SYNTHESIS OF HEXAGONAL BORON NITRIDE IN THE EXISTENCE OF FLUXING AGENTS

by
MUHAMMED ÖZ

THESIS SUBMITTED TO
THE GRADUATE SCHOOL OF NATURAL AND APLIED SCIENCES
OF
ABANT İZZET BAYSAL UNIVERSITY
IN PARTIAL FULLFILMENT OF THE REQUIREMENTS FOR THE
DEGREE DOCTOR OF PHILOSOPHY
IN
THE DEPARMENT OF CHEMISTRY

JUNE, 2013

Approval of the Graduate School of Natural and Applied Sciences.

Prof. Dr. Yaşar DÜRÜST
Director

I certify that this thesis satisfies all the requirements as a thesis for the degree of Doctor of Philosophy.

Prof. Dr. Çetin BOZKURT
Head of Department

This is to certify that we have read this thesis and that in our opinion it is fully adequate, in scope and quality, as a thesis for the degree of Doctor of Philosophy.

Prof. Dr. Çetin BOZKURT
Supervisor

Examining Committee Members

1. Prof. Dr. Çetin BOZKURT
2. Prof. Dr. Salih Zeki YILDIZ
3. Prof. Dr. İzzet MORKAN
4. Prof. Dr. İbrahim BELENLİ
5. Prof. Dr. Mustafa ÇULHA

ABSTRACT

SYNTHESIS OF HEXAGONAL BORON NITRIDE IN THE EXISTENCE OF FLUXING AGENTS

ÖZ, Muhammed
Ph.D., Department of Chemistry
Supervisor: Prof. Dr. Çetin BOZKURT

June 2013, 114 pages

Hexagonal boron nitride, one of the polymorph of boron nitride is important synthetic products in materials science. It is commercially valuable compound for industrial applications due to its special chemical and physical properties. Therefore, hBN has been the subject of recent interests for twenty years.

Some additives are known to catalytically affect the hBN formation. However, they have various functions at high temperature processes; such as a reducing agent, absorption of impurities, and retention of mixture at liquid phase at the melting temperature for a longer time thus increasing interaction at the interface of solids. Also, they are used to control grain size of crystalline solids as in optimum time-temperature conditions during sintering.

In this study, hBN was synthesized with the modified O'Connor method in presence of representative metal carbonates, acetates, and hydroxides in different amounts at different temperatures under ammonia atmosphere. Structural properties of the synthesized materials were determined by Fourier Transform Infrared

Spectroscopy, (FT-IR), X-Ray Diffraction, (XRD), Scanning Electron Microscopy, (SEM), and Transmission Electron Microscopy, (TEM).

FT-IR investigations confirmed the formation hBN and XRD patterns of the samples were indexed as hBN and calculated lattice parameters were very close to reported values of hBN. Addition of representative metal salts (especially lithium and calcium salts) into the reaction mixture decreased the formation temperature of hBN and overcome the internal stress. Also, usages of salts improved the formation of the nano structures at any temperature applied in experiments. The accompanying anions in the fluxing agents did not virtually have significant effect on the crystallization behavior of hBN.

Finally, the effect of fluxing agents on the synthesis of hBN was determined that addition of more than 20 % of metal salts into the boron oxide and urea mixture was found optimum for increasing the rate and yield of hBN formation.

Keywords: Hexagonal Boron Nitride, O'Connor Method, Characterization, XRD, TEM, Nanocrystal, Catalyst, Fluxing Agent.

ÖZET

HEGZAGONAL BOR NİTRÜRÜN ERİME NOKTASI DÜŞÜRÜCÜ MADDELER VARLIĞINDA SENTEZİ

ÖZ, Muhammed
Doktora, Kimya Bölümü
Tez danışmanı: Prof. Dr. Çetin BOZKURT

Haziran 2013, 114 sayfa

Bor nirürün polimorflarından biri olan hegzagonal bor nitrür malzeme biliminde önemli bir sentetik üründür. Özel kimyasal ve fiziksel özellikleri bakımından ticari uygulamalar bakımından değerli bir bileşiktir. Bu nedenle hBN son yirmi yılda yoğun bir şekilde araştırmalara konu olmaktadır.

Bazı katkıların hBN oluşumunu katalitik olarak etkilediği bilinmektedir. Ancak, onların indirgeyici öğe olarak, safsızlıkların absorbsiyonu ve katıların ara yüzeyinde etkileşimi arttırarak karışımı erime sıcaklığında uzun süre alıkoyması gibi yüksek sıcaklık işlemlerinde çeşitli fonksiyonu vardır. Ayrıca, sinterleşme esnasında uygun zaman sıcaklık ilişkisinde kristal katıların tanecik büyüklüğünü kontrol etmek için kullanılır.

Bu çalışmada, hBN modfiye O'Connor yöntemi kullanılarak temsilci metal karbonatları, asetatları ve hidroksitleri varlığında farklı miktarlarda ve farklı sıcaklıkta amonyak atmosferinde sentezlenmiştir. Sentezlenen maddelerin yapısal özellikleri Fourier Dönüsüm Kızılötesi Spektroskopisi (FT-IR), X-Isını Kırınım

Ölçeri (XRD), Taramalı Elektron Mikroskobu, (SEM) ve Geçirimli Elektron Mikroskobu (TEM) kullanılarak belirlenmiştir.

FT-IR araştırmaları hBN oluşumunu doğrulamıştır ve örneklerin XRD motifleri hBN olarak endekslenmiştir ve hesaplanan örgü parametreleri bildirilen hBN değerlerine oldukça yakındır. Temsilci metal tuzlarının (özellikle de lityum ve kalsiyum tuzları) reaksiyon karışımına eklenmesi hBN oluşum sıcaklığını düşürmekte ve iç gerilimin üstesinden gelmektedir. Katkıların kullanımı uygulanan her sıcaklıkta nano yapıların oluşumunu sağlamaktadır. Eritici maddelerle eşlenilen anyonların hBN'nin kristallenme davranışları üzerinde neredeyse belirgin anlamlı etkisi yoktur.

Sonuç olarak, hBN sentezi üzerindeki eritici öğelerin etkisi bor oksit ve üre karışımına % 20'den fazla metal tuzu eklendiğinde, hBN oluşumunun verimini ve hızını arttırmak için en iyi koşul olarak belirlenmiştir.

Anahtar Kelimeler: Hegzagonal Bor Nitrür, O'Connor Metodu, Karakterizasyon, XRD, TEM, Nanokristal, Katalizör, Eritici Katkılar

DEDICATED TO MY FATHER

ABDURRAHMAN ÖZ

ACKNOWLEDGMENTS

I would like to express my appreciation and gratitude to my supervisor Prof. Dr. Çetin BOZKURT for his endless support, encouragement, inspiration and guidance at all stages of my studies.

I would like to thank my committee members Prof. Dr. Salih Zeki YILDIZ, Prof. Dr. İzzet Amour MORKAN, Prof. Dr. İbrahim BELENLİ, and Prof. Dr. Mustafa ÇULHA for their teaching doctrine, sincerities and helps.

I would like to express my sincere gratitude to Prof. Dr. Ahmet VARİLCİ for his laboratory support.

My sincere thanks also goes to Assist. Prof. Dr. Erhan BUDAK, Assist. Prof. Dr. Gürcan YILDIRIM, Sevgi POLAT ALTINTAŞ, Nevin SOYLU, and the staff of Physics Department of A. İ. B. U., for their friendships, support, and help in analysis of samples.

I would like to express my sincere gratitude to my family for their great support, love, endless patience and encouragement during my study.

Finally, I apologize to those whom I can not mention, however, have not forgotten.

TABLE OF CONTENTS

ABSTRACT..... iii

ÖZET..... v

ACKNOWLEDGEMENTS..... viii

TABLE OF CONTENTS..... ix

LIST OF TABLES..... xiii

LIST OF FIGURES..... xiv

LIST OF ABBREVIATIONS..... xxi

CHAPTER 1

1. INTRODUCTION..... 1

1.1. Basis of Boron Nitride..... 2

1.1.1. Hexagonal Boron Nitride…..... 3

1.1.2. Other Main Forms of Boron Nitride…..... 4

1.2. Synthesis of Hexagonal Boron Nitride..... 5

1.3. Solid State Reactions..... 8

1.4. Flux Agents and Usage..... 10

1.5. Characterization of Hexagonal Boron Nitride..... 12

1.5.1. FT-IR Spectroscopy..... 12

1.5.2. X-Ray Powder Diffraction (XRD)..... 13

1.5.3. Electron Microscopy..... 15

1.5.3.1. Scanning Electron Microscopy (SEM)..... 15

1.5.3.2. Transmission Electron Microscopy (TEM)..... 16

1.6. Scope of This Study..... 18

CHAPTER 2

2. LITERATURE SURVEY..... 19

2.1. Literature Survey on Boron Nitride..... 19

2.2. Literature Survey on Flux Agents..... 20

2.3. Literature Survey on Nanocrystalline Boron Nitride..... 23

CHAPTER 3

3. EXPERIMENTAL and INSTRUMENTAL PROCESSES..... 26

3.1. Materials..... 26

3.2. Synthesis of hBN Samples..... 26

3.3. Preparation of BN Samples..... 27

3.3.1. Ball-Mill Grinder..... 27

3.3.2. Camara Furnace..... 28

3.3.3. Tube Furnace..... 29

3.4. Characterization of hBN Samples..... 31

3.4.1. FT-IR Spectroscopy..... 31

3.4.2. XRD Measurement…..... 31

3.4.3. SEM Analysis..... 32

3.4.4. TEM Analysis..... 33

3.5. Sample Calculations..... 33

3.5.1. Calculation of Lattice Parameters..... 33

3.5.2. Determination of Grain Size..... 34

3.5.2.1. Debye-Scherer Method..... 35

3.5.2.2. Williamson-Hall Method..... 35

3.5.3. Calculation of Graphitization Index..... 37

CHAPTER 4

4. RESULTS..... 38

4.1. Effect of Representative Metal Carbonates on Synthesis of hBN..... 38

4.1.1. FT-IR Spectroscopy of hBN Samples in the Presence of Metal Carbonates..... 38

4.1.2. XRD Analysis of hBN Samples in the Presence of Metal Carbonates..... 43

4.1.3. Scanning Electron Microscopy Observations of hBN Samples in the Presence of Metal Carbonates..... 51

4.2. Effect of Representative Metal Acetates on Synthesis of hBN..... 53

4.2.1. FT-IR Spectroscopy of hBN Samples in the Presence of Metal Acetates..... 54

4.2.2. XRD Analysis of hBN Samples in the Presence of Metal Acetates..... 57

4.2.3. Scanning Electron Microscopy Observations of hBN Samples in the Presence of Metal Acetates..... 62

4.3. Effect of Representative Metal Hydroxides on Synthesis of hBN..... 66

4.3.1. FT-IR Spectroscopy of hBN Samples in the Presence of Metal Hydroxides..... 66

4.3.2 XRD Analysis of hBN Samples in the Presence of Metal Hydroxides..... 69

4.3.3. Scanning Electron Microscopy Observations of hBN Samples in the Presence of Metal Hydroxides..... 77

4.4. Low Temperature Trials of Representative Metals Salts Additions on hBN Synthesis..... 80

4.4.1. FT-IR Spectroscopy of hBN Samples Synthesized at Low Temperatures..... 80

4.4.2. XRD Analysis of hBN Samples Synthesized at Low Temperature..... 83

4.4.3. Scanning Electron Microscopy Analysis of hBN Samples Synthesized at Low Temperature..... 88

4.5. Effect of Metals of the Metal Salts on the Formation of hBN..... 93

4.6. The Effect of Anions in the Metal Salts on the hBN Synthesis..... 96

4.7. Transmission Electron Microscopy Observations for hBN Samples.... 100

CHAPTER 5

5. DISCUSSION..... 103

CHAPTER 6

6. CONCLUSION…..... 106

REFERENCES…..... 108

CIRRICULUM VITAE..... 114

LIST OF TABLES

Table 1.1. Some properties of BN morphologies determined by XRD..... 15

Table 3.1. Flux agents (Used as additive into boron oxide and urea mixture)..... 27

Table 4.1. Lattice Parameters, Average Grain Size, Microstrain and Graphitization Index of Metal Carbonates..... 48

Table 4.2. Lattice Parameters, Average Grain Size, Microstrain and Graphitization Index of Metal Acetates..... 60

Table 4.3. Lattice Parameters, Average Grain Size, Microstrain and Graphitization Index of Metal Hydroxides..... 74

Table 4.4. Lattice Parameters, Average Grain Size, Microstrain and Graphitization Index of Low Temperature Trials..... 86

Table 4.5. Comparison of effect of the anions of salts..... 97

LIST OF FIGURES

Figure 1.1 The comparison of the hBN and graphite..... 3

Figure 1.2 Comparison of the phases of BN and carbon..... 4

Figure 1.3 The routes of synthesis of BN..... 6

Figure 1.4 Redistribution of HO–B–N–H monomer..... 7

Figure 1.5 Trimerization of the monomer..... 7

Figure 1.6 Formation of macromolecules of BN..... 7

Figure 1.7 Crystalline BN..... 8

Figure 1.8 Diagram showing the reaction interface..... 9

Figure 1.9 IR spectra samples of hBN and cBN..... 12

Figure 1.10 The X-ray diffraction spectra of hBN, rBN, tBN, cBN, and wBN.. 14

Figure 1.11 Samples of SEM images of BN..... 16

Figure 1.12 Sample TEM images of BN (a) nanotube (b) nanowire form of BN..... 17

Figure 3.1 Pascall Engineering, 1600-VS-A roll mixer and alumina jar..... 28

Figure 3.2 Sieve..... 28

Figure 3.3 Temperature rates of experiments until precursor stage..... 29

Figure 3.4 Proterm PLF 140/5 Camera Furnace..... 29

Figure 3.5 Temperature rates of experiments..... 30

Figure 3.6 Proterm PTF 15/75/450 Tube Furnace..... 30

Figure 3.7 Shimadzu 8400S FT-IR spectrometer..... 31

Figure 3.8 Rigaku Multiflex XRD..... 32

Figure 3.9 Jeol JSM 6390LV SEM..... 32

Figure 3.10 Jeol JEM 2100F HRTEM..... 33

Figure 3.11 The schematically Williamson-Hall plot..... 36

Figure 4.1 FT-IR spectra of the hBN samples with increasing amounts of Li_2CO_3 a) 1 % Li_2CO_3, b) 10 % Li_2CO_3, c) 20 % Li_2CO_3, d) 30 % Li_2CO_3, and e) 40 % Li_2CO_3..... 40

Figure 4.2 FT-IR spectra of the hBN samples with increasing amounts of Na_2CO_3, a) 1 % Na_2CO_3, b) 10 % Na_2CO_3, c) 20 % Na_2CO_3, d) 30 % Na_2CO_3, and e) 40 % Na_2CO_3..... 41

Figure 4.3 FT-IR spectra of the hBN samples with increasing amounts of K_2CO_3, a) 1 % K_2CO_3, b) 10 % K_2CO_3, c) 20 % K_2CO_3, d) 30 % K_2CO_3, and e) 40 % K_2CO_3..... 41

Figure 4.4 FT-IR spectra of the hBN samples with increasing amounts of $Mg(OH)CO_3$, a) 1 % $Mg(OH)CO_3$, b) 10 % $Mg(OH)CO_3$, c) 20 % $Mg(OH)CO_3$, d) 30 % $Mg(OH)CO_3$, and e) 40 % $Mg(OH)CO_3$..... 42

Figure 4.5 FT-IR spectra of the hBN samples with increasing amounts of $CaCO_3$, a) 1 % $CaCO_3$, b) 10 % $CaCO_3$, c) 20 % $CaCO_3$, d) 30 % $CaCO_3$, and e) 40 % $CaCO_3$..... 42

Figure 4.6 The XRD diffractogram of commercial hBN..... 43

Figure 4.7 Comparison of XRD patterns of plain hBNs (1) prepared according to O'Connor method and pure (commercial) hBNs (2)..... 44

Figure 4.8 XRD patterns of the hBN in the presence of Li_2CO_3 where, 1) 1 %, 2) 10 %, 3) 20 %, 4) 30 %, and 5) 40 % Li_2CO_3..... 45

Figure 4.9 XRD patterns of the hBN in the presence of Na_2CO_3 where, 1) 1 %, 2) 10 %, 3) 20 %, 4) 30 %, and 5) 40 % Na_2CO_3..... 45

Figure 4.10 XRD patterns of the hBN in the presence of K_2CO_3 where, 1) 1 %, 2) 10 %, 3) 20 %, 4) 30 %, and 5) 40 % K_2CO_3..... 46

Figure 4.11 XRD patterns of the hBN in the presence of $Mg(OH)CO_3$ where, 1) 1 %, 2) 10 %, 3) 20 %, 4) 30 %, and 5) 40 % $Mg(OH)CO_3$..... 46

Figure 4.12 XRD patterns of the hBN in the presence of $CaCO_3$ where, 1) 1 %, 2) 10 %, 3) 20 %, 4) 30 %, and 5) 40 % $CaCO_3$..... 47

Figure 4.13 Average grain size (Debye-Scherrer Method) of hBN versus amount with the use of metal carbonates..... 49

Figure 4.14 Average grain size (Williamson-Hall Method) of hBN versus amount with the use of metal carbonates..... 49

Figure 4.15 Graphitization index of hBN synthesized with different metal carbonates..... 50

Figure 4.16 Selected SEM images of hBNs synthesized in the presence of Li_2CO_3..... 51

Figure 4.17 Selected SEM images of hBNs synthesized in the presence of Na_2CO_3..... 52

Figure 4.18 Selected SEM images of hBNs synthesized in the presence of K_2CO_3..... 52

Figure 4.19 Selected SEM images of hBNs synthesized in the presence of $Mg(OH)CO_3$..... 53

Figure 4.20 Selected SEM images of hBNs synthesized in the presence of $CaCO_3$..... 53

Figure 4.21 FT-IR spectra of the hBN samples with increasing amounts of $Li(CH_3CO_2)$, a) 1 % $Li(CH_3CO_2)$, b) 10 % $Li(CH_3CO_2)$, c) 20 % $Li(CH_3CO_2)$, d) 30 % $Li(CH_3CO_2)$, and e) 40 % $Li(CH_3CO_2)$..... 54

Figure 4.22 FT-IR spectra of the hBN samples with increasing amounts of $Na(CH_3CO_2)$, a) 1 % $Na(CH_3CO_2)$, b) 10 % $Na(CH_3CO_2)$, c) 20 % $Na(CH_3CO_2)$, d) 30 % $Na(CH_3CO_2)$, and e) 40 % $Na(CH_3CO_2)$..... 55

Figure 4.23 FT-IR spectra of the hBN samples with increasing amounts of $K(CH_3CO_2)$, a) 1 % $K(CH_3CO_2)$, b) 10 % $K(CH_3CO_2)$, c) 20 % $K(CH_3CO_2)$, d) 30 % $K(CH_3CO_2)$, and e) 40 % $K(CH_3CO_2)$..... 55

Figure 4.24 FT-IR spectra of the hBN samples with increasing amounts of $Mg(CH_3CO_2)_2$, a) 1 % $Mg(CH_3CO_2)_2$, b) 10 % $Mg(CH_3CO_2)_2$, c) 20 % $Mg(CH_3CO_2)_2$, d) 30 % $Mg(CH_3CO_2)_2$, and e) 40 % $Mg(CH_3CO_2)_2$..... 56

Figure 4.25 FT-IR spectra of the hBN samples with increasing amounts of $Ca(CH_3CO_2)_2$, a) 1 % $Ca(CH_3CO_2)_2$, b) 10 % $Ca(CH_3CO_2)_2$, c) 20 % $Ca(CH_3CO_2)_2$, d) 30 % $Ca(CH_3CO_2)_2$, and e) 40 % $Ca(CH_3CO_2)_2$..... 56

Figure 4.26 XRD patterns of the hBN in the presence of $Li(CH_3CO_2)$ where, 1) 1 %, 2) 10 %, 3) 20 %, 4) 30 %, and 5) 40 % $Li(CH_3CO_2)$..... 57

Figure 4.27 XRD patterns of the hBN in the presence of $Na(CH_3CO_2)$ where, 1) 1 %, 2) 10 %, 3) 20 %, 4) 30 %, and 5) 40 % $Na(CH_3CO_2$..... 58

Figure 4.28 XRD patterns of the hBN in the presence of $K(CH_3CO_2)$ where, 1) 1 %, 2) 10 %, 3) 20 %, 4) 30 %, and 5) 40 % $K(CH_3CO_2)$..... 58

Figure 4.29 XRD patterns of the hBN in the presence of $Mg(CH_3CO_2)_2$ where, 1) 1 %, 2) 10 %, 3) 20 %, 4) 30 %, and 5) 40 % $Mg(CH_3CO_2)_2$..... 59

Figure 4.30 XRD patterns of the hBN in the presence of $Ca(CH_3CO_2)_2$ where, 1) 1 %, 2) 10 %, 3) 20 %, 4) 30 %, and 5) 40 % $Ca(CH_3CO_2)_2$..... 59

Figure 4.31 Average grain size (Debye-Scherrer Method) of hBN versus amount with the use of acetates..... 61

Figure 4.32 Average grain size (Williamson-Hall Method) of hBN versus amount with the use of acetates..... 61

Figure 4.33 Graphitization index of hBN synthesized with different metal acetates..... 62

Figure 4.34 Selected SEM images of hBNs synthesized in the presence of $Li(CH_3CO_2)$..... 63

Figure 4.35 Selected SEM images of hBNs synthesized in the presence of $Na(CH_3CO_2)$..... 64

Figure 4.36 Selected SEM images of hBNs synthesized in the presence of $K(CH_3CO_2)$..... 64

Figure 4.37 Selected SEM images of hBNs synthesized in the presence of $Mg(CH_3CO_2)_2$..... 65

Figure 4.38 Selected SEM images of hBNs synthesized in the presence of $Ca(CH_3CO_2)_2$..... 65

Figure 4.39 FT-IR spectra of the hBN samples with increasing amounts of LiOH, a) 1 % LiOH, b) 10 % LiOH, c) 20 % LiOH, d) 30 % LiOH, and e) 40 % LiOH..... 67

Figure 4.40 FT-IR spectra of the hBN samples with increasing amounts of NaOH, a) 1 % NaOH, b) 10 % NaOH, c) 20 % NaOH, d) 30 % NaOH, and e) 40 % NaOH..... 67

Figure 4.41 FT-IR spectra of the hBN samples with increasing amounts of KOH, a) 1 % KOH, b) 10 % KOH, c) 20 % KOH, d) 30 % KOH, and e) 40 % KOH..... 68

Figure 4.42 FT-IR spectra of the hBN samples with increasing amounts of $Mg(OH)_2$, a) 1 % $Mg(OH)_2$, b) 10 % $Mg(OH)_2$, c) 20 % $Mg(OH)_2$, d) 30 % $Mg(OH)_2$, and e) 40 % $Mg(OH)_2$..... 68

Figure 4.43 FT-IR spectra of the hBN samples with increasing amounts of $Ca(OH)_2$, a) 1 % $Ca(OH)_2$, b) 10 % $Ca(OH)_2$, c) 20 % $Ca(OH)_2$, d) 30 % $Ca(OH)_2$, and e) 40 % $Ca(OH)_2$..... 69

Figure 4.44 XRD patterns of the hBN in the presence of LiOH where, 1) 1 %, 2) 10 %, 3) 20 %, 4) 30 %, and 5) 40 % LiOH..... 70

Figure 4.45 XRD patterns of the hBN in the presence of NaOH where, 1) 1 %, 2) 10 %, 3) 20 %, 4) 30 %, and 5) 40 % NaOH..... 71

Figure 4.46 XRD patterns of the hBN in the presence of KOH where, 1) 1 %, 2) 10 %, 3) 20 %, 4) 30 %, and 5) 40 % KOH..... 71

Figure 4.47 XRD patterns of the hBN in the presence of $Mg(OH)_2$ where, 1) 1 %, 2) 10 %, 3) 20 %, 4) 30 %, and 5) 40 % $Mg(OH)_2$..... 72

Figure 4.48 XRD patterns of the hBN in the presence of $Ca(OH)_2$ where, 1) 1 %, 2) 10 %, 3) 20 %, 4) 30 %, and 5) 40 % $Ca(OH)_2$..... 72

Figure 4.49 Average grain size (Debye-Scherrer Method) of hBN versus amount with the use of metal hydroxides..... 75

Figure 4.50 Average grain size (Williamson-Hall Method) of hBN versus amount with the use of metal hydroxides..... 75

Figure 4.51 Graphitization index of hBN synthesized with different metal hydroxides..... 76

Figure 4.52 Selected SEM images of hBNs synthesized in the presence of LiOH..... 77

Figure 4.53 Selected SEM images of hBNs synthesized in the presence of NaOH..... 78

Figure 4.54 Selected SEM images of hBNs synthesized in the presence of KOH..... 78

Figure 4.55 Selected SEM images of hBNs synthesized in the presence of $Mg(OH)_2$..... 79

Figure 4.56 Selected SEM images of hBNs synthesized in the presence of $Ca(OH)_2$..... 79

Figure 4.57 FT-IR spectra of the hBN samples synthesized with 40 % Li_2CO_3 at different temperatures a) 1000 °C, b) 1150 °C, c) 1300 °C, and d) 1450 °C..... 81

Figure 4.58 FT-IR spectra of the hBN samples synthesized with 40 % $Li(CH_3CO_2)$ at different temperatures a) 1150 °C, b) 1300 °C, and c) 1450 °C..... 81

Figure 4.59 FT-IR spectra of the hBN samples synthesized with 40 % LiOH at different temperatures a) 1150 °C, b) 1300 °C, and c) 1450 °C..... 82

Figure 4.60 FT-IR spectra of the hBN samples synthesized with 10 % $CaCO_3$ at different temperatures a) 1150 °C, b) 1300 °C, and c) 1450 °C..... 82

Figure 4.61 Synthesis of hBN with the addition of 40 % Li_2CO_3 at different temperatures, where, 1) 1000 °C, 2) 1150 °C, 3) 1300 °C, and 4) 1450 °C..... 84

Figure 4.62 Synthesis of hBN with the addition of 40 % $Li(CH_3CO_2)$ at different temperatures, where, 1) 1150 °C, 2) 1300 °C, and 3) 1450 °C..... 84

Figure 4.63 Synthesis of hBN with the addition of 40 % LiOH at different temperatures, where, 1) 1150 °C, 2) 1300 °C, and 3) 1450 °C..... 85

Figure 4.64 Synthesis of hBN with the addition of 10 % $CaCO_3$ at different temperatures, where, 1) 1150 °C, 2) 1300 °C, and 3) 1450 °C..... 85

Figure 4.65 Average grain size (Debye-Scherrer Method) of hBN at increasing temperatures with the use of representative metals..... 87

Figure 4.66 Average grain size (Williamson-Hall Method) of hBN at increasing temperatures with the use of representative metals..... 87

Figure 4.67 Graphitization index of hBN synthesized at low temperatures with different additives..... 88

Figure 4.68 Selected SEM images of hBNs synthesized in presence of Li_2CO_3 at 1300 °C..... 89

Figure 4.69 Selected SEM images of hBNs synthesized in presence of Li_2CO_3 at 1150 °C..... 90

Figure 4.70 Selected SEM images of hBNs synthesized in presence of $Li(CH_3CO_2)$ at 1300 °C..... 90

Figure 4.71 Selected SEM images of hBNs synthesized in presence of $Li(CH_3CO_2)$ at 1150 °C..... 91

Figure 4.72 Selected SEM images of hBNs synthesized in presence of LiOH at 1300 °C..... 91

Figure 4.73 Selected SEM images of hBNs synthesized in presence of LiOH at 1150 °C..... 92

Figure 4.74 Selected SEM images of hBNs synthesized in presence of $CaCO_3$ at 1300 °C..... 92

Figure 4.75 Selected SEM images of hBNs synthesized in presence of $CaCO_3$ at 1150 °C..... 93

Figure 4.76 Comparison of XRD patterns of hBNs prepared with different additives, where 1) 40 % Li_2CO_3, 2) 40 % Na_2CO_3, 3) 40 % K_2CO_3, 4) 40 % $MgOHCO_3$, and 5) 40 % $CaCO_3$..... 95

Figure 4.77 Comparison of XRD patterns of hBNs prepared with different additives, where 1) 40 % $Li(CH_3CO_2)$, 2) 40 % $Na(CH_3CO_2)$, 3) 40 % $K(CH_3CO_2)$, 4) 40 % $Mg(CH_3CO_2)_2$, and 5) 40 % $Ca(CH_3CO_2)_2$..... 95

Figure 4.78 Comparison of XRD patterns of hBNs prepared with different additives, where 1) 40 % LiOH, 2) 40 % NaOH, 3) 40 % KOH, 4) 40 % $Mg(OH)_2$, and 5) 40 % $Ca(OH)_2$..... 96

Figure 4.79 Comparison of XRD patterns of hBNs prepared with lithium in different anions, where 1) 40 % $Li(CH_3CO_2)$, 2) 40 % LiOH, and 3) 40 % Li_2CO_3…..... 97

Figure 4.80 Comparison of XRD patterns of hBNs prepared with sodium in different anions, where 1) 40 % $Na(CH_3CO_2)$, 2) 40 % NaOH, and 3) 40 % Na_2CO_3..... 98

Figure 4.81 Comparison of XRD patterns of hBNs prepared with potassium in different anions, where 1) 40 % $K(CH_3CO_2)$, 2) 40 % KOH, and 3) 40 % K_2CO_3..... 98

Figure 4.82 Comparison of XRD patterns of hBNs prepared with magnesium in different anions, where 1) 40 % $Mg(CH_3CO_2)_2$, 2) 40 % $Mg(OH)_2$, and 3) 40 % $MgOHCO_3$..... 99

Figure 4.83 Comparison of XRD patterns of hBNs prepared with magnesium in different anions, where 1) 40 % $Ca(CH_3CO_2)_2$, 2) 40 % $Ca(OH)_2$, and 3) 40 % $CaCO_3$..... 99

Figure 4.84 Selected TEM images of hBN synthesized in the presence of Li_2CO_3 at 1450 °C..... 100

Figure 4.85 Selected TEM images of hBN synthesized in the presence of Li_2CO_3 at 1300 °C..... 101

Figure 4.86 Selected TEM images of hBN synthesized in the presence of Li_2CO_3 at 1150 °C..... 101

Figure 4.87 Selected TEM images of hBN synthesized in the presence of $Li(CH_3CO_2)$ at 1150 °C..... 101

Figure 4.88 Selected TEM images of hBN synthesized in the presence of LiOH at 1450 °C..... 102

Figure 4.89 Selected TEM images of hBN synthesized in the presence of $CaCO_3$ at 1450 °C..... 102

LIST OF ABBREVIATIONS

2θ	:	Bragg angle degree
aBN	:	Amorphous Boron Nitride
AFM	:	Atomic Force Microscope
BN	:	Boron Nitride
cBN	:	Cubic Boron Nitride
EDX	:	Energy Dispersive X-Ray Spectroscopy
FT-IR	:	Fourier Transform Infrared Spectroscopy
hBN	:	Hexagonal Boron Nitride
HR-TEM	:	High Resolution Transmission Electron Microscope
ICDD	:	The International Centre for Diffraction Data
rBN	:	Rhombohedral Boron Nitride
SEM	:	Scanning Electron Microscopy
SSR	:	Solid State Reactions
tBN	:	Turbostratic Boron Nitride
TEM	:	Transmission Electron Microscope
TGA	:	Thermal Gravimetric Analysis
wBN	:	Wurtzitic Boron Nitride
XRD	:	X-ray Diffractometer

CHAPTER 1

1. INTRODUCTION

Boron compounds have wide variety of uses in industrial applications and consumer products including many detergents, cosmetics, and enamel glazes. Moreover, they are used in ceramics, bleaching agents, insecticides, semiconductors, magnets, shielding in nuclear reactors, biological applications, and other nonmedical uses [1].

Boron nitride (with its all forms) is one of the important synthetic chemical boron compounds with chemical formula BN, consisting of boron and nitrogen atoms. It is a commercially valuable compound for industrial applications due to its special chemical and physical properties.

Hexagonal boron nitride (hBN) a polymorph of BN has layered planar structure. Therefore, it is used as lubricant at high and low temperature processes. hBN has also low dielectric constant, high electrical resistance, excellent thermal shock resistance, and high stability. Thus it is utilized in paint, dental cement, turbine shafts, and diesel turbo charges [2].

Flux agents that are carbonate of soda, potash, charcoal, coke, borax, lime, lead sulfide and minerals with phosphorus have various functions at high temperature processes, such as a reducing agent, absorption of impurities, and retention of melt in liquid phase at the melting temperature [3, 4]. Fluxes also behave as a heat transfer

medium, to increase interaction at the interface of solids and are used to control grain size of crystalline solids as in optimum time-temperature conditions during sintering [5, 6].

1.1. Basis of Boron Nitride

Boron compounds (especially borax) have been used since 2600 b.c. by Babylon, Tibet, ancient Egypt, and ancient Greek for cleaning, melting of jewels, mummifying, and healing. Turkey has the opportunity having largest boron raw deposits in the World. Also, boron and its compounds were declared by USA and NATO as strategically important material [7].

Boron nitride, was first synthesized in 1842, is the oldest known synthetic compound of boron and nitrogen with chemical formula $(BN)_x$, consisting of equal numbers of boron and nitrogen atoms. BN is isoelectronic to a similarly structured carbon lattice that has similar properties as carbon allotropes. Layered structure of BN was named as hexagonal BN is similar to graphite; therefore it is often referred to as "white graphite". Depending on its hybridization boron nitride has several crystalline forms that are; hexagonal boron nitride (hBN), rhombohedral boron nitride (rBN), cubic boron nitride (cBN) or borazon, wurzit boron nitride (wBN), zinc blende (zBN), turbostratic boron nitride (tBN), ion-bombarded boron nitride (iBN), explosion boron nitride (EBN), amber boron nitride (ABN), Showa Denko's cubic boron nitride (SBN), pyrolytic boron nitride (pBN)- the mixture of hBN and tBN-, amorphous boron nitride (aBN), elbor cubonite, αBN, βBN, γBN and more [8].

1.1.1. Hexagonal Boron Nitride

One of the most stable crystalline forms of BN is the hexagonal, also called hBN, αBN, or gBN (graphitic BN) (Figure 1.1). The crystal lattice of hBN consists of hexagonal rings forming parallel planes. In each layer, boron and nitrogen atoms are bound by strong covalent bonds (σ-bonding and sp^2-hybridization), whereas the layers are held together by weak van der Waals forces (mainly π-bonding). Atoms of boron and nitrogen are bonded to other atoms in the plane with the angle at 120° between two bonds (each boron atom is bonded to three nitrogen atoms and each nitrogen atom is bonded to three boron atoms). Additionally, it has to be pointed out that the planes are stacked on top of one another, without any horizontal displacement (boron and nitrogen are alternating along the c-axis) [1, 8, 9].

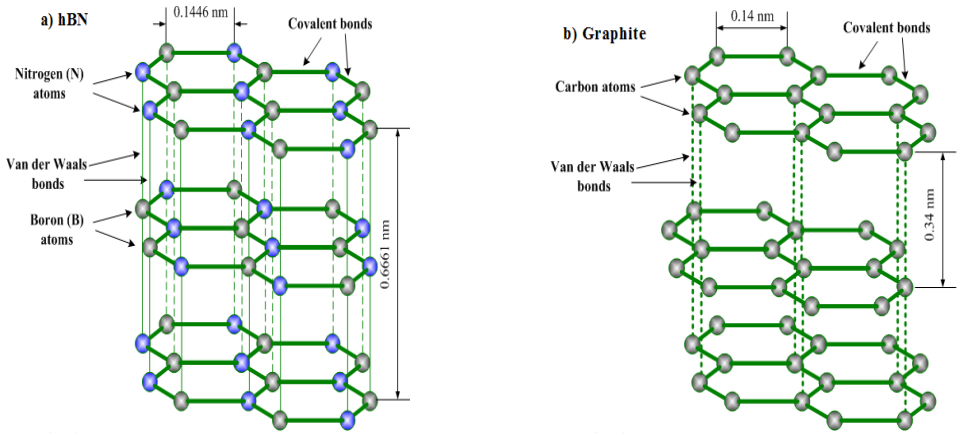

Figure 1.1 The comparison of the hBN and graphite [9].

1.1.2. Other Main Forms of Boron Nitride

The rBN has trigonal sp^2 bonding and its structure is similar to the graphite structure as well as hBN (Figure 1.2). rBN has flat sp^2 hybridized bonding and the B–N distance 144 pm while the distance between the layers is long as 333 pm. As a result of weak interaction between the layers, allows the structure to be converted other forms of BN under high pressure [8, 9].

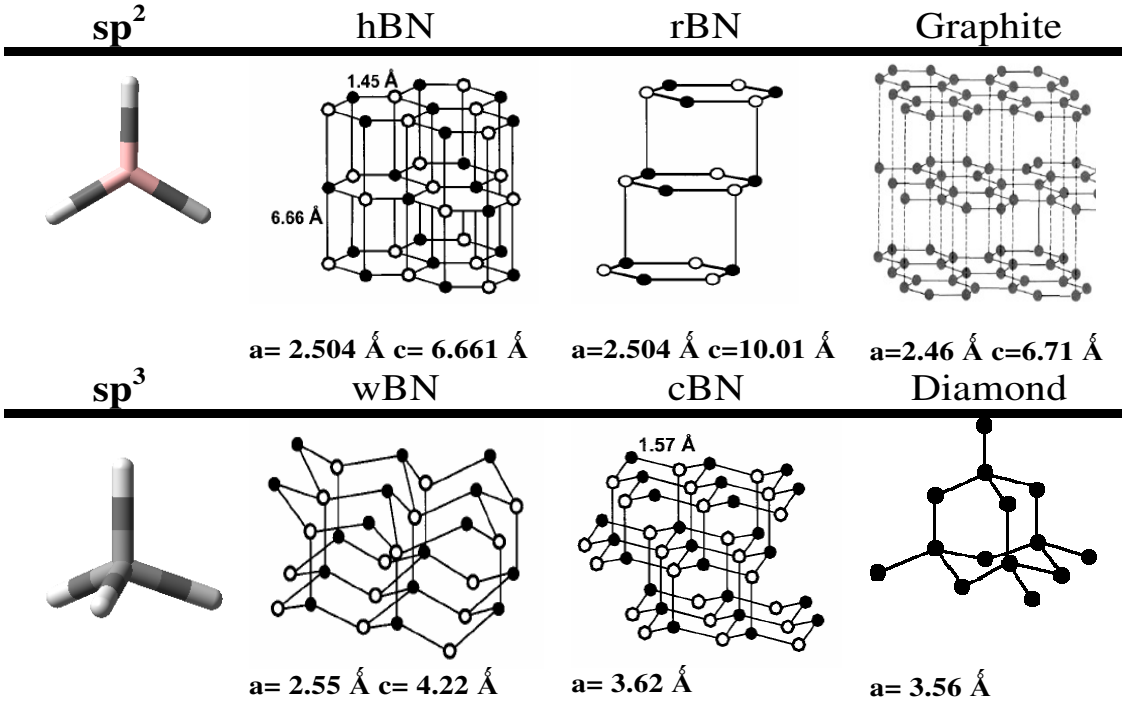

Figure 1.2 Comparison of the phases of BN and carbon [8, 9].

Boron nitride has disordered structure at low temperature (~1000 ºC) synthesis is called as turbostratic BN as well as many-layered turbostratic carbon. tBN has also layer structure similar to the hBN, the layers are mostly placed parallel, however, they do not aligned to one axis table. Meanwhile the turbostratic structure can be converted to other forms of BN by treatment at high temperatures [8, 9].

Tetrahedrally coordinated B and N atoms are called as cBN or wBN. In this arrangement atoms have sp^3 hybridization (Figure 1.2) with a 157 pm layer distance for cBN. cBN exhibits high hardness, because of short bonding lengths. In addition, cBN is also insulator due to its lack of π bonds. It can be produced from the hexagonal form of BN and others [8, 9].

1.2. Synthesis of Hexagonal Boron Nitride

BN is synthetically produced from the initial boron containing compounds in literature. The first synthesis of BN was achieved in W. H. Balmain by the action of molten boric acid on potassium cyanide. However, the product was unstable and BN did not become a commercial material until 1950s due to the difficulties in synthesis and high cost of methods [10]. Nowadays, there are several methods that are applied to produce hBN industrial scale, are summarized in figure 1.3 [11].

Three main methods are utilized for the production of hBN that are; carbothermic method, the reaction of boric acid with ammonia gas, and the reaction of nitrogen containing solid substances such as urea with boron containing substances like boric acid under nitrogen rich gases [9, 11, 12, 13].

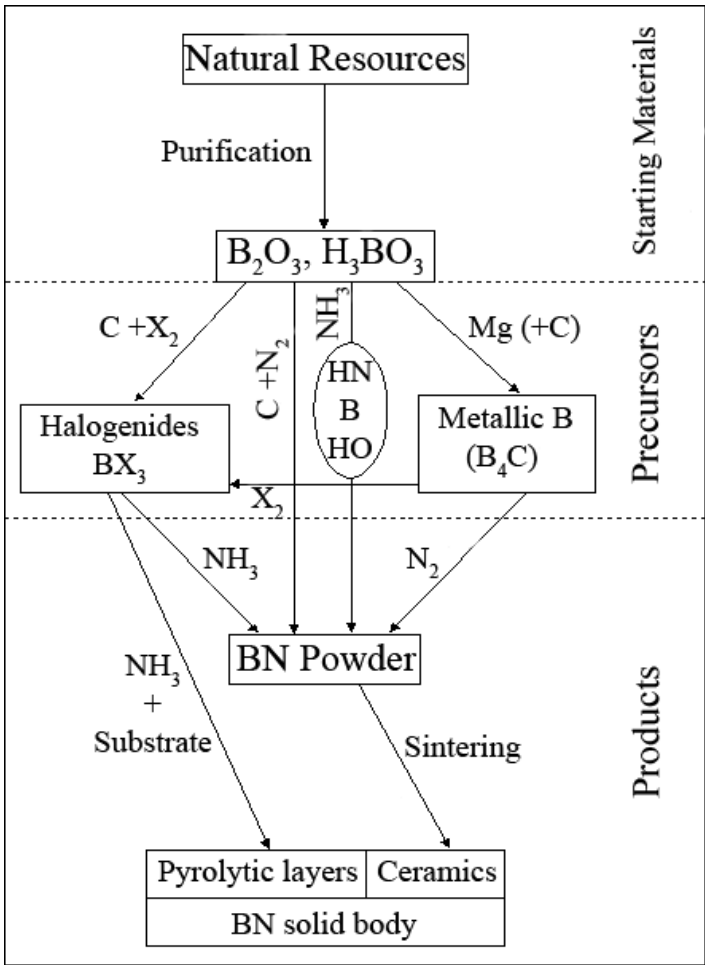

Figure 1.3 The routes of synthesis of BN [11].

In literature, one of the mechanisms that have great attention was estimated by O'Connor. It was to produce powder hBN with a simple method proposed by O'Connor by heating urea and boric acid under ammonia atmosphere at high temperatures (over 1600°C) [13]. Moreover, this is accepted as a possible method among the others and it is likely to modify hBN samples at precursor stage [14]. In the first step of proposed mechanism, an ammonia molecule approaches to the surface of a boric acid crystal. Then, the new bonds are formed (occupying HO–B–N–H monomer) and water is released as a result of the redistribution of electron densities in the system (Figure 1.4). Formations of the stable monomers are concluded by the trimerization at the second step (Figure 1.5) [9, 14].

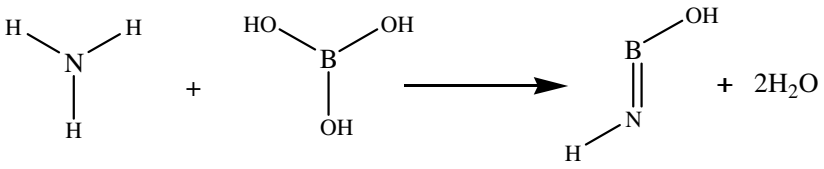

Figure 1.4 Redistribution of HO–B–N–H monomer.

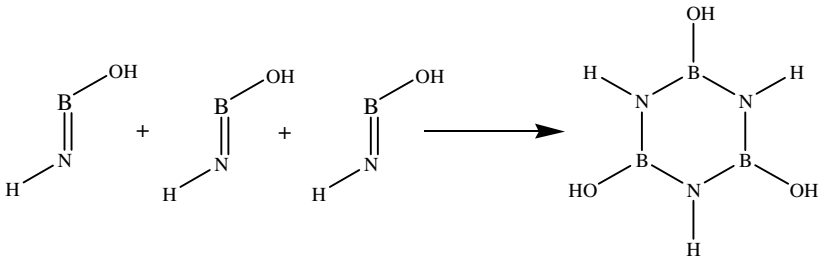

Figure 1.5 Trimerization of the monomer.

In the last step, macromolecules are possibly constituted from the bonding of monomers to the trimerized BNs (Figure 1.6). The estimated growth of BN continues to form the intermediate macromolecules depending on reactants, heating temperature, and reaction atmosphere (Figure 1.7) [1, 5, 14]. The –O–H and –H groups at the end of macromolecules are constitutional part and recommended chain terminating step of the two dimensional hBN layers [15].

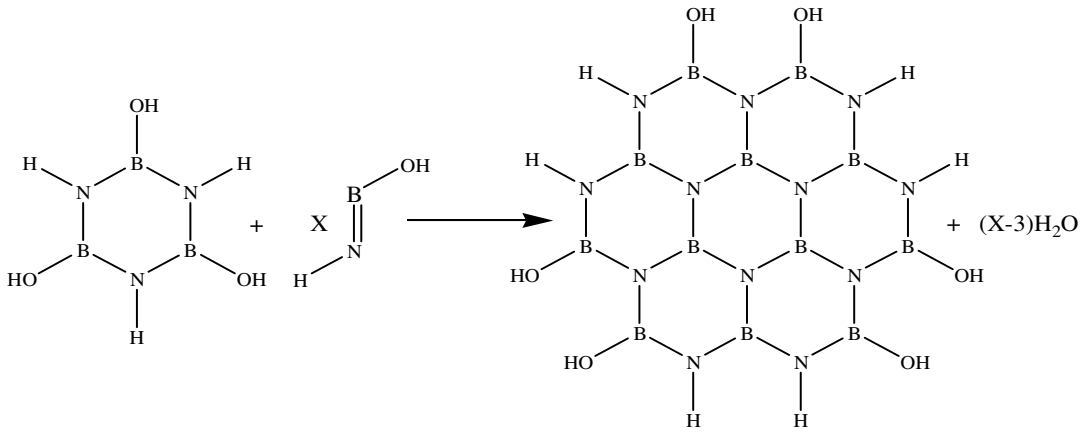

Figure 1.6 Formation of BN macromolecules.

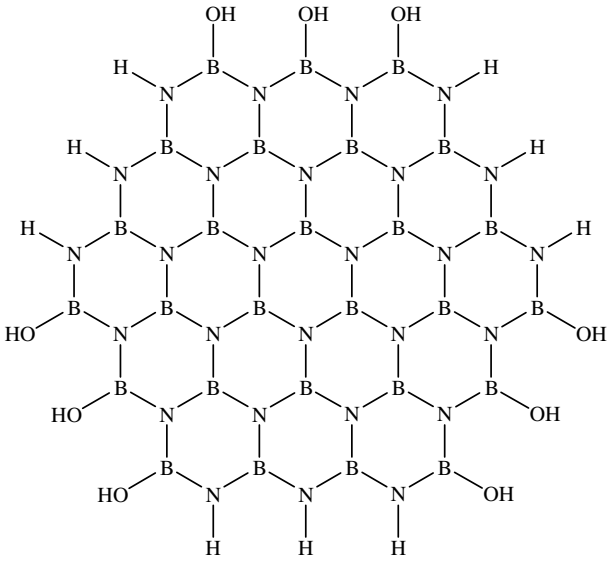

Figure 1.7 Crystalline BN.

1.3. Solid State Reactions

Production of hBN is carried with various methods such as chemical vapor deposition (CVD), carbothermic and high temperature annealing of boron and nitrogen compounds in solid state reactions (SSR) [1, 8]. SSR is mainly called as solventless reaction or dry media reaction that is a chemical reaction, in which solvents are not used. Therefore, the SSRs have many advantages compared to other methods. It is an economic synthesis method to eliminate solvents resulting the less cost. Eliminating the solvent from the reaction system means that a SSR produces more product than a normal reaction and it is friendlier for environment. Since there is no solvent usage, there is no waste at the end of the reaction [16].

The preparation of polycrystalline solids from a mixture of solid starting materials is achieved by the SSRs that are widely used method containing the mechanisms that has phase changes, formation of phase boundaries, rate process changes in solids, nucleation, diffusion processes, and diffusion-controlled SSRs.

Solids mostly react at the interface of another solid, or in the case of a liquid-solid reaction, react with the liquid molecule at solid interface where one can imagine that reaction occurs when the layers become mixed (Figure 1.8) [17].

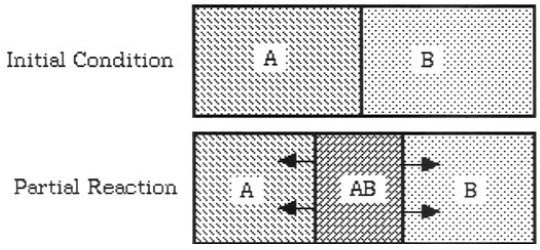

Figure 1.8 Diagram showing the reaction interface [17].

When two particles are involved in a reaction very close to each other, it undergoes SSRs with ease due to the transportation or interchange of cations and/or anions to form a new compound. Therefore, the degree of the dispersion and mixing of one reacting solid with another is driving force for the overall mechanism of SSRs [17].

There are several conditions under which a SSR takes place. Furnace techniques are used high temperatures to encourage reactions without solvents. In a melting technique, the reactants are mixed and melted together. The melted reactants interact in the liquid state and become a paste, which then hardens into a solid. Gas reactions are also observed in SSRs in presence of highly reactive gases. Therefore, scientists expose the reaction mixture to a stream of reactive gas.

Solids usually do not react together at room temperature over normal time scales and it is necessary to heat them to much higher temperatures, often to 2000 °C [18]. Such high temperatures are to induce diffusion of the reactants, but this depends strongly on the system studied. Some SSRs already proceed at temperatures as low as 100 °C.

Many solids react easily with reactive gases like chlorine, iodine, oxygen etc. Such reactions are often carried out in a tube furnace that is open ended on both sides and through which the gas is passed at which it reaches to high temperatures often to 2000 °C [18].

The factors on which the feasibility and rate of a SSR include, reaction conditions, structural properties of the reactants, surface area of the solids, their reactivity and the thermodynamic free energy change associated with the reaction [16].

1.4. Flux Agents and Usage

Usage of any kind of additives as a fluxing agent in the BN synthesis has some applications that resulted in positive effect on the formation of different polymorph of BN [1, 19, 20, 21]. General definition of flux is done as a chemical compound, which melts lower than the SSR temperature, which means it dissolves one or more of the components and allows materials transport to reaction rank, without entering into the SSR. Preferably, the end product should be insoluble in the flux or flux itself, should be removed at cleaning stage [17].

Flux can be used as cleaning agent, flowing agent, or purifying agent in chemical reactions. Some of the widely preferred fluxes are carbonate of soda, potash, charcoal, coke, borax, lime, lead sulfide and certain minerals containing phosphorus [3]. These agents have various functions at high temperature processes such as reducing agent and absorption of impurities. In the process of smelting, fluxes render a slag more liquid at the smelting temperature [4]. Molten flux also serves as a heat transfer medium, facilitating interaction at the interface of solids [5].

In addition, fluxing agents are used to control grain size of crystalline solids as a common practice in time-temperature conditions during sintering [6].

The dissolution of solids in molten phase is the miscibility in solvents as melts of borates, fluorides, or even metals when solvent is selected as a flux, which is possible to bring down the melting temperature of the solute or mixture [22, 23]. Performing SSRs in the form of molten phase (mostly dependent to dissolution) at high-temperature solvents by fluxes (e.g., Bi, Sn, halide salts, or alkali metals) is a method that has served to increase the diffusion and reactivity of solids in the molten phase [23, 24]. It should be emphasized that the treatment of the surface with flux is one of the most powerful methods of controlling the rate of SSR that increase diffusion rates in these reactions [25].

In SSRs, the phases formed at the reactant surfaces by diffusion of thermally activated atoms through the interfaces and this mass transport needs high temperatures and high energy consumption in order to complete the reaction and formation of the compound [3, 6]. This is directly related to the surface contact between grains of each solid and slow solid state diffusion often results in long reaction times.

Flux agents are generally expressed as catalyst in solid state synthesis of hBN [19, 20, 21, 26], however, their wetting, smelting, and reducing properties are ignored. The high crystalline BN produced when mixed proper fluxes, which increase the longevity of the molten phase in which the BN product grows. In this method, by-product or fluxing agent itself, form a low melting flux, which would allow the BN crystallites to remain in a molten salt medium for a longer period of time, enabling increased crystallization [24].

1.5. Characterization of Hexagonal Boron Nitride

1.5.1. FT-IR Spectroscopy

Infrared spectroscopy (IR) is used to characterize BN products which gives information on the vibrational and rotational modes of motion of a polyatomic systems and hence an important technique for identification and characterization of a substance.

In the literature, IR spectra of polymorph of BN (cubic and hexagonal) were throughly discussed the other forms were not detailed. Whether a BN sample is hexagonal or cubic can be determined by FTIR spectroscopy. Because of the strong covalent bonding of cBN is expected to have high frequency lattice vibration but the bonding in the flat sp^2 6-ring of hBN is stronger than in the cBN (Figure 1.9), as indicated by the higher frequency BN vibrations exhibited by hBN υ_{LO} =1610 cm^{-1} -IR inactive- and υ_{LO} = 1370 cm^{-1} -IR active- on the other hand, frequency B–N vibrations exhibited by cBN are υ_{LO} = 1304 cm^{-1} -IR inactive- and υ_{LO} = 1054 cm^{-1} -IR active [1].

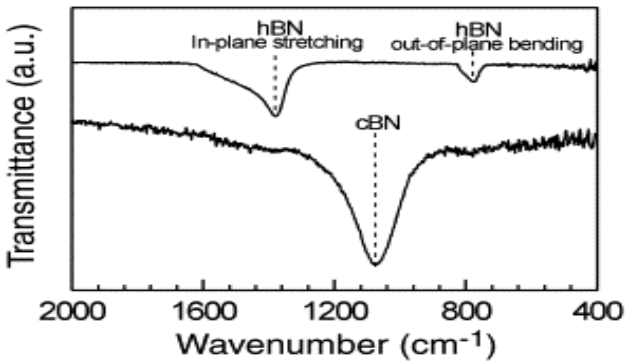

Figure 1.9 IR spectra samples of hBN and cBN [27].

1.5.2. X-Ray Powder Diffraction (XRD)

Powder BN samples are generally analyzed by x-ray powder diffraction (XRD) to determine grain size, crystallinity, graphitization index, and the lattice parameters. It is an analytical technique used for phase identification of a crystalline material and can provide information on unit cell dimensions. The analyzed material is finely ground, homogenized, and average bulk composition is determined.

X-ray diffraction is based on constructive interference of monochromatic X-rays and a crystalline sample at which X-rays are generated by a cathode ray tube. When conditions satisfy Bragg's Law ($n\lambda=2d \sin \theta$), the interaction of the incident rays with the sample produces constructive interference and a diffracted ray. By scanning the sample through a range of 2θ angles, all possible diffraction directions of the lattice should be attained due to the random orientation of the powdered material. Since each crystal has a set of unique d-spacings and conversion of the diffraction peaks to d-spacings allows identification of the matter. Typically, this is achieved by comparison of d-spacings with standard reference patterns.

Crystal forms of BN are characterized by X-ray diffraction method and layer types and the distance between the layers of boron nitride phases is found X-ray diffraction measurements [10]. The peaks observed at around $2\theta = 25°$ correspond to the distance (~333 pm) between the layers of the sp^2 networks as in the hexagonal form of BN. The peaks around $2\theta = 40\text{-}50°$ are derived from atoms in the sp^2 or sp^3-6-layer rings. The species having sp^3 hybridized layers gives peak $2\theta = 40\text{-}50°$ with ~210 pm layer distance (in cBN), while the sp^2 hybridized layers have $2\theta = 40\text{-}50°$ with ~145 pm. Turbostratic form of BN shows two broad diffraction peaks around $2\theta = 25°$ and 40-50° (Figure 1.10) [10].

The average grain sizes of BN are calculated according to the Debye-Scherrer and Williamson-Hall methods indicating the structure in three dimensional order [1, 28, 29]. However they are a useful method to study of many powder patterns of chemical compound which is synthesized under different conditions, might reveal trends in the crystallite size/strain that can be related to the properties of the product [1, 28, 29].

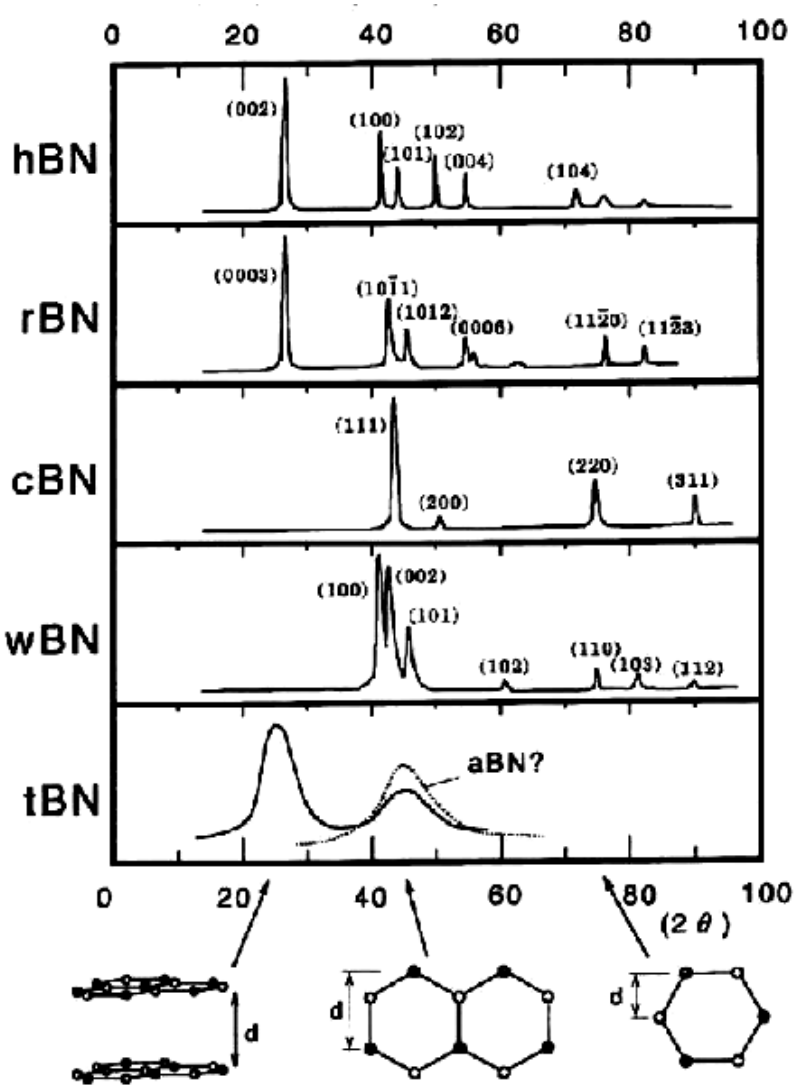

Figure 1.10 The X-ray diffraction spectra of hBN, rBN, tBN, cBN, and wBN [10].

The graphitization index enhances the explanation of ordered layer structure of BN and designates the similarities of graphite-like nature. The higher value of graphitization index was interpreted as less three-dimensional ordering in hBN and vice versa [28, 29]. The low value of graphitization index indicates higher crystalline (graphitic) and layered form of hBN.

Table 1.1. Some properties of BN morphologies determined by XRD

Crystallic Configuration	Turbostratic	Quasi-Turbostratic	Quasi-Graphitic	Graphitic
Graphitic Index	>100	50±25	10±5	3±1
Crystal Size (nm)	20-60	100-300	250-1500	500-3500
Mean Particles Size (micron)	3.0	3.5	8.0	10.0

1.5.3. Electron Microscopy

1.5.3.1. Scanning Electron Microscopy (SEM)

Scanning electron microscopy (SEM) is a type of method that is used to determine of morphology and crystalline nature of solids and visualize of BN in micro scale. To understand how SEM is able to view crystalline surface such a low units, the working principle of SEM must be considered. It uses a focused beam of high-energy electrons to generate a variety of signals at the surface of solid specimens. Then the signals provide information about the sample including external morphology, surface topography, and crystalline structure and orientation of materials that derive from electron-sample interactions. Finally, the electron beam is

generally scanned in a raster-scan pattern, and the beam's position is combined with the detected signal to produce an image [30].

In most applications, data are collected over a selected area of the surface of the sample, and two dimensional images are generated that displays spatial variations in these properties. Areas ranging from approximately 1 cm to 5 microns in width can be imaged in a scanning mode using conventional SEM techniques. The SEM is also capable of performing analyses of selected point locations on the sample; this approach is especially useful in qualitatively or semi-quantitatively determining chemical compositions (using energy dispersive spectroscopy, EDS), crystalline structure, and crystal orientations [30].

Boron nitride samples are crystalline compounds that they could be imaged with SEM (Figure 1.11)and morphology, topography, and crystalline structure in the range of 1 cm to 5 microns are determined in 2 dimensional visions [1, 20, 31].

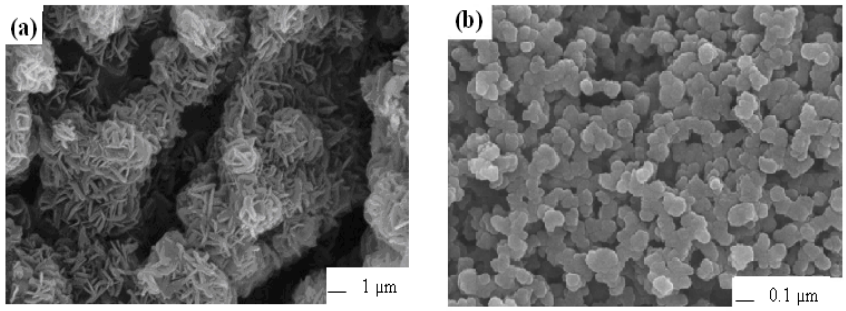

Figure 1.11 Samples of SEM images of BN [20, 31].

1.5.3.2. Transmission Electron Microscopy (TEM)

Solid compounds could be visualized by the transmission electron microscopy (TEM). If the solid is crystalline, the electrons are diffracted by atomic planes inside the material. Therefore it is possible to form a transmission electron

diffraction pattern from electrons that have passed through a thin specimen. When the accelerating potential is increased, higher energy electrons can penetrate distances of several microns into a solid or are diffracted from the regular array of atoms at the surface of a crystal. Then these transmitted electrons could be focused due to their wavelike character and influence of the electric and magnetic field to the negatively charged property. Thus, their very short wavelength would allow the specimen to be imaged with a spatial resolution. Most modern TEMs use an electron accelerating voltage between 100 kV and 300 kV and 0.2 nm resolutions, that, it is possible to image individual atomic planes or columns of atoms [30]. Therefore high magnifications have made the TEM a valuable tool in life sciences such as medical, biological and materials research.

BN samples are analyzed to imagine the nanoscale crystal structure and morphology and nature of compound in individual atomic planes or columns of atoms by TEM. Nanowire, nanotube and other nanostructured boron nitride could be determined with the planar and other frames with use of TEM [32].

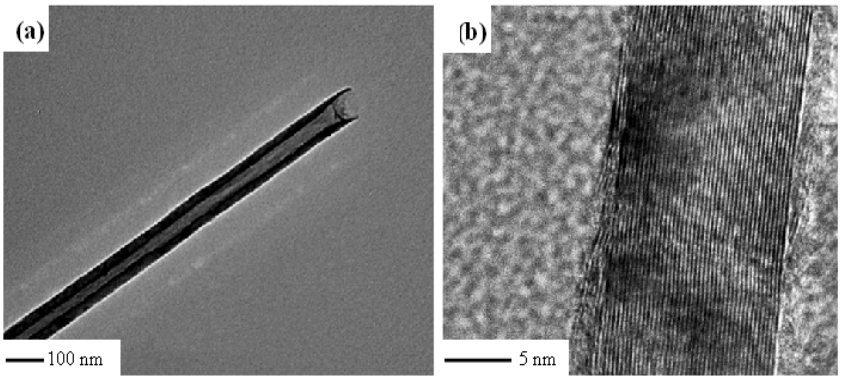

Figure 1.12 Sample TEM images of BN (a) nanotube (b) nanowire form of BN [32].

1.6. Scope of This Study

hBN is an important material for industry since it is used as solid surface lubricant at high temperatures for metal processes and aerospace applications as an insulator for electronics, reducer of wear and friction for ceramics and polymers, and shield for radioactive spread.

The objective of this thesis is to synthesize the hBN in the presence of fluxing agents at optimum temperatures and to characterize samples by FT-IR, XRD, SEM, and TEM.

The role of the additives on the formation of hBN and the identification of the effect of additives on the formed BN will be systematically determined. In general, objectives of this study are determined as follows:

To determine the effect of amount of fluxes,

To exhibit the influence of additives in the form of anion or cation component,

To improve crystallinity of hBN,

To reduce the synthesis temperature of hBN,

To increase the grain size of hBN,

To compare grain sizes of hBN with different fluxes,

To analyze and determine morphology of hBN samples in nanoscale.

CHAPTER 2

2. LITERATURE SURVEY

2.1. Literature Survey on Boron Nitride

Boron nitride is a synthetic compound that had been investigated in details in the last decades but the first synthesis method from binary compounds was suggested by Balmain [33] in 1842. Afterwards the nitridation of boron was achieved at a range of 500-950 °C when heated in a stream of ammonia due to the analogy structural form of BN to carbon [13]. Hubacek et al., was also determined the positive effect of ammonia gas as decreasing oxide content of the samples in 1988. They had used the chlorinated compounds together with ammonia gas in order to remove oxygen due to the reduction property of the chlorine [34].

Later, reaction mechanism was proposed for formation and growth of hBN from oxidic boron compounds in 1992 and the perfect crystalline BN (larger than 50 nm size and lower than interlayer spacing 0.335 nm) was obtained when the working temperature was not lower than 1500 °C besides low hydroxyl end groups [35]. In 1993, addition of B_2O_3 was found to be effective on the crystallization of amorphous BN and increased crystallinity of BN at high temperature (1350–1450 °C) by Choi et al. The amorphous BN with B_2O_3 were crystallized and transformed to cBN with catalyst [36]. In 1996, chemical reactions of hBN synthesis and their mechanisms

are discussed by Hubacek and Ueki. They were suggested a ternary B–N–O diagram for virtual compositions of hBN ceramic and preceding materials. Decomposition and crystallization of BN powder were characterized during sintering and hydrolysis of ceramic in the synthesis. The polymerization was assigned as a controlling chemical process due to the dynamic model they had applied to the covalent characterized systems, [11]. Recently, Kubota et al. reported the production high quality hBN crystals at a elevated temperatures such as 2100 °C by using a nickel–molybdenum solvent [37].

2.2. Literature Survey on Flux Agents and Boron Nitride

In solid state reactions, formations of crystals are directly related to the surface contact between grains of each solid, and slow solid state diffusion. Performing SSRs in the form of molten phase (mostly dependent to dissolution) at high-temperature solvents (fluxes) is a method at which has served to increase the diffusion and reactivity of solids in the molten phase [24]. In this method, fluxing agent forms a low melting mixture which would allow the solid crystallites to remain in a molten salt medium for a longer period of time, enabling increased crystallization [24].

In 2004, hBN were synthesized by the modified O'Connor method in the presence of various metal nitrates and the crystallization degree and grain growth of hBN can be improved by intercalation with various transition metals at a relatively lower temperature (1320 K) by Budak and Bozkurt. They suggested that interlayer spacing was affected due to the electronic interaction between hBN and valence orbital of metal and the reduction reaction between the metal and h-BN overcomes

the internal stress [38]. Another study that used modified O'Connor method, representative metals exhibited a positive effect on the crystallization of hBN due to the d-π interaction and they caused the formation of nano-scale products at a relatively low temperature [1].

In carbothermal synthesis of hBN additives had used and had found positive effects. For instance; metal carbonates prevented the formation of boron suboxide at low temperatures and of boron carbide at high temperatures. Therefore the ordering of the structure and growth of the boron nitride grains in the presence of metal carbonates were not explained not only by its catalytic effect but also role of a catalyst-solvent effect [39].

In a study, Na_2CO_3 was used as catalyst to improve the crystallite thickness, particle size, and the yield of hBN, and utilization of Na_2CO_3 and NH_3 together was found to have a significant contribution to these parameters. hBN powder with high yield and relatively large particle size was obtained at low temperature and sodium carbonate addition was explained by formation of a sodium borate melt from which hBN crystallized via the reaction of borate and nitrogen ions in the melt. [19].

Effect of $CaCO_3$ on the carbothermic formation of hBN was investigated by adding $CaCO_3$ to the activated carbon-boric oxide mixture. The yield and grain size of hBN were found higher and specific surface area was determined lower than the products obtained from plain mixtures. The mechanism was suggested as calcium borate liquid formation by $CaCO_3$, resulting the dissolution of N_2 (g) as N^{3-} or N^{-} depending on the basicity of the calcium borate phase and dissolved nitrogen reacted with $(BO_3)^{3-}$ in basic melts or more complex anions like $(B_2O_5)^{4-}$ in acidic melts [20].

Catalytic effect of alkaline earth oxides, (MgO, CaO and BaO in the form of carbonates), was investigated on the formation of hBN by the reaction of boron oxide and carbon under nitrogen atmosphere in 2008. Addition of alkaline earth oxides into B_2O_3–C mixtures was found to have noticeable raise in the amount and particle size of hBN [21].

Alkoy and friends obtained tBN powders by nitridation of boron oxide (B_2O_3) with an inert filler material ($Ca_3(PO_4)_2$) under the flow of ammonia (NH_3) gas at 900 °C. Calcium phosphate $Ca_3(PO_4)_2$ with a high specific surface area was used as an inert filler material to provide sufficient reaction surface to the boric oxide, which is a viscous fluid at the reaction temperatures [26].

In the presence of Li_2CO_3 the degree of boron nitriding was found higher than ordinary synthesis of BN. In addition, formation of the BN was supported by the processes of desorption of impurities on the surface of boron and soot by the molten lithium carbonate in the carbothermal synthesis and also by loosening of the charge during dissociation of this compound [39].

In the literature, the effect of the metal acetates has not been discussed until now; however former study of our group was to search effect of metal carbonyls on the synthesis of hBN. In this study the metal carbonyls had no significant effect on interlayer spacing at different temperatures, nevertheless, the grain size and yield increased with metal carbonyls [40].

Different forms of BN phases were determined in the presence of LiOH via the carbothermic method in literature [41]. Higher yield of BN and hexagonal and rhombohedral forms of BN was ensured with the LiOH additions. The role of lithium explained that it intensifies the reaction by entering into the lattice of BN layers. [42].

2.3. Literature Survey on Nanocrystalline Boron Nitride

Production and usage of nanoscale compounds has been spread over broad application area. BN nano materials which are mainly obtained from the hBN are an advantageous material for high temperature processes surpassing the carbon nano structures. Moreover, nanocrystalline BN has aroused continuous and increasing research interest during the past decades owing to the special chemical and physical properties. After the tight-binding calculations which had proposed the formation of nanotubes from hBN and due to the similarities derived from the electronic structure of carbon nanotubes, studies had started to focus on BN nano structures since 1995 [43].

The first traces of the BN nano structures were reported in the form of mullti-walled tubes by a carbon-free plasma discharge method between a BN-packed tungsten rod and a cooled copper electrode [43]. However, pure BN nanotubes had been synthesized with HfB_2 electrodes in a nitrogen atmosphere by arc discharge and this route leaded to the formation of highly crystalline tubes with reduced numbers of layers such as one or two layers of tubes [44].

In general, various techniques including plasma-arc, laser ablation, and chemical vapor-phase synthesis have been employed to produce bulk amounts of nanocrystalline BNs. For instance, a high-yield plasma-arc method was used to production of macroscopic amounts of pure BN nanotubes and double-walled nanotubes maintained by this method. In this type of route, BN-coated crystalline nanoparticles were formed, whose cores can be preferentially etched leaving behind hollow BNs [45].

In a study, BN nanotubes had been produced by thermal annealing method at 1000°C with the previously ball milled elemental boron powders in ammonia gas for a long period at room temperature. A metastable material was formed consisting of disordered BN and nanocrystalline boron which was then increased from those metastable and chemically activated structures during heat treatment in the presence of nitrogen gas [46]. Later, ball-milling and annealing method were improved by production of nanosized boron particle via ball-milling and ultrasonicated in ethanol in order to break up large aggregates resulting the multi-walled cylindrical and bamboo nanotubes as well as nanowires. In addition, effect of different reaction gases, annealing temperatures, and different catalysts (Fe, Co, and stainless steel) were discussed and different kinds of nano structures persisted in the different nature with high-yield and high-density [47]. Moreover, a purification process was investigated for BN nanostructures which were prepared by using a ball milling and annealing method and it was found that dispersion, selective chemical leaching with HCl, partial thermal oxidization and hot water washing treatments showed up production of high purity BN nanotubes that was feasible for other synthesis methods [48].

BN nanotubes of diameter 6.6 nm and length 50–100 nm and fullerenes of size 0.7 nm were synthesized by the arc-melting method mixing a powder mixture of boron and iron oxide in a nitrogen gas. The stability of their atomic structure and the electronic state were estimated by theoretical calculations. [49]. Moreover, BN nanotubes with different structures were produced by reacting boric acid with ammonia gas in the presence of a mixture of activated carbon and Fe particles. The purified BN nanotubes were devised in high yields by heating boric acid with multi-walled carbon nanotubes in the 1000–1300 °C range [50].

NH_4Cl and $NH_4Cl–NaN_3$ was mixed with MgB_2 for production of nanocrystalline BN with needle-like and hollow spherical morphology. It was found that amount of NaN_3, heat and high pressure had a significant effect on the size of the hollow spheres [51].

In this study, formation of BN nano structures was not expected and principally it was suggested as to synthesize highly crystalline hBN at a lower temperature. However the nano forms of BN was also persisted in the samples with other crystalline polymorphs.

CHAPTER 3

3. EXPERIMENTAL and INSTRUMENTAL PROCESSES

3.1. Materials

Boron oxide (Fluka, 97%), urea (Fluka, 99%), lithium carbonate (Merck, 98.5%), lithium acetate (Alfa Aesar, 63%), lithium hydroxide (Merck, 56%), sodium carbonate (Merck, 99.9%), sodium acetate (Merck, 99%), sodium hydroxide (Merck, 97%), potassium carbonate (Merck, 99%), potassium acetate (Merck, 99%), potassium hydroxide (Carlo Erba, 85%), magnesium hydroxy carbonate(Merck), magnesium acetate (Merck, 99.5%), magnesium hydroxide (Fluka, 99%), calcium carbonate (Surechem, 98%), calcium acetate (Merck, 95%), calcium hydroxide (Riedel-de Haen, 95%), Potassium bromide (Merck, for FT-IR), ammonia (Linde Co. 99.9%) ethanol (Spanivskiy, 96%), and hydrochloric acid (Merck, 37%) obtained commercially were used without any purification.

3.2. Synthesis of hBN Samples

The modified O'Connor method [13] was applied to synthesize hBN in the presence of flux agents (Table 3.1). The mixture prepared by 1 g of boron oxide and 2 g of urea was homogenized in ball-mill grinder, and then mixed with different

amounts of fluxes (1, 10, 20, 30, and 40 %) to determine the optimum percent ratio of the flux (metal carbonates, acetates, and hydroxides) in the mixture. Then, mixture was then pre-heated to 200°C for 2 hours in the furnace and a precursor was obtained. Finally, the obtained precursor was pulverized in mortar and heated in tube furnace under ammonia atmosphere (120 mL/min) at different temperatures starting from 1450 °C to the lower temperatures at which the hexagonal form of BN transformed to turbostratic form. Unreacted boric oxide and inert filler material were removed from the reaction products with an acidic leaching in ~1 M HCl solution and in ethanol. Purification was completed when samples were dried in an oven at 100°C.

Table 3.1. Flux agents (Used as additive into boron oxide and urea mixture)

Metal Carbonates	Metal Acetates	Metal Hydroxides
Li_2CO_3, Na_2CO_3, K_2CO_3, $Mg(OH)CO_3$, $CaCO_3$.	$Li(CH_3COO)$, $Na(CH_3COO)$, $K(CH_3COO)$, $Mg(CH_3COO)_2$, $Ca(CH_3COO)_2$.	LiOH, NaOH, KOH, $Mg(OH)_2$, $Ca(OH)_2$.

3.3. Preparation of BN Samples

3.3.1. Ball-Mill Grinder

A mixture of boron oxide and urea were ground in a ball mill rotated on a roll mixer (Pascall Engineering, 1600-VS-A roll mixer) at medium speed for 4 hours to obtain homogenous mixture. The resultant powder was sieved and 125 μm mixture particles were collected.

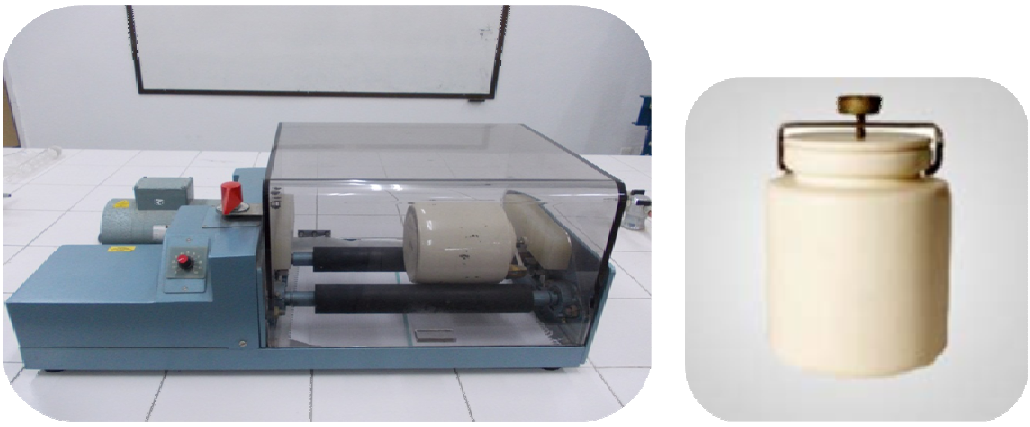

Figure 3.1 Pascall Engineering, 1600-VS-A roll mixer and alumina jar.

Figure 3.2 Sieve.

3.3.2. Camara Furnace

The precursor preparation was performed with Proterm PLF 140/5 (average heating speed: 10°C/min) camara furnace at 200 °C under open atmosphere for 2 hours and stayed in until the room temperature. The heating rate of samples until precursor stage is given figure 3.3.

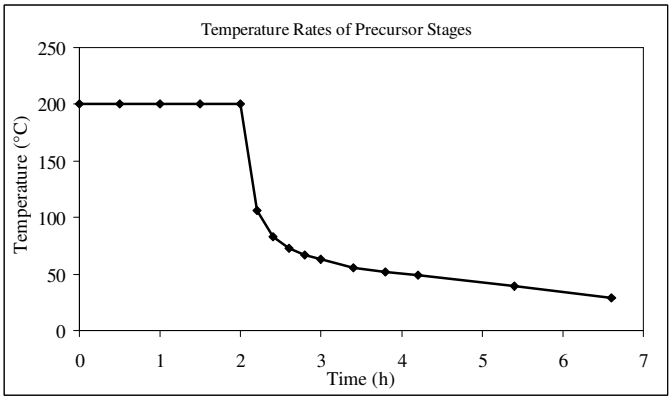

Figure 3.3 Temperature rates of experiments until precursor stage.

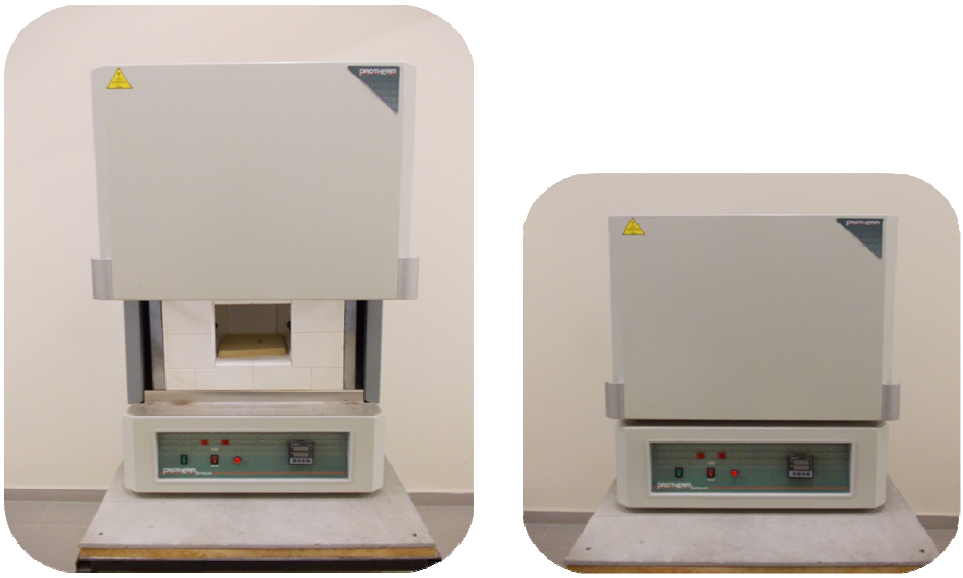

Figure 3.4 Proterm PLF 140/5 Camara Furnace.

3.3.3. Tube Furnace

Final heating process was carried out with Proterm PTF 15/75/450 tube furnace (average heating speed: 16°C/min) at different temperatures (1000 °C, 1150 °C, 1300 °C, and 1450°C) under ammonia atmosphere (ammonia flow rate adjusted as 120mL/min by using flow meter) under open atmosphere for 3 hours. The temperature rates of experiments are given in figure 3.5.

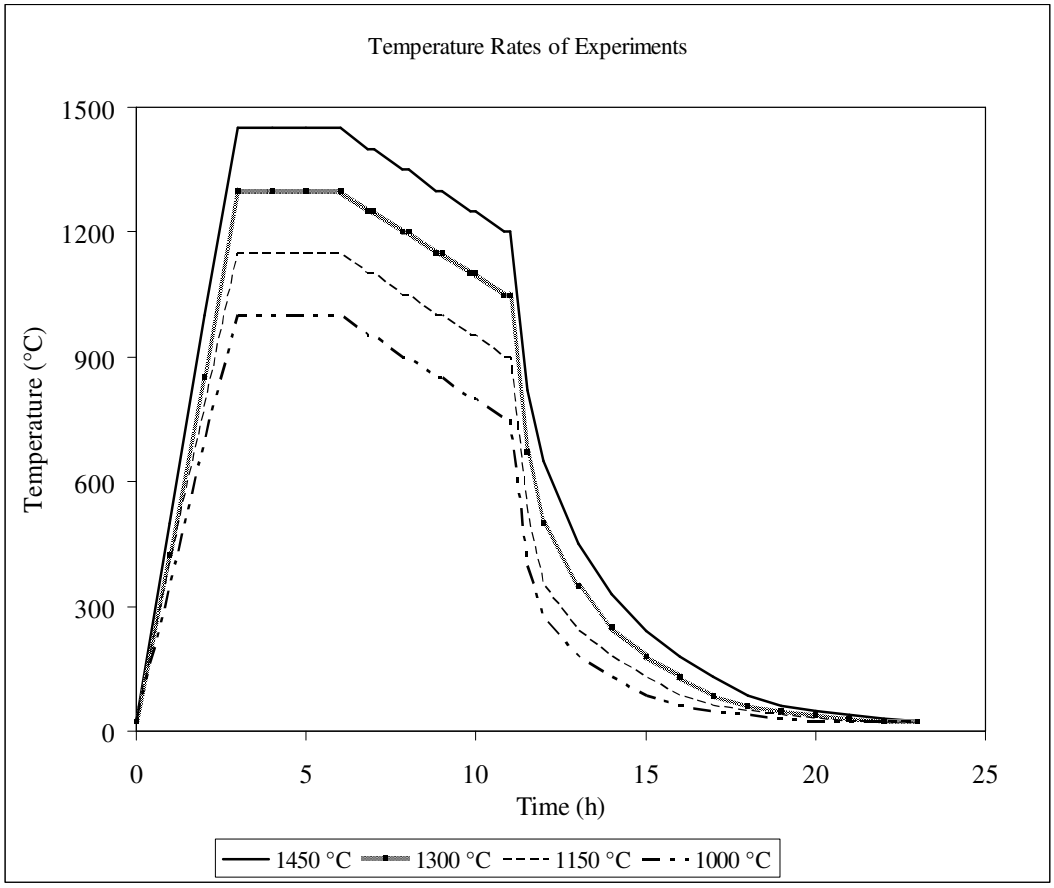

Figure 3.5 Temperature rates of experiments.

Figure 3.6 Proterm PTF 15/75/450 Tube Furnace.

3.4. Characterization of hBN Samples

3.4.1. FT-IR Spectroscopy

FT-IR spectra of samples in KBr pellets were recorded on a Shimadzu 8400S spectrometer in the range of 400 – 4000 cm^{-1}. All KBr pellets composed of 0.0004 g of sample and 0.0196 g of KBr were prepared in the same weight in order to obtain comparable FT-IR spectra.

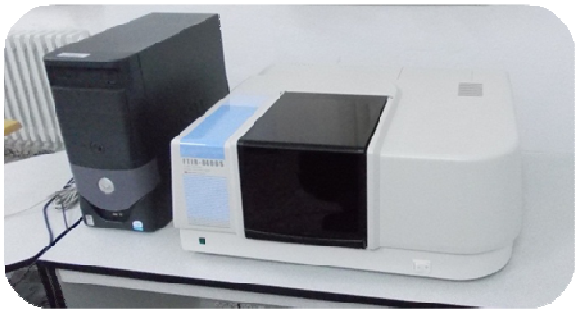

Figure 3.7 Shimadzu 8400S FT-IR spectrometer.

3.4.2. XRD Measurement

XRD characterization of hBN samples was performed with Rigaku DMAX 2000/PC and Rigaku Multiflex diffractometer using CuK_{α} radiation (40 kV/30 mA, Goniometer: MultiFlex + goniometer (with a shutter), Div Slit: ½ deg., Sct Slit: ½ deg., Rec Slit: 0.15 mm, Scan Speed: 5 deg / min., Attachment: Standard sample holder) between the 10º and 90º.

Figure 3.8 Rigaku Multiflex XRD.

3.4.3. SEM Analysis

The morphology of surface was studied by JEOL JST-6400 scanning electron microscope (SEM) and micrographs were taken by Zeiss Evo 50 after dispersion of powders on a carbon sticker and coating with gold.

Figure 3.9 Jeol JSM 6390LV SEM.

3.4.4. TEM Analysis

TEM images were obtained from the JEOL JEM 2100F HR-TEM over the range 100 nm and 5 nm. Samples were suspended in ethanol by ultrasonic bath and a drop of suspended solution put onto the copper-carbon Holey grid and then dried at room temperature at least for one day before the TEM analysis.

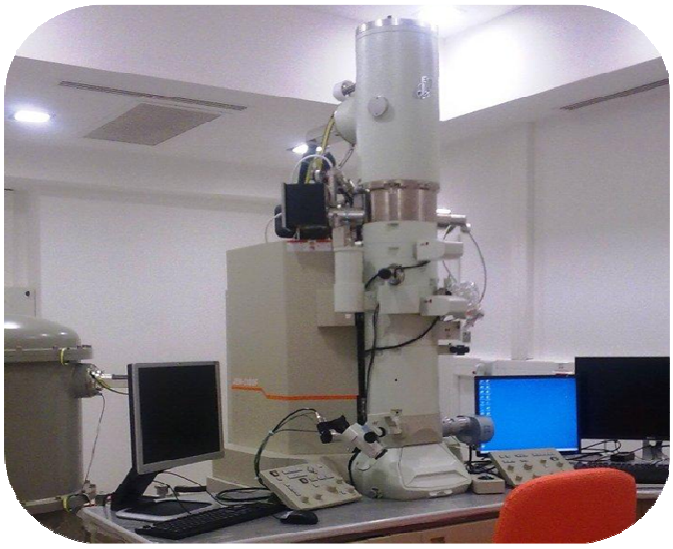

Figure 3.10 Jeol JEM 2100F HRTEM.

3.5. Sample Calculations

3.5.1. Calculation of Lattice Parameters

Lattice parameters of the samples were calculated by using following equation for hexagonal systems.

$$\frac{1}{d^2} = \frac{4}{3} x \left[\frac{h^2 + hk + k^2}{a^2} \right] + \frac{l^2}{c^2}$$

d: Interlayer spacing

h, k, l : Related Miller indices

a, c: Lattice parameters

Calculation of “a” parameter of hBN:

For 110 peak of hBN d is 1.2501 Å

$$\frac{1}{(1.2501)^2} = \frac{4}{3} x \left[\frac{1^2 + 1x1 + 1^2}{a^2} \right] + \frac{(0)^2}{c^2}$$

$$a = 2.5002$$

Calculation of “c” parameter of hBN:

For 002 peak of hBN d is 3.3290 Å

$$\frac{1}{(3.3290)^2} = \frac{4}{3} x \left[\frac{0^2 + 0x0 + 0^2}{a^2} \right] + \frac{2^2}{c^2}$$

$$c = 6.6580$$

3.5.2. Determination of Grain Size

The powder pattern includes information about the average size and strain within the crystallites composing a given powder, from the diffraction pattern. The information about crystallite size depends on the nature of the methods and is an average value for particle size and grain size analysis. These methods contain Debye-Scherer, Williamson-Hall, and Warren-Averbach, however most prevalent one is Debye-Scherer and nowadays others also come into prominence due to the most reasonable results.

3.5.2.1. Debye-Scherer Method

In this method, the XRD patterns are used for determination of average crystallite size or grain size in order to interpret the hBN products however this is not an absolute value for size identification.

Scherer equation relates the peak breadth of a specific phase of a material to the mean crystallite size of that material.

$$L = \frac{K \quad \lambda}{\beta \quad \cos \quad \theta}$$

where, β is difference of the width of the peak at half maximum intensity of a specific phase (h k l) in radians of reference material and sample.

K is a constant that varies with the method of taking the breadth (0.9)

λ is the wavelength of incident X-Rays (CuK_{α}=1.504 Å).

2θ is the center angle of the peak of sample

L is the crystallite size.

3.5.2.2. Williamson-Hall Method

This method is attributed to G.K.Williamson and his student, W.H.Hall relies on the principle that the approximate formula for size broadening, β_L, and strain broadening, β_e, vary quite differently with respect to Bragg angle, θ

$$\beta_L = \frac{K\lambda}{L \quad \cos\theta} \quad , \qquad \beta_e = \quad C_{\varepsilon} \quad \tan\theta$$

One contribution varies as 1/cosθ and the other as tanθ. If both contributions are present then their combined effect should be determined by convolution which is

assumed either a simple sum or sum of squares in the simplification of Williamson and Hall method. Then sum up the former of these formulas then one get:

$$\beta_{tot} = \beta_L + \beta_e = C_\varepsilon \tan\theta + \frac{K\lambda}{L\cos\theta}$$

If this equation is multiplied by cosθ it turns into:

$$\beta_{tot}\cos\theta = C_\varepsilon \sin\theta + \frac{K\lambda}{L}$$

and when it is pretended to the standard equation for a straight line (m = slope; c = intercept)

$$y = mx + c$$

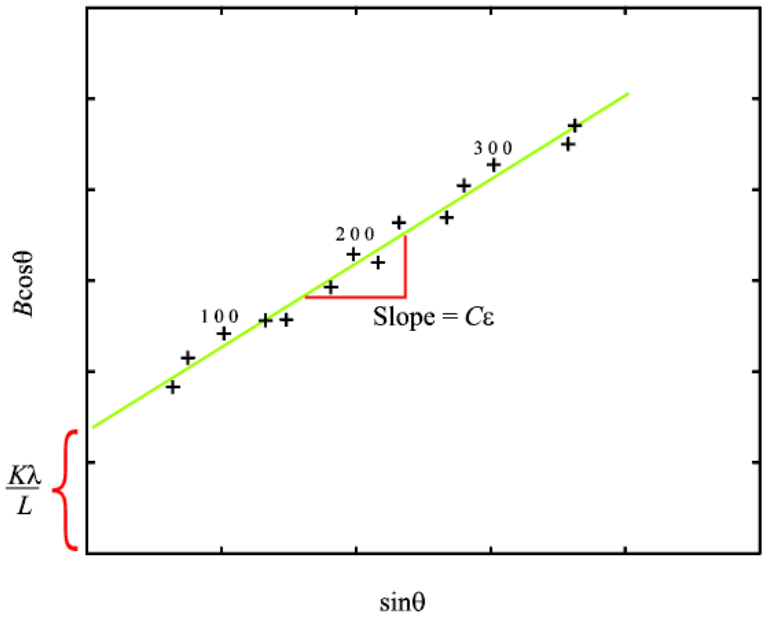

Figure 3.11 The schematically Williamson-Hall plot.

Then, it is possible to find the strain component of samples from the slope (C_ε) and the size component (Kλ/L) from the intercept by plotting $\beta_{tot}\cos\theta$ versus sinθ that is known as a Williamson-Hall plot given in figure 3.9 (this plot could alternatively be expressed in reciprocal space parameters, β* versus d*).

The Williamson-Hall method includes many assumptions such as its values are an average and should not be considered as absolute values. However it can be a useful method to study of many powder patterns of the same chemical compound which is synthesized under different conditions, might reveal trends in the crystallite size/strain that can be related to the properties of the product. This method was also used for determination of grain/crystalline strain/size of the hBN by using the XRD patterns in this study [52].

3.5.3. Calculation of Graphitization Index

The degree of crystallization of the hBN phase was evaluated in terms of the "graphitization index" (G.I.) as three dimensional order is the ratio of (102) plane into the (100) and (101) directions [28, 29], as

$$G.I = \frac{Area(100) \quad + \quad Area(101)}{Area(102)}$$

CHAPTER 4

4. RESULTS

In this study, experiments were performed with boric oxide and urea mixtures with additional fluxes; in order to investigate the formation of hBN by O'Connor method by nitridation of B_2O_3. Findings and results pertaining to the effect of additives amount on the solid state production of hBN will be presented. Finally, results related to the effects of various fluxes on this process will be given.

4.1. Effect of Representative Metal Carbonates on Synthesis of hBN

The fluxes that were used as additive in boron oxide and urea mixture had possible effects on the formation of hBN. Representative metal carbonates (Li_2CO_3, Na_2CO_3, K_2CO_3, $Mg(OH)CO_3$, and $CaCO_3$) were used in synthesis of hBN with different amounts at high temperatures such as 1450 °C.

4.1.1. FT-IR Spectroscopy of hBN Samples in the Presence of Metal Carbonates

First traces of hBN formation and first findings related to the structure of hBN are characterized by fourier transform infrared spectroscopy (FT-IR) [1, 38, 53, 54, 55]. In the FT-IR spectrum, the absorbtion frequencies in the range of 600-800

cm^{-1} belong to deformation vibrations of O–B–O in trigonal coordination of boron in the structure, at 900-1100 cm^{-1} to vibrations B–O in tetrahedral coordination of boron in the structure and at 1100-1400 cm^{-1} in trigonal one. The strong band at 1387 cm^{-1} is result of the in plane stretching vibration of hBN while the medium band at 801 cm^{-1} is derived from its out of plane bending vibration, [1, 56, 57]. The bands at around 2420-2620 cm^{-1} are ascribed to the vibrations of B–H, at 2800-3100 cm^{-1} to the valence vibrations of the bonds of C–H, at 3000-3500 cm^{-1} to the vibrations of N–H and 3200-3600 cm^{-1} to the vibrations of the O–H groups [1, 56, 57].

FT-IR spectra of the hBN samples provide us information of present phases in the existence of representative metal carbonates. The main absorbtion bands of hBN were determined at 810, 1370, 2520, and 3424 cm^{-1} denoting the out of plane B–N, in plane B–N, end group vibrations of B–H, and vibrations of O–H or N–H groups, respectively. –B–OH, and –N–H groups identified in the FT–IR spectra attributed to termination of the two-dimensional hBN macromolecules that they are the constitutional components [8, 58]. Moreover, the disappearance or weakening of the band at about 3400 cm^{-1} is the signal of decrease in the N–H and O–H groups indicates possibly increase in crytallinity.

The FT-IR spectra of the hBN synthesized in the presence of the metal carbonates had the approximately same absorption peaks of hBN as in given literature [1]. The in-plane and out-of-plane vibrations of hBN were determined in the whole samples. The peak observed at 3400 cm^{-1} is mainly derived from the O–H stretching vibration of the terminal O–H and also N–H groups, however, the peak weakened or disappeared by the increasing amount of metal carbonates indicating the lowering the number of end groups [1, 38]. It was clearly understood that as the amount of additives increased, the –N–H, –B–OH and –B–O stretching vibrations

decreased or were not observed. As it is given in figures 4.1, 4.2, 4.3, 4.4, and 4.5 there were not significant difference on the FT-IR spectra of when the metal carbonates were used as additives.

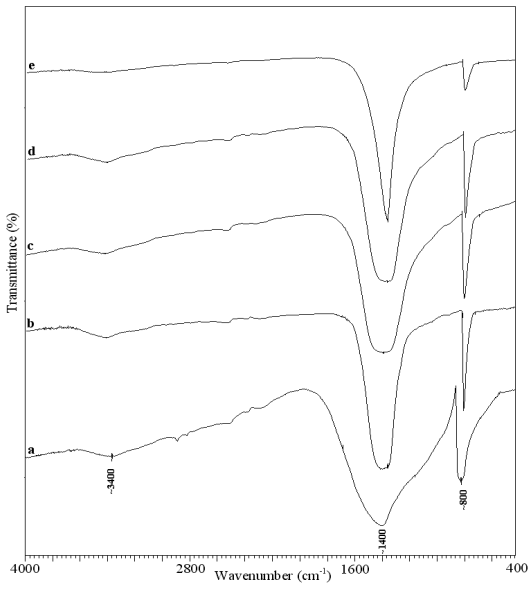

Figure 4.1 FT-IR spectra of the hBN samples with increasing amounts of Li_2CO_3 a) 1 % Li_2CO_3, b) 10 % Li_2CO_3, c) 20 % Li_2CO_3, d) 30 % Li_2CO_3, and e) 40 % Li_2CO_3.

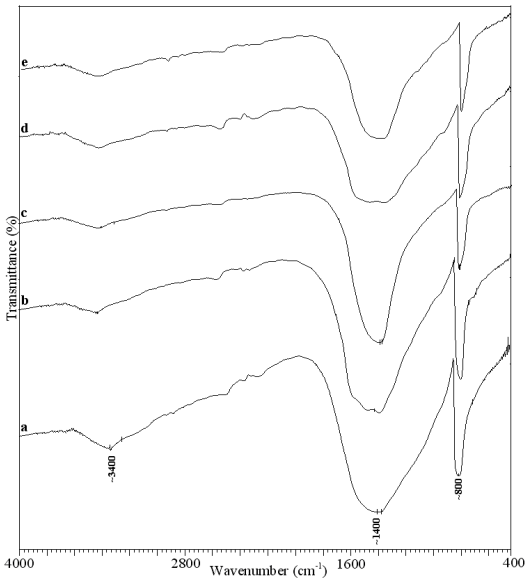

Figure 4.2 FT-IR spectra of the hBN samples with increasing amounts of Na_2CO_3, a) 1 % Na_2CO_3, b) 10 % Na_2CO_3, c) 20 % Na_2CO_3, d) 30 % Na_2CO_3, and e) 40 % Na_2CO_3.

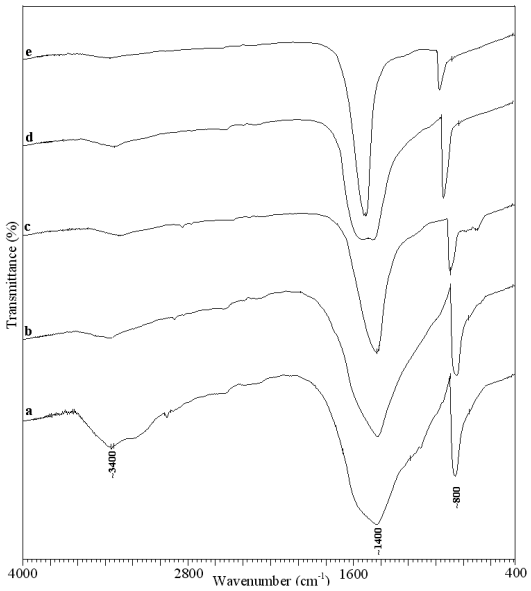

Figure 4.3 FT-IR spectra of the hBN samples with increasing amounts of K_2CO_3, a) 1 % K_2CO_3, b) 10 % K_2CO_3, c) 20 % K_2CO_3, d) 30 % K_2CO_3, and e) 40 % K_2CO_3.

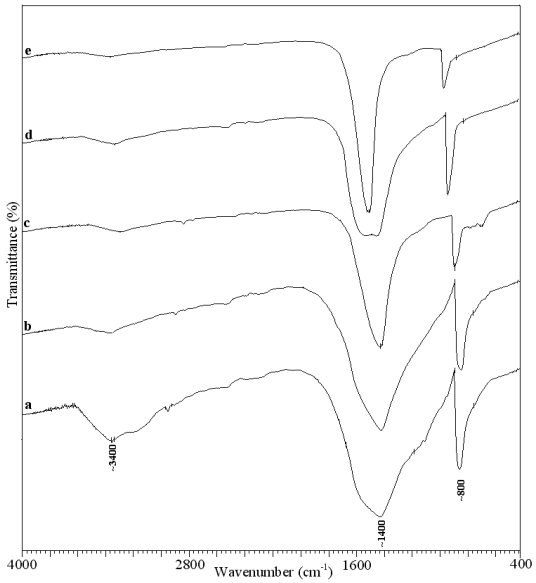

Figure 4.4 FT-IR spectra of the hBN samples with increasing amounts of $Mg(OH)CO_3$, a) 1 % $Mg(OH)CO_3$, b) 10 % $Mg(OH)CO_3$, c) 20 % $Mg(OH)CO_3$, d) 30 % $Mg(OH)CO_3$, and e) 40 % $Mg(OH)CO_3$.

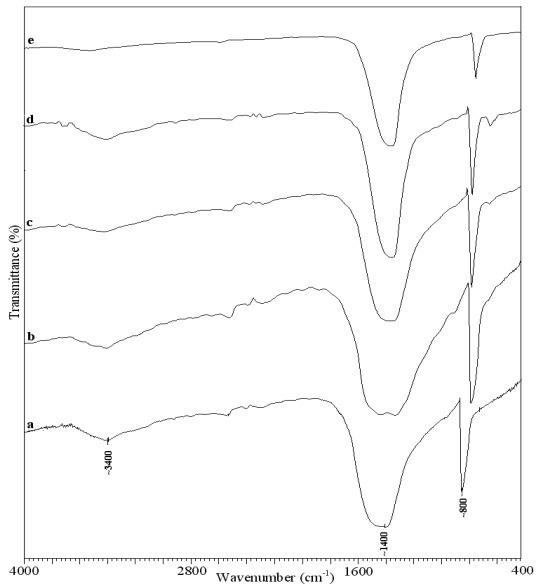

Figure 4.5 FT-IR spectra of the hBN samples with increasing amounts of $CaCO_3$, a) 1 % $CaCO_3$, b) 10 % $CaCO_3$, c) 20 % $CaCO_3$, d) 30 % $CaCO_3$, and e) 40 % $CaCO_3$.

4.1.2. XRD Analysis of hBN Samples in the Presence of Metal Carbonates

XRD analysis was applied for crystal structure examination of the hBN such as composition and crystallinity in the presence of the metal carbonates and the results were compared to original XRD pattern of standard hBN (ICDD card no: 34 - 421). The main peaks (002, 100, 101, 102, 004, 110, and 112) of original hBN is given in difractogram (Figure 4.6) however, 002, 10X, 004, 110, and 112 peaks essentially persisted in all diffractograms even the usage of small flux additions. The lattice parameters of hBN samples were calculated from the XRD patterns and were compared with literature values (a= 2.504 Å, c= 6.656 Å, d= 3.328 Å).

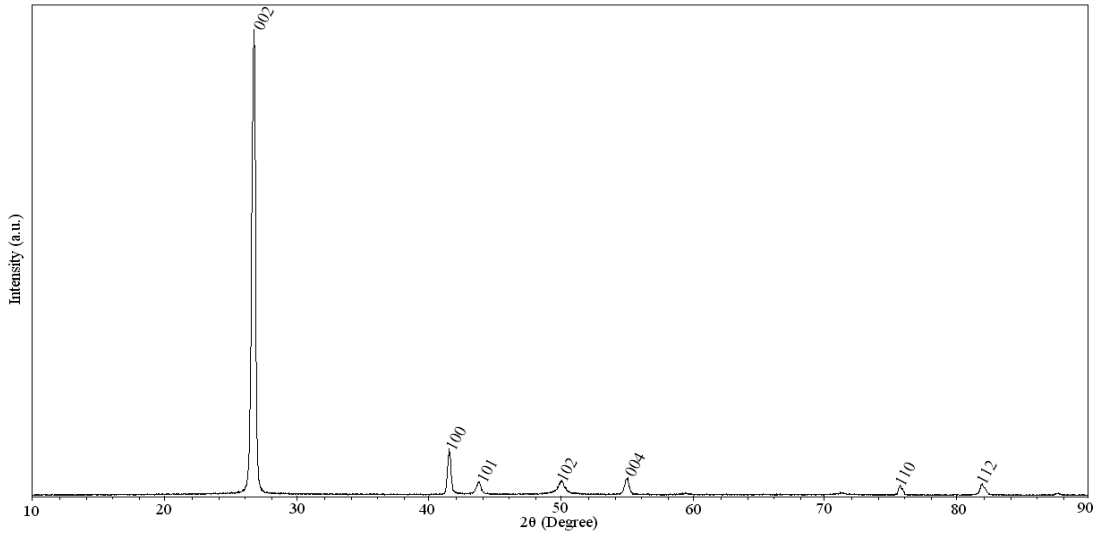

Figure 4.6 The XRD diffractogram of commercial hBN

Some of the XRD diffractograms of hBN in this study included the peaks at 100 and 101 together appearing as one peak (in Na_2CO_3, K_2CO_3 diffractograms). Moreover, 002 and other main peaks sharpened when the amount of additives was high. In some of our samples (as containing Li_2CO_3, $Mg(OH)CO_3$, $CaCO_3$), the 100 and 101 peaks were completely separated and they were nearly same peaks as in

original hBN (Figure 4.7). In addition, the appearance of the peak at 102 indicated the high crystalline hBN compounds with high amounts of additives. The amount of the metal carbonates had significant importance in the crystallite and average grain size determined according to Debye-Scherrer and Williamson-Hall method and the lattice parameters (Table 4.1).

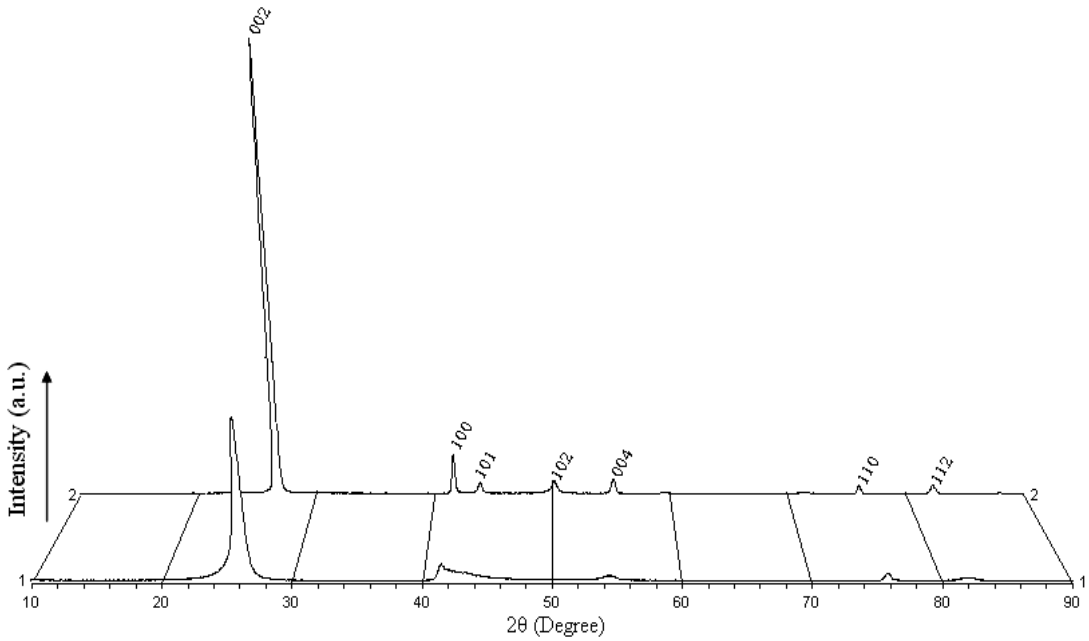

Figure 4.7 Comparison of XRD patterns of plain hBNs (1) prepared according to O'Connor method and pure (commercial) hBNs (2).

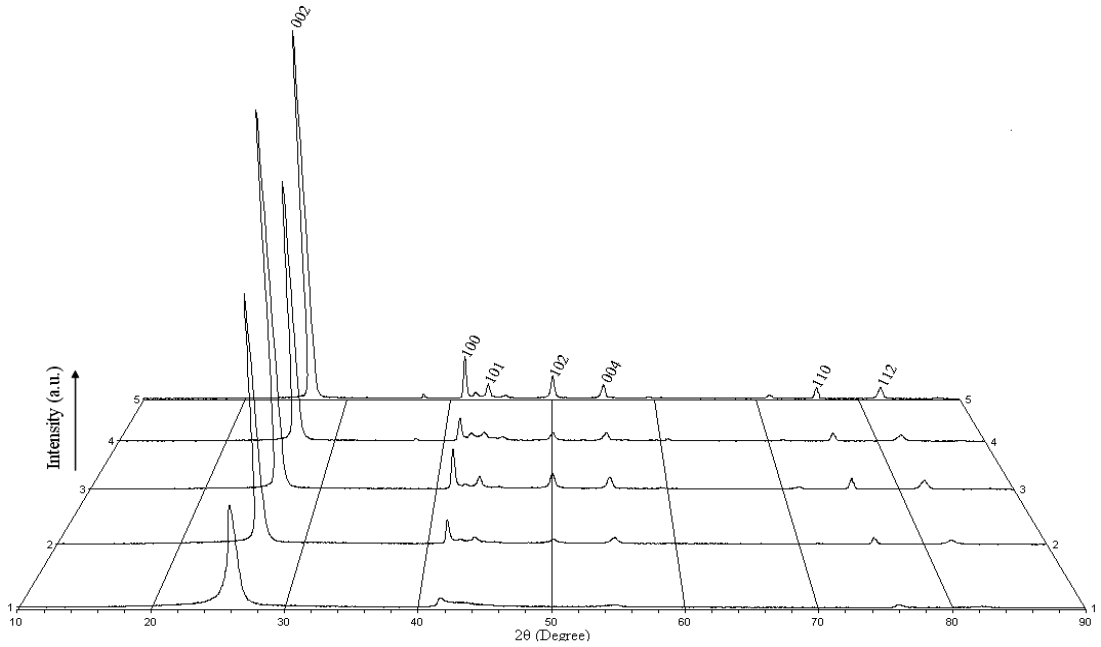

Figure 4.8 XRD patterns of the hBN in the presence of Li_2CO_3 where, 1) 1 %, 2) 10 %, 3) 20 %, 4) 30 %, and 5) 40 % Li_2CO_3.

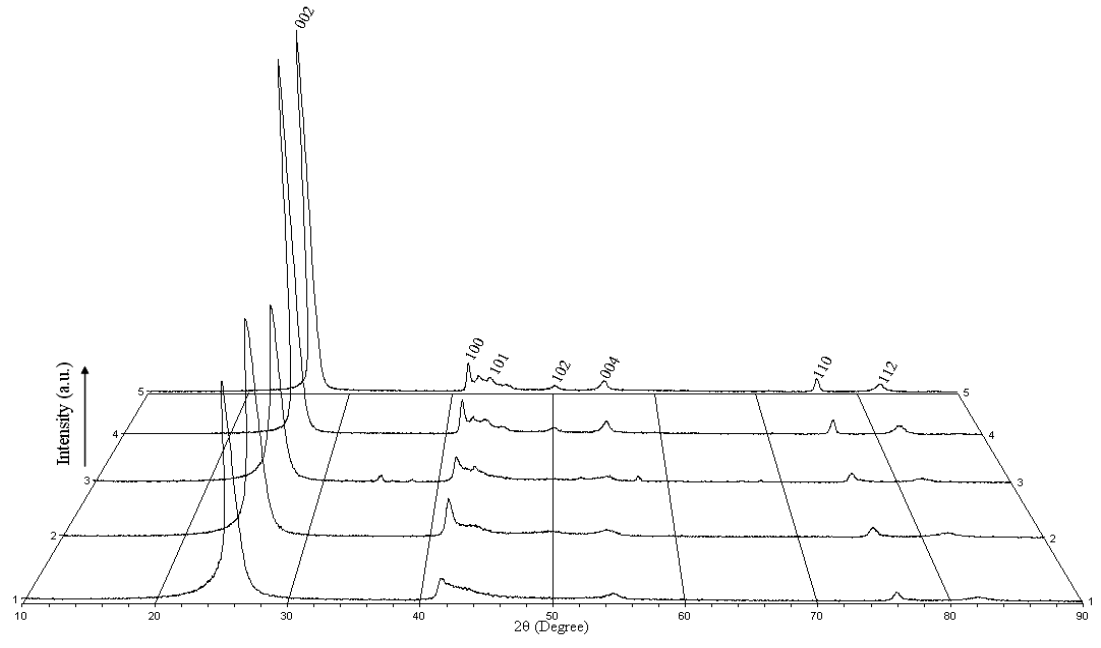

Figure 4.9 XRD patterns of the hBN in the presence of Na_2CO_3 where, 1) 1 %, 2) 10 %, 3) 20 %, 4) 30 %, and 5) 40 % Na_2CO_3.

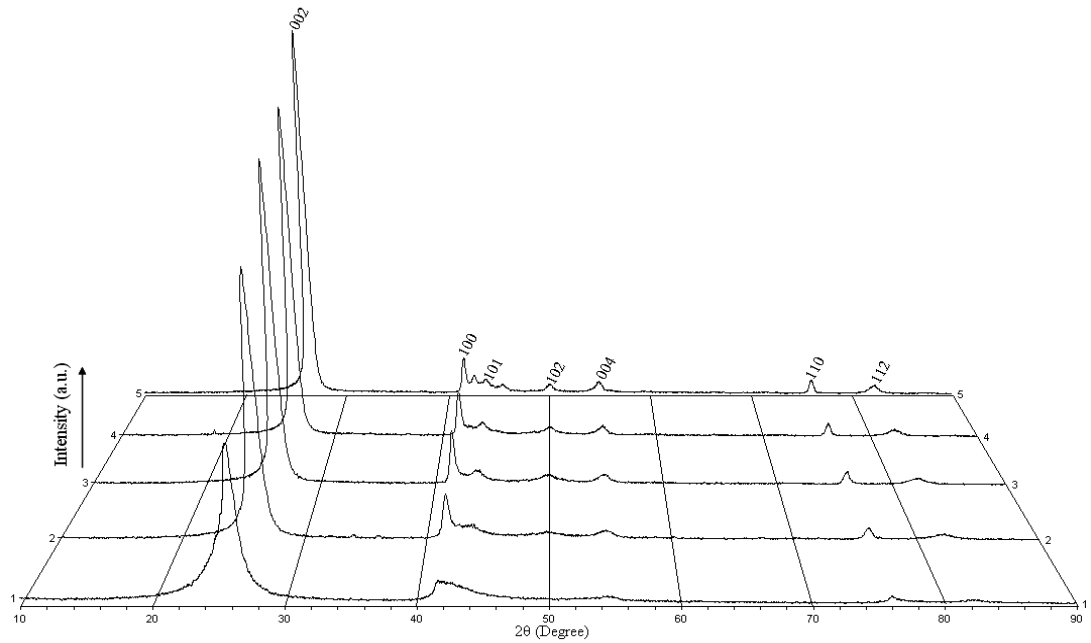

Figure 4.10 XRD patterns of the hBN in the presence of K_2CO_3 where, 1) 1 %, 2) 10 %, 3) 20 %, 4) 30 %, and 5) 40 % K_2CO_3.

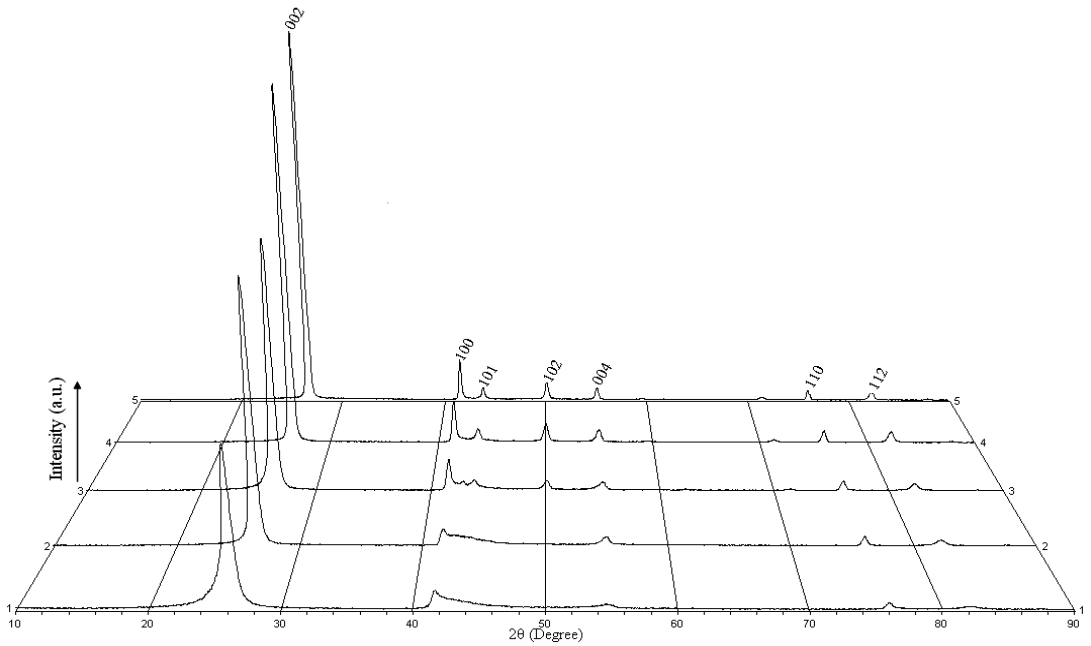

Figure 4.11 XRD patterns of the hBN in the presence of $Mg(OH)CO_3$ where, 1) 1 %, 2) 10 %, 3) 20 %, 4) 30 %, and 5) 40 % $Mg(OH)CO_3$.

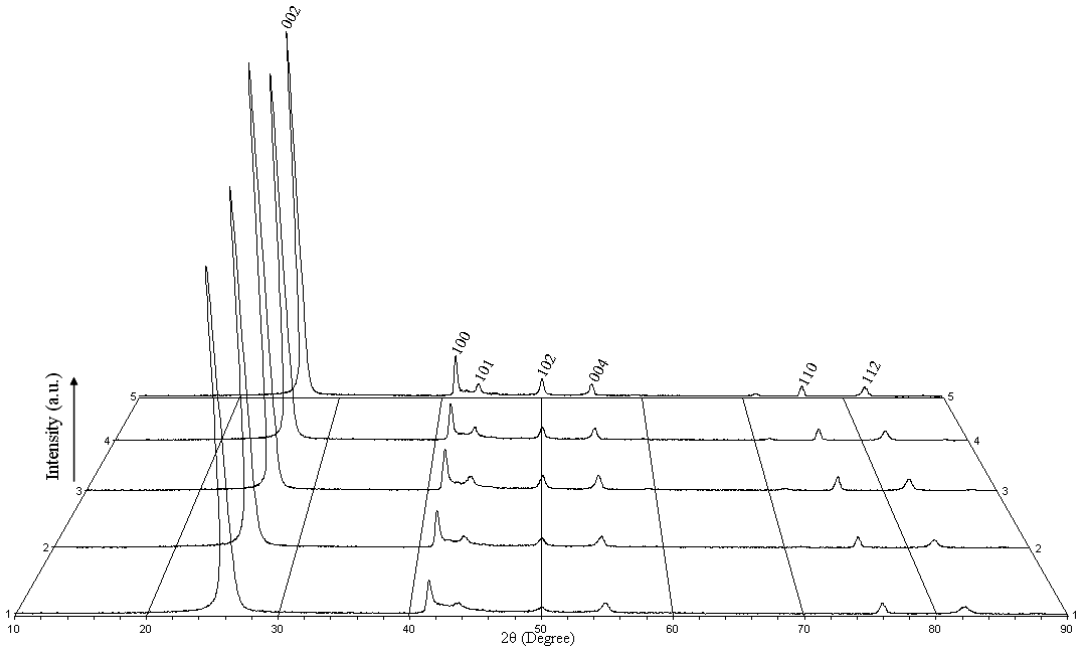

Figure 4.12 XRD patterns of the hBN in the presence of $CaCO_3$ where, 1) 1 %, 2) 10 %, 3) 20 %, 4) 30 %, and 5) 40 % $CaCO_3$.

Grain size of hBN is calculated from the XRD pattern by using the peak at 002 for Debye-Scherrer and all seven peaks for Williamson-Hall method [52] (Figure 4.13 and 4.14). According to the both methods, the grain sizes of hBN were found that there was an increase in the grain size with the increasing amount of metal carbonates in this study. In addition, the slope of line in Williamson-Hall method indicated that strain broadening was accepted as very small [59] resulting very sharp (narrower) 002 peak indicating high crystallinity. When Ca, Li, and Mg carbonates were used in the synthesis, the significant rise in the grain size of hBN was observed (Figure 4.14).

Table 4.1. Lattice Parameters, Average Grain Size, Microstrain and Graphitization Index of Metal Carbonates

	Lattice Parameters (Å)			**Average Grain Size (nm)**			
Flux Agents	**a**	**c**	**d**	**Debye-Scherer Method**	**Williamson-Hall Method**	**M* (%)**	**G****
1 % Li_2CO_3	2.502	6.724	3.362	12.0	N.A	N.A	N.D.
10 % Li_2CO_3	2.504	6.674	3.337	37.5	14.34	-0.048	3.10
20 % Li_2CO_3	2.506	6.682	3.341	37.7	44.02	0.079	2.10
30 % Li_2CO_3	2.504	6.680	3.340	30.0	44.23	0.086	2.84
40 % Li_2CO_3	2.504	6.674	3.337	43.0	44.41	0.014	1.91
1 % Na_2CO_3	2.504	6.752	3.376	11.2	N.A	N.A	N.D.
10 % Na_2CO_3	2.502	6.756	3.378	8.4	N.A	N.A	N.D.
20 % Na_2CO_3	2.502	6.724	3.362	9.0	N.A	N.A	N.D.
30 % Na_2CO_3	2.502	6.684	3.342	16.6	6.76	-0.185	3.20
40 % Na_2CO_3	2.502	6.662	3.331	20.1	10.82	0.027	3.06
1 %K_2CO_3	2.504	6.752	3.376	6.2	N.A	N.A	N.D.
10 % K_2CO_3	2.502	6.738	3.369	9.0	5.63	0.289	2.52
20 % K_2CO_3	2.502	6.704	3.352	12.7	9.85	0.480	2.18
30 % K_2CO_3	2.504	6.692	3.346	13.7	6.35	-0.144	2.81
40 % K_2CO_3	2.502	6.668	3.334	23.9	10.93	0.039	3.18
1 % $MgOHCO_3$	2.502	6.728	3.364	11.1	N.A	N.A	N.D.
10 % $MgOHCO_3$	2.502	6.688	3.344	18.7	N.A	N.A	N.D.
20 % $MgOHCO_3$	2.504	6.680	3.340	18.6	14.73	-0.070	3.02
30 % $MgOHCO_3$	2.504	6.688	3.344	28.9	23.74	-0.042	2.54
40 % $MgOHCO_3$	2.504	6.662	3.331	52.9	46.38	-0.017	2.30
1 % $CaCO_3$	2.506	6.706	3.353	22.3	10.15	-0.108	4.33
10 % $CaCO_3$	2.506	6.704	3.352	27.2	12.12	-0.142	3.64
20 % $CaCO_3$	2.504	6.670	3.335	22.6	12.01	-0.209	3.84
30 % $CaCO_3$	2.504	6.682	3.341	26.0	16.08	-0.099	2.87
40 % $CaCO_3$	2.506	6.684	3.342	34.4	31.47	0.043	2.27

N.A.; Not Applicable, N.D.; Not detected, M*; Microstrain, G**; Graphitization Index.

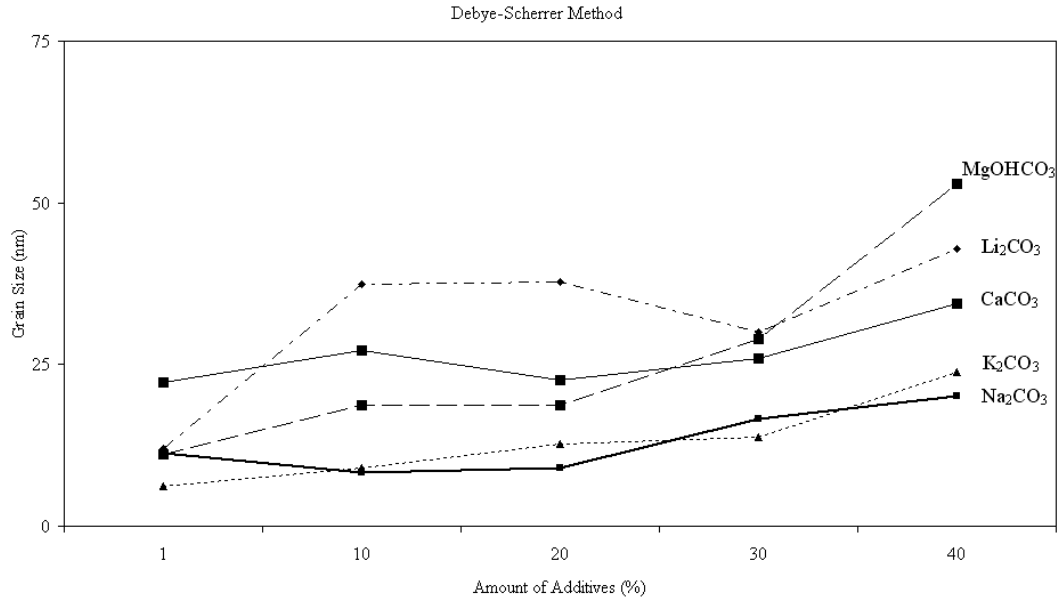

Figure 4.13 Average grain size (Debye-Scherrer Method) of hBN versus amount with the use of metal carbonates.

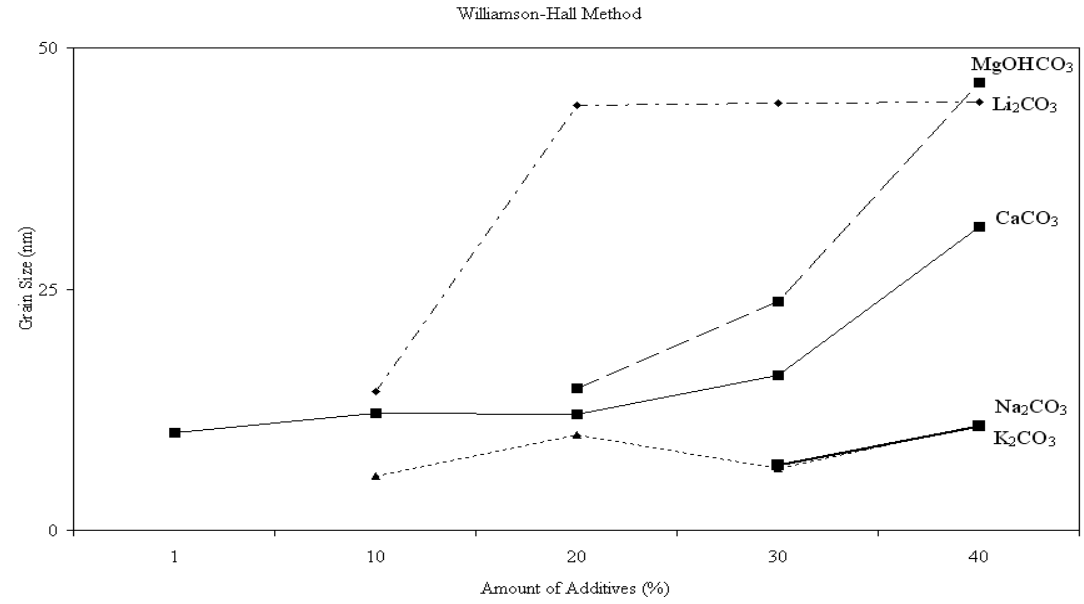

Figure 4.14 Average grain size (Williamson-Hall Method) of hBN versus amount with the use of metal carbonates.

Graphitization index is the ratio of total area under the 100 and 101 peaks to the area of 102 peak which corresponds the ordered layer structure of hBN due to the similarity of graphite [28, 29]. The graphitization index value such as 1.6 indicates higher crystalline hBN and the value about 50 is considered to be the upper limit for the least three dimensionally ordered BN [28, 29]. In this study, its value was lower than 4.5 for hBN when the amounts of fluxing agents were not lower than 10 %. In general, graphitization index of hBN synthesized in presence of metal carbonates decreased with increasing amount of them (Figure 4.15). Lithium carbonate additions resulted the formation of highly crystalline hBN with an approximate graphitization index value 1.9 because of arising the formation to three dimensional ordered structure of hBN.

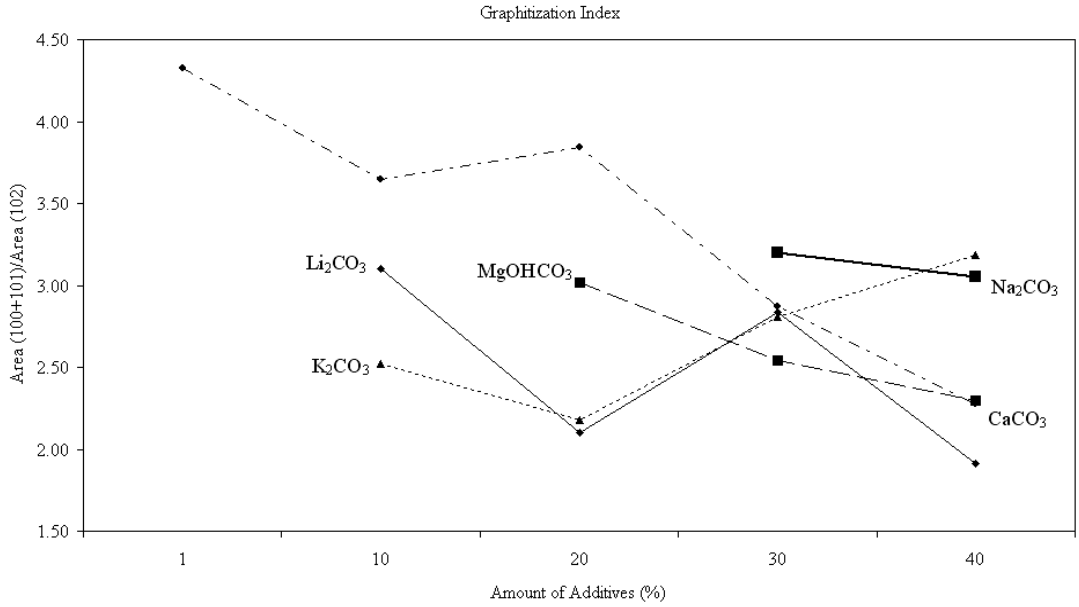

Figure 4.15 Graphitization index of hBN synthesized with different metal carbonates.

4.1.3. Scanning Electron Microscopy Observations of hBN Samples in the Presence of Metal Carbonates

The morphologic analysis of the hBN was performed by using SEM [60]. The samples that were well crystallized and the morphology of the BN powder showed an irregularly grained powder while some of SEM images of hBN particles appear plate-like. The SEM images given below exhibit that some of the synthesized hBN samples had homogeneous plates ($CaCO_3$, Li_2CO_3), rod-like (Li_2CO_3), and tubular form (Li_2CO_3) (Figure 4.16, 4.17, 4.18, 4.19, and 4.20). Porous bulk solids are seen in images of hBN samples (in K_2CO_3 additives) coated with amorphous solids while others have plates, flakes, and hexagons. The porous structure (when K_2CO_3 additive was used in synthesis) of hBN may be resulted from the escape of any intermediate gases from BN lattice [61, 62].

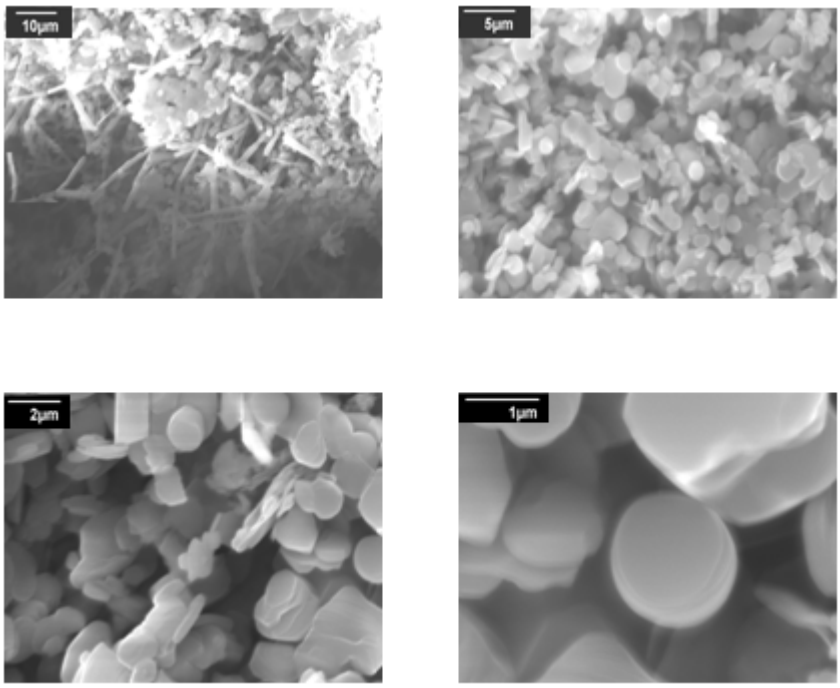

Figure 4.16 Selected SEM images of hBNs synthesized in the presence of Li_2CO_3.

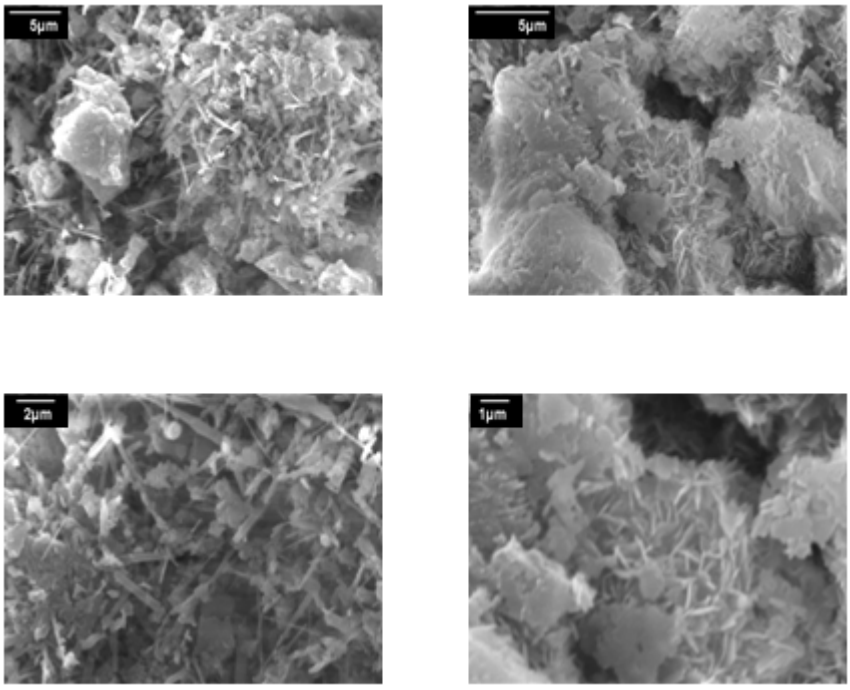

Figure 4.17 Selected SEM images of hBNs synthesized in the presence of Na_2CO_3.

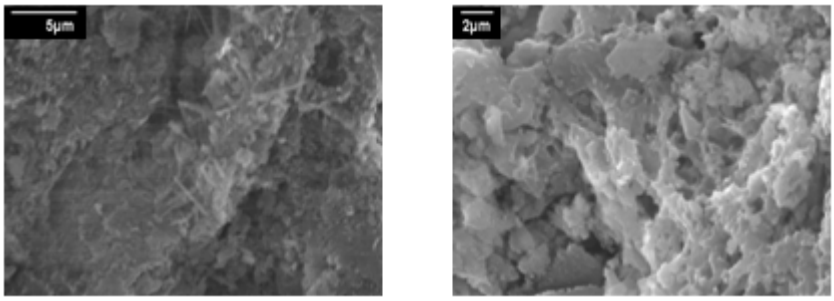

Figure 4.18 Selected SEM images of hBNs synthesized in the presence of K_2CO_3.

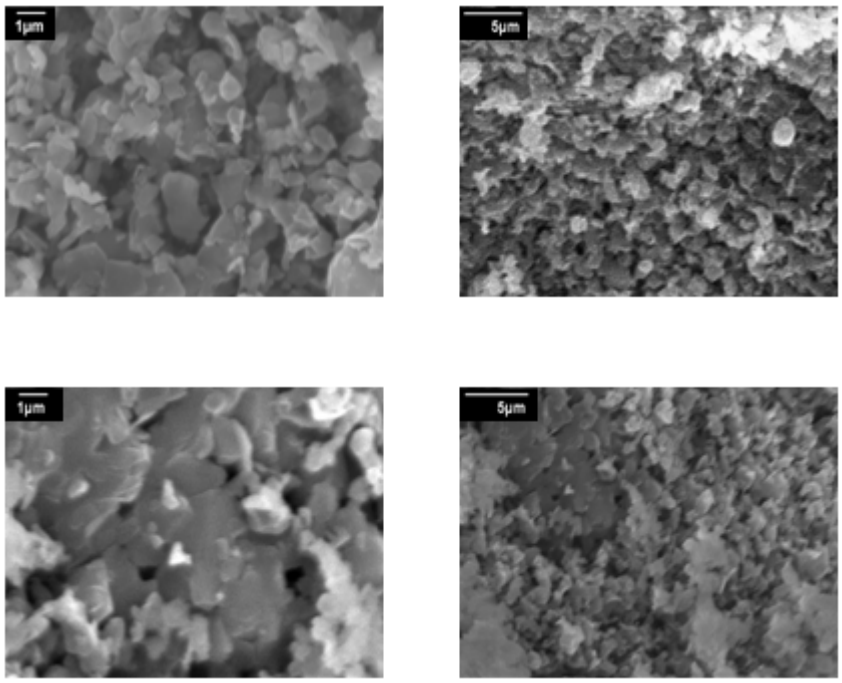

Figure 4.19 Selected SEM images of hBNs synthesized in the presence of $Mg(OH)CO_3$.

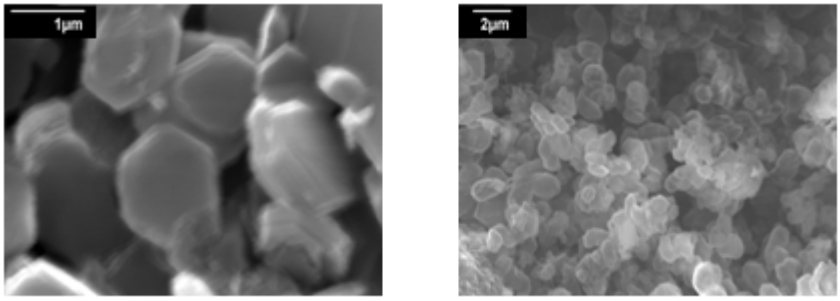

Figure 4.20 Selected SEM images of hBNs synthesized in the presence of $CaCO_3$.

4.2. Effect of Representative Metal Acetates on Synthesis of hBN

Representative metal acetates ($Li(CH_3CO_2)$, $Na(CH_3CO_2)$, $K(CH_3CO_2)$, $Mg(CH_3CO_2)_2$, and $Ca(CH_3CO_2)_2$) were used in boron oxide and urea mixture with several amounts at high temperatures such as 1450 °C that will be given below including the analysis with FT-IR, XRD, and SEM.

4.2.1. FT-IR Spectroscopy of hBN Samples in the Presence of Metal Acetates

Comparison of the FT-IR spectra of the synthesized hBN in the presence of the metal acetates in different amounts is given in figures 4.21, 4.22, 4.23, 4.24 and 4.25. The peaks located at about ~1400 cm^{-1} and ~800 cm^{-1} clearly indicated the in-plane and out-of-plane vibrations of hBN respectively. The peak observed at ~3400 cm^{-1} was attributed as vibration of the terminal O–H and N–H groups, however, strength of that peak was affected from amount of metal acetates which indicating the lowering the end groups [1, 53]. Also in plane and out of plane vibrations was observed at 1400 and 800 cm^{-1} due to the ordered structure of E_{1u} and A_{2u} modes respectively when the high amounts of additives were used.

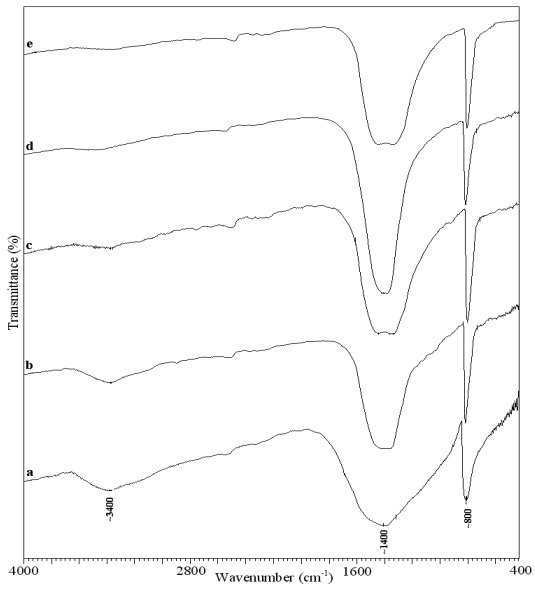

Figure 4.21 FT-IR spectra of the hBN samples with increasing amounts of $Li(CH_3CO_2)$, a) 1 % $Li(CH_3CO_2)$, b) 10 % $Li(CH_3CO_2)$, c) 20 % $Li(CH_3CO_2)$, d) 30 % $Li(CH_3CO_2)$, and e) 40 % $Li(CH_3CO_2)$.

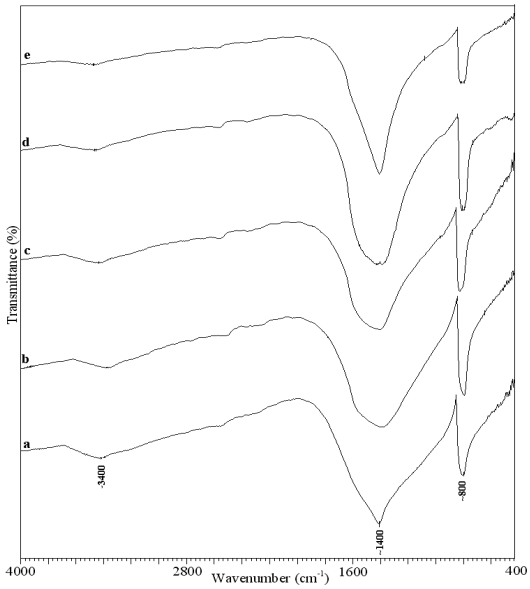

Figure 4.22 FT-IR spectra of the hBN samples with increasing amounts of $Na(CH_3CO_2)$, a) 1 % $Na(CH_3CO_2)$, b) 10 % $Na(CH_3CO_2)$, c) 20 % $Na(CH_3CO_2)$, d) 30 % $Na(CH_3CO_2)$, and e) 40 % $Na(CH_3CO_2)$.

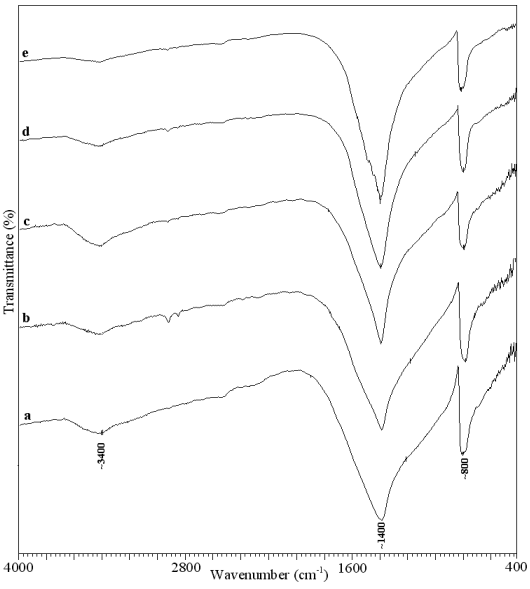

Figure 4.23 FT-IR spectra of the hBN samples with increasing amounts of $K(CH_3CO_2)$, a) 1 % $K(CH_3CO_2)$, b) 10 % $K(CH_3CO_2)$, c) 20 % $K(CH_3CO_2)$, d) 30 % $K(CH_3CO_2)$, and e) 40 % $K(CH_3CO_2)$.

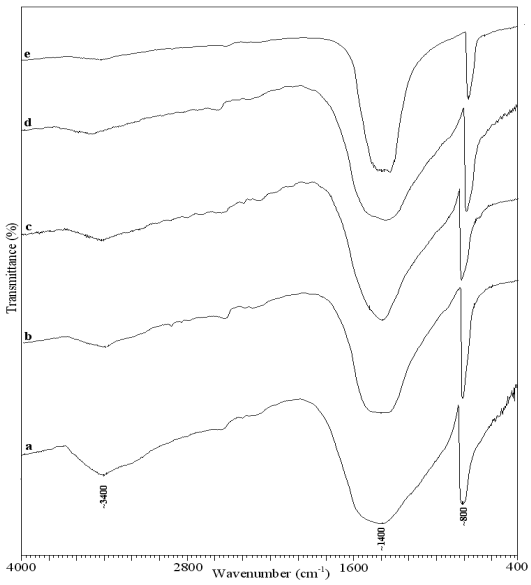

Figure 4.24 FT-IR spectra of the hBN samples with increasing amounts of $Mg(CH_3CO_2)_2$, a) 1 % $Mg(CH_3CO_2)_2$, b) 10 % $Mg(CH_3CO_2)_2$, c) 20 % $Mg(CH_3CO_2)_2$, d) 30 % $Mg(CH_3CO_2)_2$, and e) 40 % $Mg(CH_3CO_2)_2$.

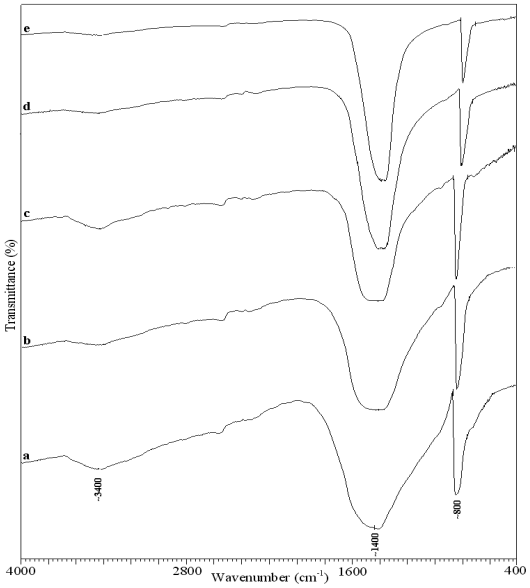

Figure 4.25 FT-IR spectra of the hBN samples with increasing amounts of $Ca(CH_3CO_2)_2$, a) 1 % $Ca(CH_3CO_2)_2$, b) 10 % $Ca(CH_3CO_2)_2$, c) 20 % $Ca(CH_3CO_2)_2$, d) 30 % $Ca(CH_3CO_2)_2$, and e) 40 % $Ca(CH_3CO_2)_2$.

4.2.2. XRD Analysis of hBN Samples in the Presence of Metal Acetates

In most diffractograms the main peaks of original hBN were observed in figure 4.26, 4.27, 4.28, 4.29, and 4.30. In XRD patterns of lithium and calcium acetates, the peaks at 100 and 101 were completely separated that the hBN formation was affirmatively proved with high crystallinity. In addition, the amount of the metal acetates had significant importance to increase the crystallinity, grain size and the lattice parameters as well as metal carbonates. Lattice parameters (Table 4.2) of hBN samples were calculated from the XRD patterns were close to the literature values.

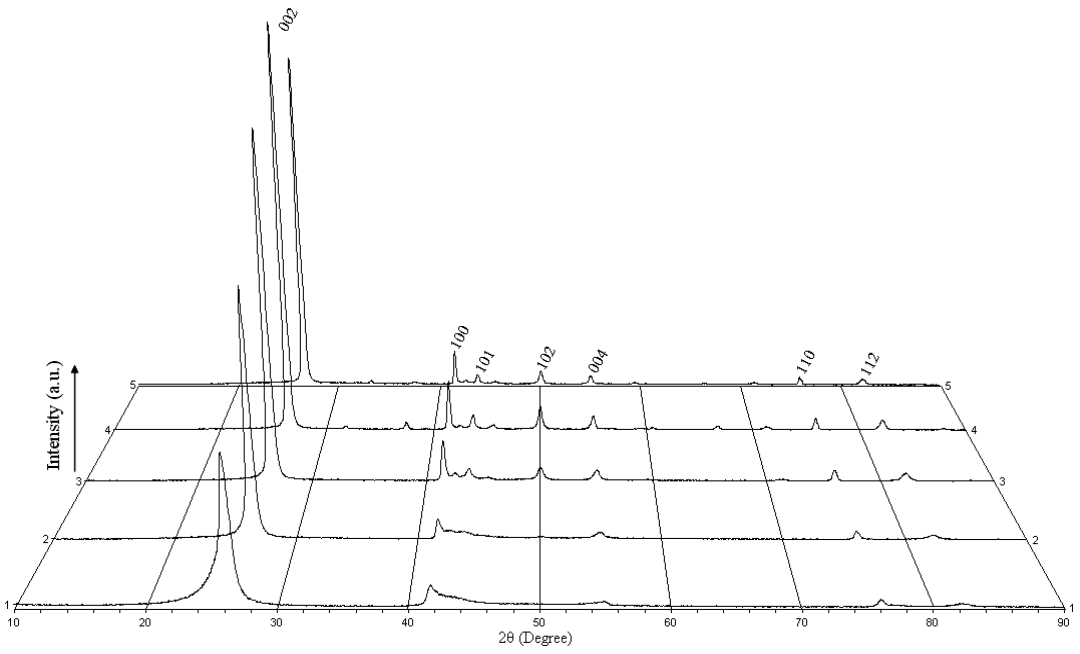

Figure 4.26 XRD patterns of the hBN in the presence of $Li(CH_3CO_2)$ where, 1) 1 %, 2) 10 %, 3) 20 %, 4) 30 %, and 5) 40 % $Li(CH_3CO_2)$.

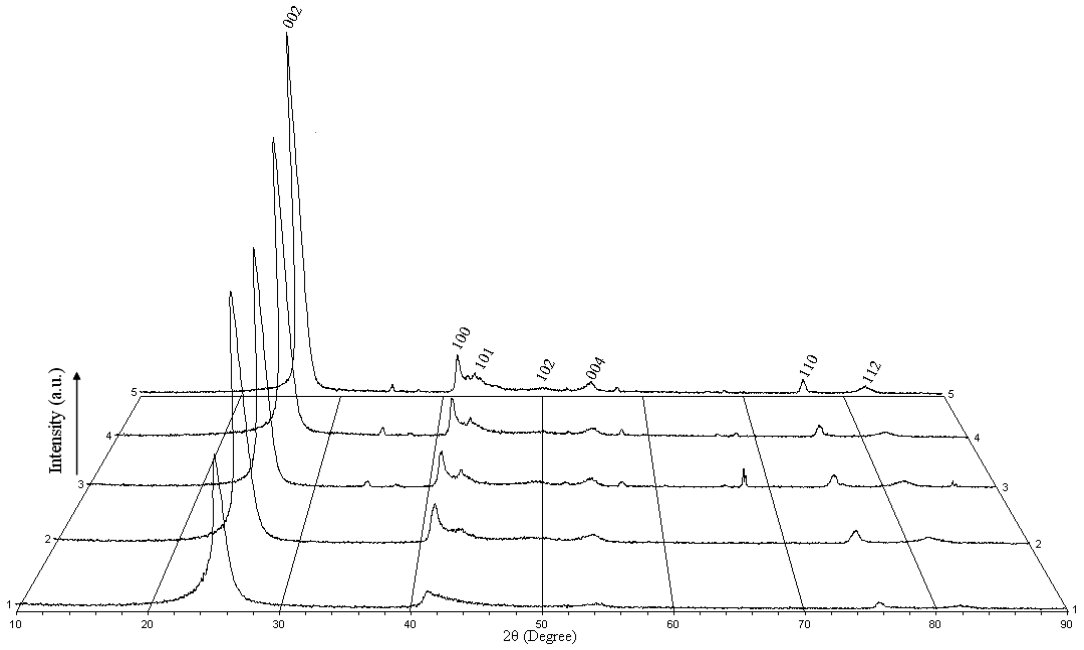

Figure 4.27 XRD patterns of the hBN in the presence of $Na(CH_3CO_2)$ where, 1) 1 %, 2) 10 %, 3) 20 %, 4) 30 %, and 5) 40 % $Na(CH_3CO_2)$.

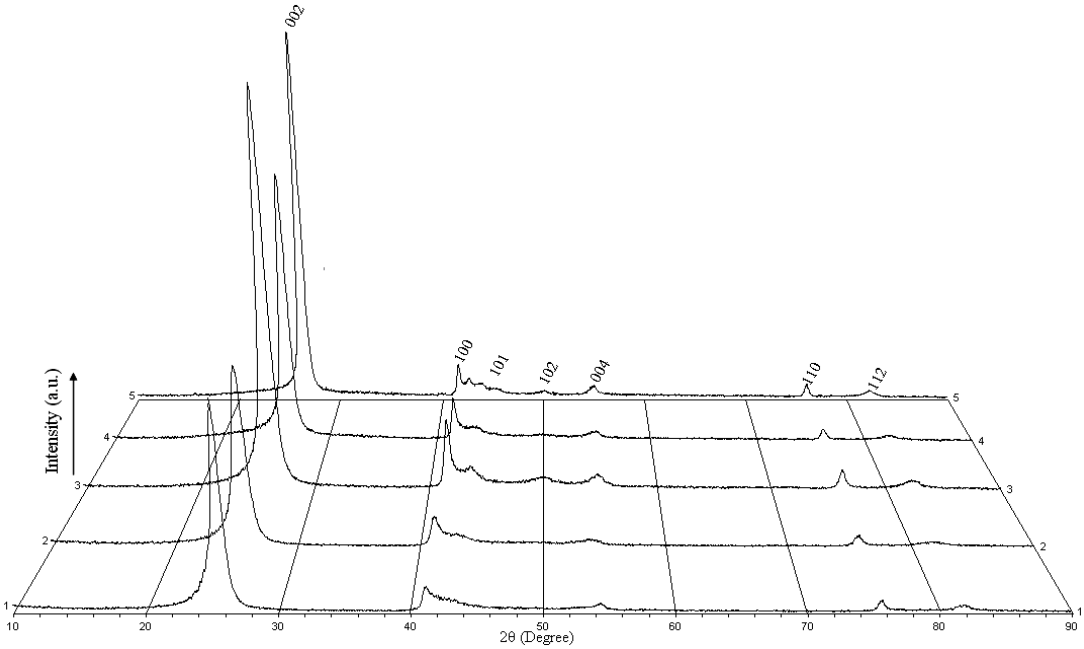

Figure 4.28 XRD patterns of the hBN in the presence of $K(CH_3CO_2)$ where, 1) 1 %, 2) 10 %, 3) 20 %, 4) 30 %, and 5) 40 % $K(CH_3CO_2)$.

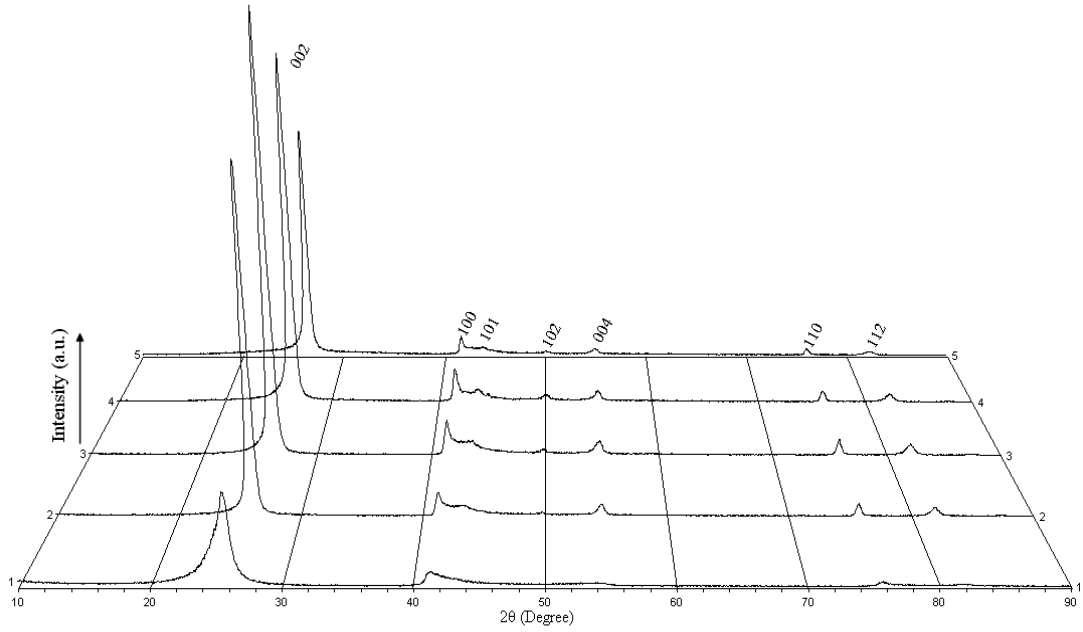

Figure 4.29 XRD patterns of the hBN in the presence of $Mg(CH_3CO_2)_2$ where, 1) 1 %, 2) 10 %, 3) 20 %, 4) 30 %, and 5) 40 % $Mg(CH_3CO_2)_2$.

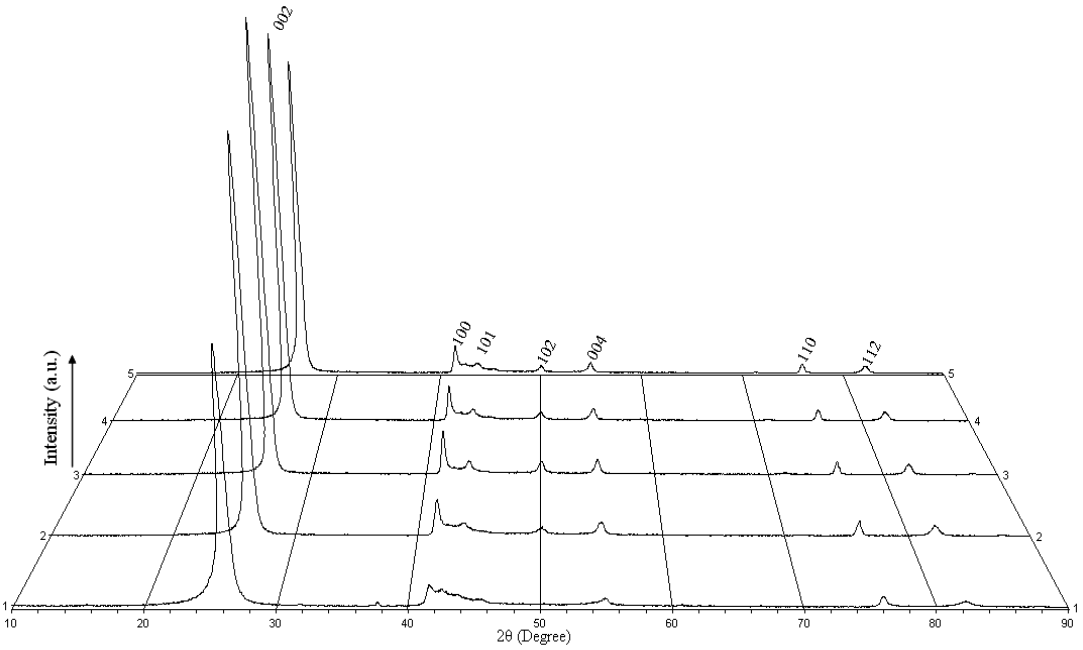

Figure 4.30 XRD patterns of the hBN in the presence of $Ca(CH_3CO_2)_2$ where, 1) 1 %, 2) 10 %, 3) 20 %, 4) 30 %, and 5) 40 % $Ca(CH_3CO_2)_2$.

Average grain size of the hBN samples were calculated by Debye-Scherrer and Williamson-Hall methods. The addition of $Li(CH_3CO_2)$ had significant contribution to the grain size whereas $Na(CH_3CO_2)$ had the lowest or no important effect on the grain size or crystallinity (Figures 4.31 and 4.32). The average grain size of hBN samples in the existence of lithium, calcium, and magnesium acetates was affected due to the reaction surface rise or catalyst effect of them.

Table 4.2. Lattice Parameters, Average Grain Size, Microstrain and Graphitization Index of Metal Acetates

	Lattice Parameters (Å)			**Average Grain Size (nm)**			
Flux Agents	**a**	**c**	**d**	**Debye-Scherer Method**	**Williamson-Hall Method**	**M* (%)**	**G****
1 % $Li(CH_3CO_2)$	2.502	6.718	3.359	9.598	N.A.	N.A.	N.D.
10 % $Li(CH_3CO_2)$	2.502	6.682	3.341	19.860	N.A.	N.A.	N.D.
20 % $Li(CH_3CO_2)$	2.504	6.684	3.342	26.580	24.78	0.051	2.53
30 % $Li(CH_3CO_2)$	2.506	6.684	3.342	55.998	64.58	0.065	2.02
40 % $Li(CH_3CO_2)$	2.506	6.672	3.336	54.049	89.43	0.110	1.97
1 % $Na(CH_3CO_2)$	2.512	6.858	3.429	8.605	N.A.	N.A.	N.D.
10 % $Na(CH_3CO_2)$	2.512	6.866	3.433	8.568	N.A.	N.A.	N.D.
20 % $Na(CH_3CO_2)$	2.516	6.840	3.420	10.640	N.A.	N.A.	N.D.
30 % $Na(CH_3CO_2)$	2.504	6.726	3.363	11.006	N.A.	N.A.	N.D.
40 % $Na(CH_3CO_2)$	2.504	6.712	3.356	13.129	N.A.	N.A.	N.D.
1 % $K(CH_3CO_2)$	2.516	6.856	3.428	10.456	N.A.	N.A.	N.D.
10 % $K(CH_3CO_2)$	2.512	6.900	3.450	7.301	N.A.	N.A.	N.D.
20 % $K(CH_3CO_2)$	2.502	6.712	3.356	9.553	7.19	0.267	4.48
30 % $K(CH_3CO_2)$	2.502	6.71	3.355	10.399	N.A.	N.A.	N.D.
40 % $K(CH_3CO_2)$	2.502	6.688	3.344	16.619	11.81	0.316	3.31
1 % $Mg(CH_3CO_2)_2$	2.512	6.868	3.434	5.765	N.A.	N.A.	N.D.
10 % $Mg(CH_3CO_2)_2$	2.514	6.790	3.395	23.183	N.A.	N.A.	N.D.
20 % $Mg(CH_3CO_2)_2$	2.51	6.754	3.377	20.959	N.A.	N.A.	N.D.
30 % $Mg(CH_3CO_2)_2$	2.504	6.694	3.347	18.427	8.00	-0.204	4.46
40 % $Mg(CH_3CO_2)_2$	2.504	6.688	3.344	22.791	16.84	0.194	4.09
1 % $Ca(CH_3CO_2)_2$	2.504	6.746	3.373	14.432	N.A.	N.A.	N.D.
10 % $Ca(CH_3CO_2)_2$	2.502	6.682	3.341	20.776	9.41	-0.254	4.24
20 % $Ca(CH_3CO_2)_2$	2.504	6.680	3.340	32.288	17.97	-0.087	3.30
30 % $Ca(CH_3CO_2)_2$	2.506	6.698	3.349	36.619	13.83	-0.127	3.64
40 % $Ca(CH_3CO_2)_2$	2.504	6.684	3.342	26.231	15.49	-0.038	3.99

N.A.; Not Applicable, N.D.; Not detected, M*; Microstrain, G**; Graphitization Index.

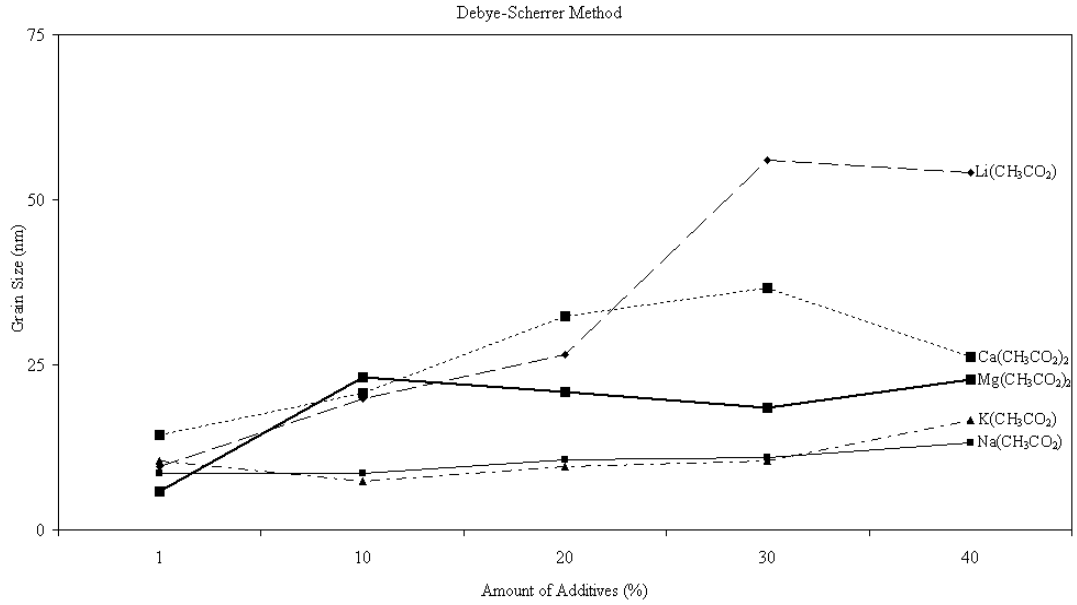

Figure 4.31 Average grain size (Debye-Scherrer Method) of hBN versus amount with the use of acetates.

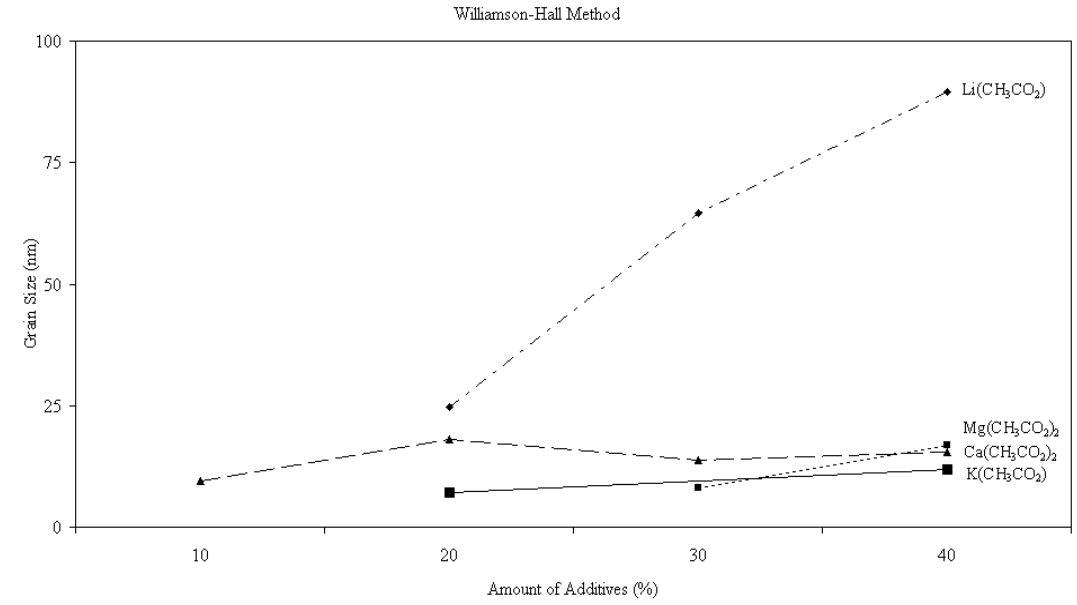

Figure 4.32 Average grain size (Williamson-Hall Method) of hBN versus amount with the use of acetates.

The calculated graphitization index of the hBN samples exhibited high crystallinity with low values at the high amount of metal acetates were used, however, increase in amount of $Na(CH_3CO_2)$ in mixtures was not sufficient to decrease the graphitization index (Figure 4.33). Meanwhile, the lowest graphitization index resulted from $Li(CH_3CO_2)$ additions to boron oxide and urea mixture as an indication of most graphitic morphology and usage of other metal acetates promoted the layered form with the high amounts except for $Ca(CH_3CO_2)_2$.

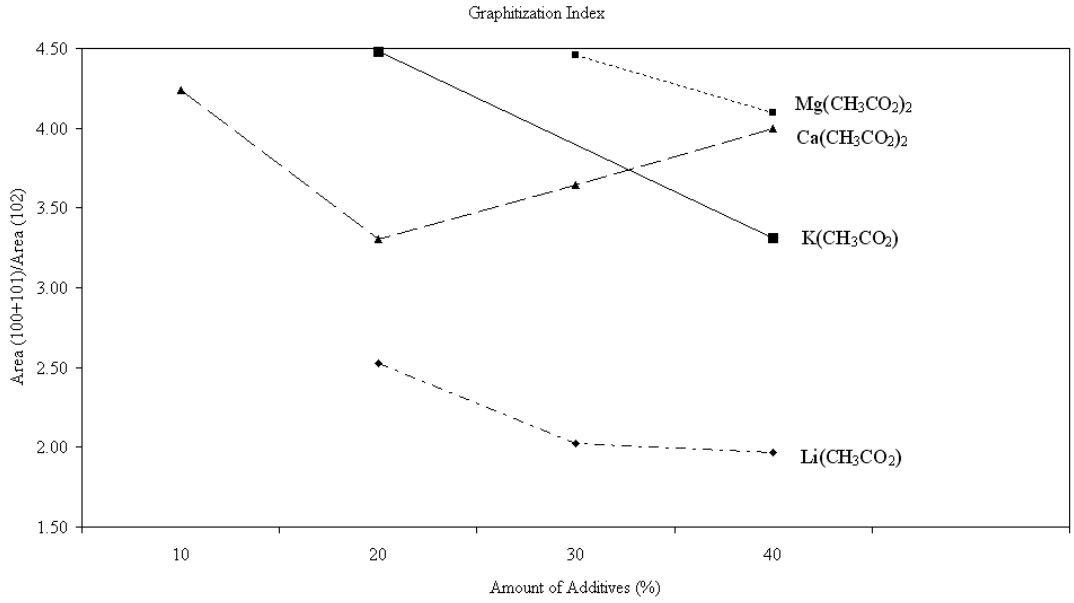

Figure 4.33 Graphitization index of hBN synthesized with different metal acetates.

4.2.3. Scanning Electron Microscopy Observations of hBN Samples in the Presence of Metal Acetates

The morphology of the hBN powder, was identified by SEM, showed irregular grained powder and had an ordered shape or tubular structures with covered amorphous forms [60]. hBN samples had irregular grained powder with fractures that the particles were jagged shapes (Figures 4.34, 4.35, 4.36, 4.37, and 4.38). However,

some of SEM images of hBN particles appeared plate-like (in $Li(CH_3CO_2)$) and had a tubular rod-like shape ($Mg(CH_3CO_2)_2$, $Ca(CH_3CO_2)_2$). The SEM images given below exhibited that some of the synthesized hBNs samples were in mixed granular form that both amorphous porous bulk BN ($Na(CH_3CO_2)$) and crystalline hBNs.

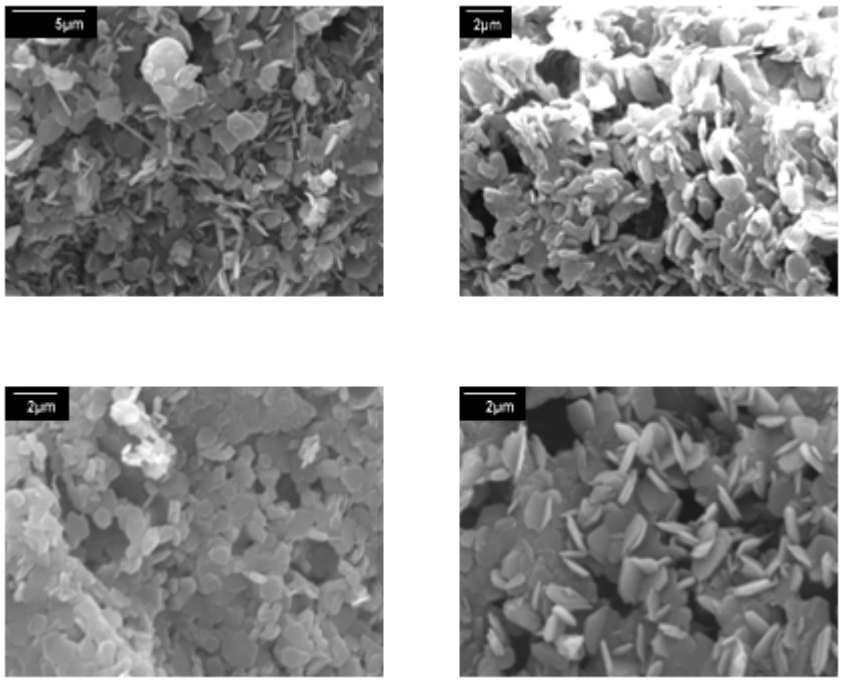

Figure 4.34 Selected SEM images of hBNs synthesized in the presence of $Li(CH_3CO_2)$.

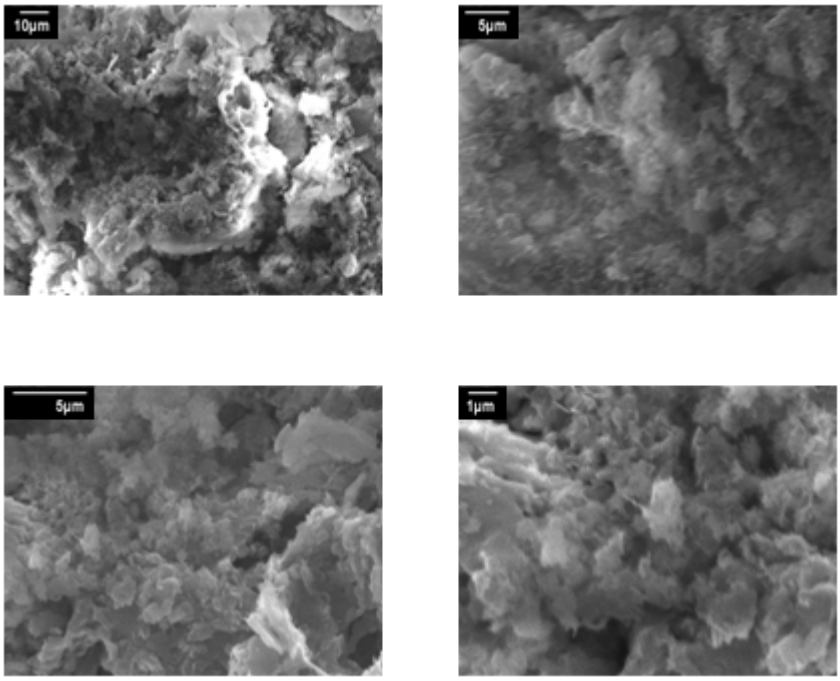

Figure 4.35 Selected SEM images of hBNs synthesized in the presence of $Na(CH_3CO_2)$.

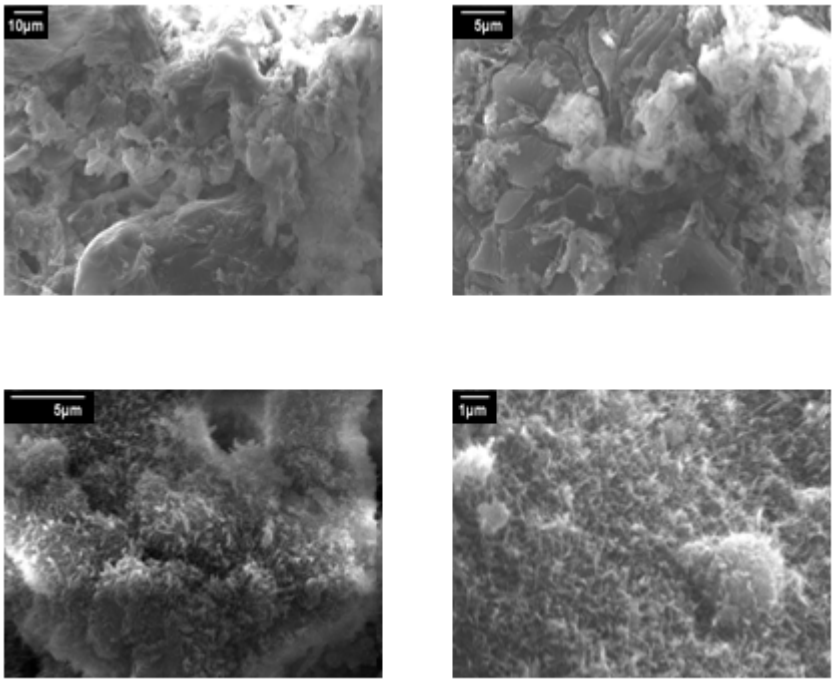

Figure 4.36 Selected SEM images of hBNs synthesized in the presence of $K(CH_3CO_2)$.

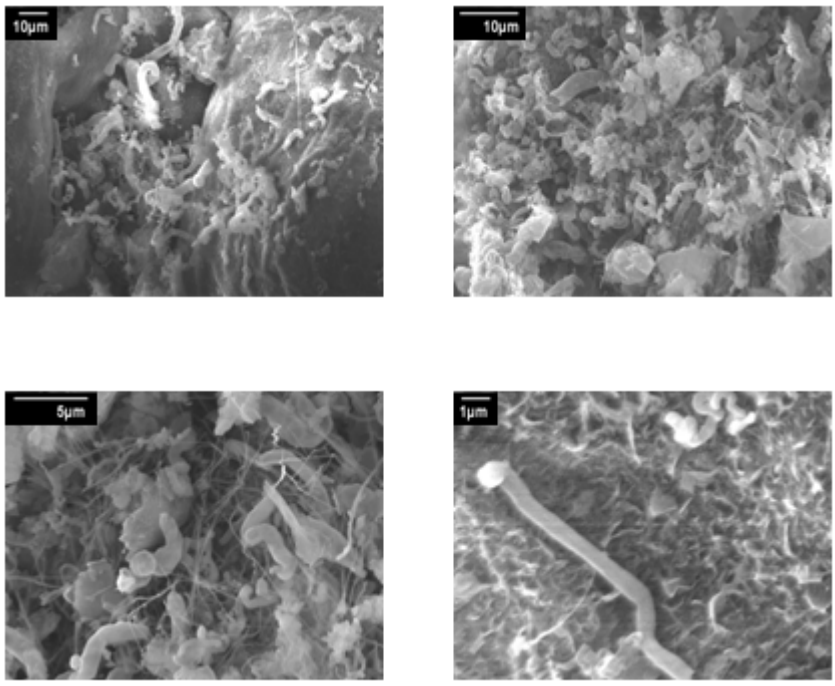

Figure 4.37 Selected SEM images of hBNs synthesized in the presence of $Mg(CH_3CO_2)_2$.

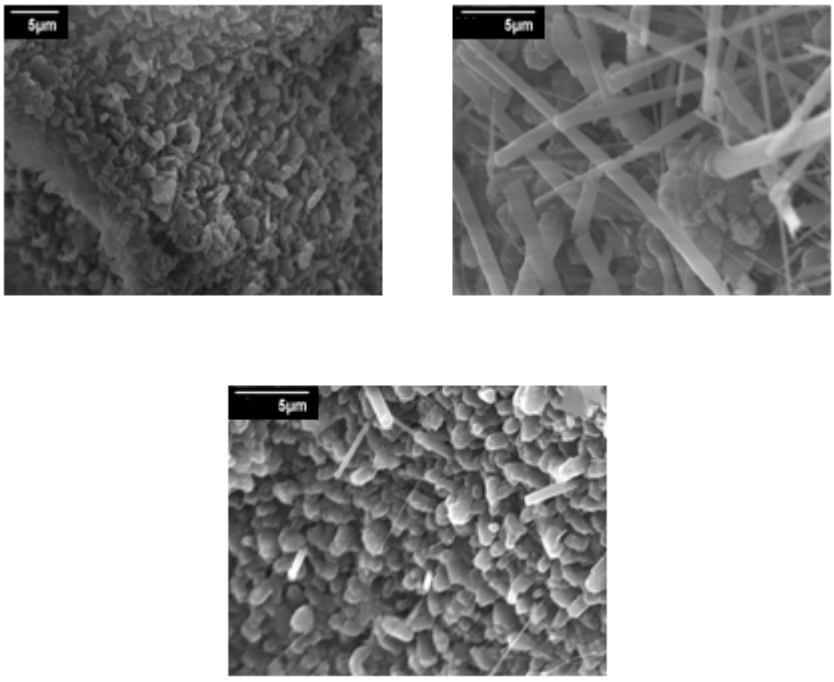

Figure 4.38 Selected SEM images of hBNs synthesized in the presence of $Ca(CH_3CO_2)_2$

.

4.3. Effect of Representative Metal Hydroxides on Synthesis of hBN

Representative metal hydroxides (LiOH, NaOH, KOH, $Mg(OH)_2$, and $Ca(OH)_2$) were used in boron oxide and urea mixtures with different amounts at high temperatures such as 1450 °C that will be given below including the analysis with FT-IR, XRD, and SEM.

4.3.1. FT-IR Spectroscopy of hBN Samples in the Presence of Metal Hydroxides

The formation of hBN was characterized by FT-IR spectroscopy is established in figures 4.39, 4.40, 4.41, 4.42, and 4.43. The FT-IR spectra of the hBN synthesized in the presence of the metal hydroxides included the vibrations assigned for hBN such as peaks at ~3400 cm^{-1}, ~1400 cm^{-1}, and ~800 cm^{-1} as in given literature [1, 38]. The peaks at ~1400 cm^{-1} and ~800 cm^{-1} indicated the in-plane and out-of-plane vibrations of hBN respectively. The peak observed at ~3400 cm^{-1} is mainly derived from the stretching vibration of the terminal O–H and N–H end groups. They disappeared when high amount of metal hydroxides were used whereas less content of additives would indicated broad peak at ~3400 cm^{-1}. Moreover the sharpness and change in peaks of these modes explained the order and layered structure of hBN. In plane and out of plane peaks turned to sharp when the amount of metal hydroxides increased as indication of three dimensional order.

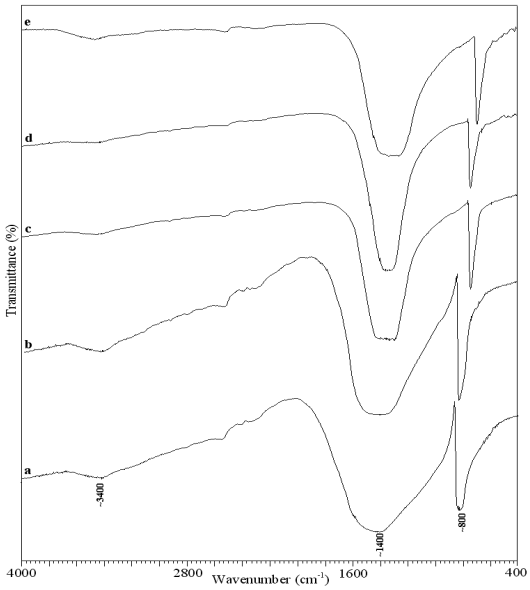

Figure 4.39 FT-IR spectra of the hBN samples with increasing amounts of LiOH, a) 1 % LiOH, b) 10 % LiOH, c) 20 % LiOH, d) 30 % LiOH, and e) 40 % LiOH.

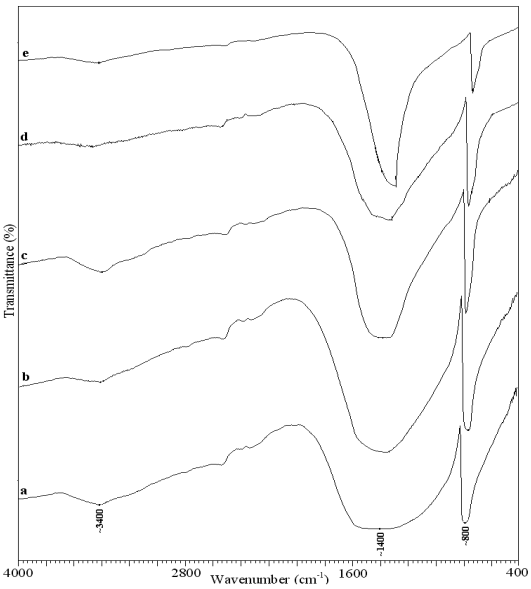

Figure 4.40 FT-IR spectra of the hBN samples with increasing amounts of NaOH, a) 1 % NaOH, b) 10 % NaOH, c) 20 % NaOH, d) 30 % NaOH, and e) 40 % NaOH.

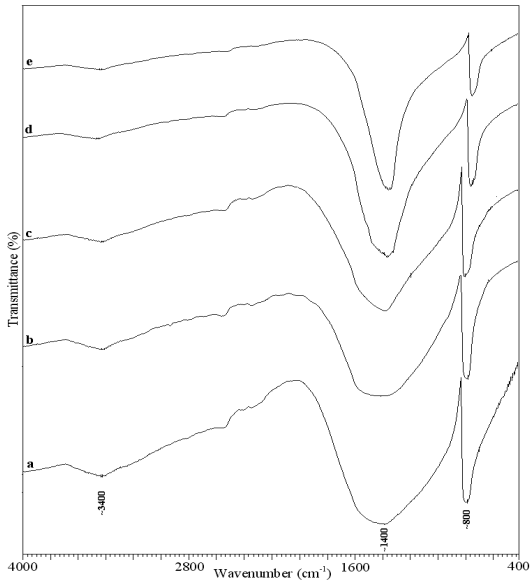

Figure 4.41 FT-IR spectra of the hBN samples with increasing amounts of KOH, a) 1 % KOH, b) 10 % KOH, c) 20 % KOH, d) 30 % KOH, and e) 40 % KOH.

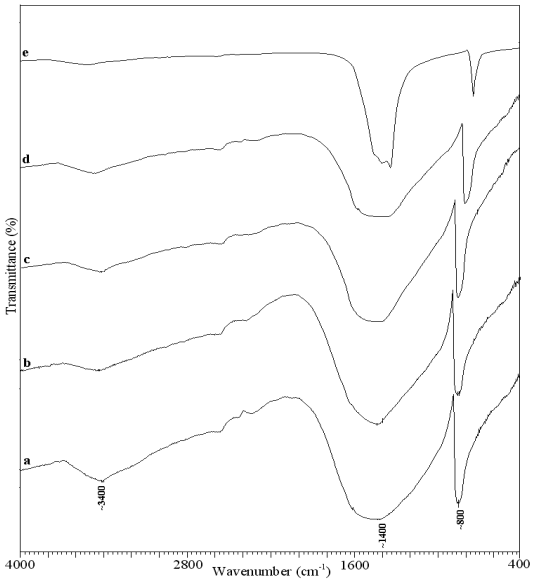

Figure 4.42 FT-IR spectra of the hBN samples with increasing amounts of $Mg(OH)_2$, a) 1 % $Mg(OH)_2$, b) 10 % $Mg(OH)_2$, c) 20 % $Mg(OH)_2$, d) 30 % $Mg(OH)_2$, and e) 40 % $Mg(OH)_2$.

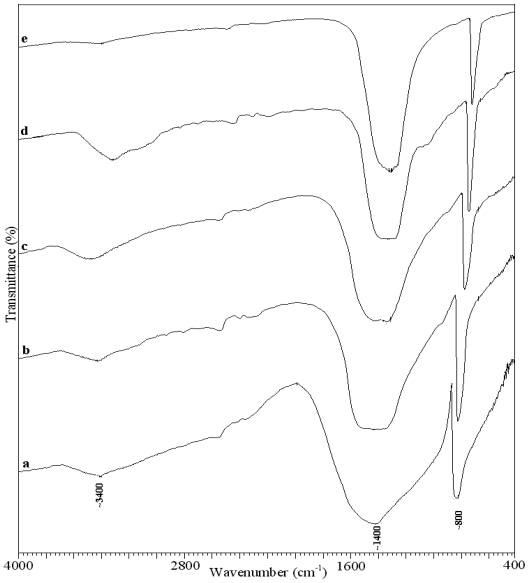

Figure 4.43 FT-IR spectra of the hBN samples with increasing amounts of $Ca(OH)_2$, a) 1 % $Ca(OH)_2$, b) 10 % $Ca(OH)_2$, c) 20 % $Ca(OH)_2$, d) 30 % $Ca(OH)_2$, and e) 40 % $Ca(OH)_2$.

4.3.2 XRD Analysis of hBN Samples in the Presence of Metal Hydroxides

Crystal structure of the hBN was analyzed by XRD and the results were compared to original hBN when metal hydroxides were used as fluxing agents. In diffractograms the main peaks of original hBN were observed (Figure 4.44, 4.45, 4.46, 4.47, and 4.48). In some of our samples (LiOH and $Ca(OH)_2$ added synthesis), complete separation of the 100 and 101 peaks indicated the three dimensional ordered hBN formations with high crystallinity and the improved lattice parameters. Appearance of the peak at 102 direction indicated the crystalline formation of hBN which was existed with high percent metal hydroxide additions (as in LiOH, NaOH, KOH, $Ca(OH)_2$ diffractograms). The diffractograms of hydroxide added samples included the 100 and 101 peaks together, when low concentration metal hydroxides were used into boron oxide and urea mixture in this study. These combined peaks as

a result of low propagation at those directions indicated small crystallite size and turbostratic form of BN because of less removal of end groups via decomposition of metal hydroxides [1, 38].

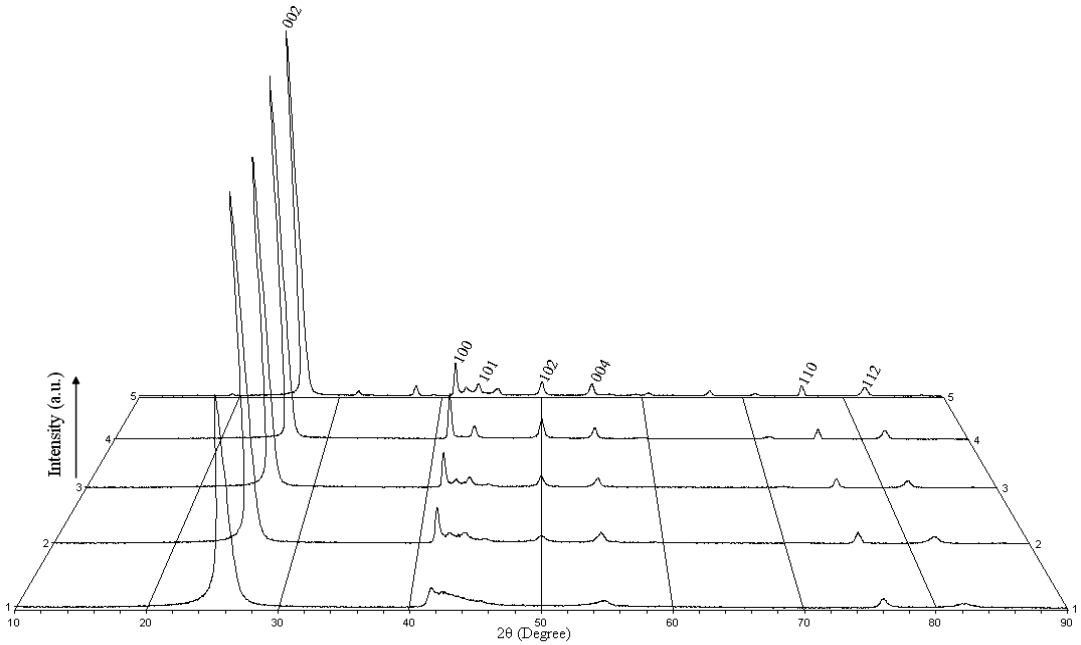

Figure 4.44 XRD patterns of the hBN in the presence of LiOH where, 1) 1 %, 2) 10 %, 3) 20 %, 4) 30 %, and 5) 40 % LiOH.

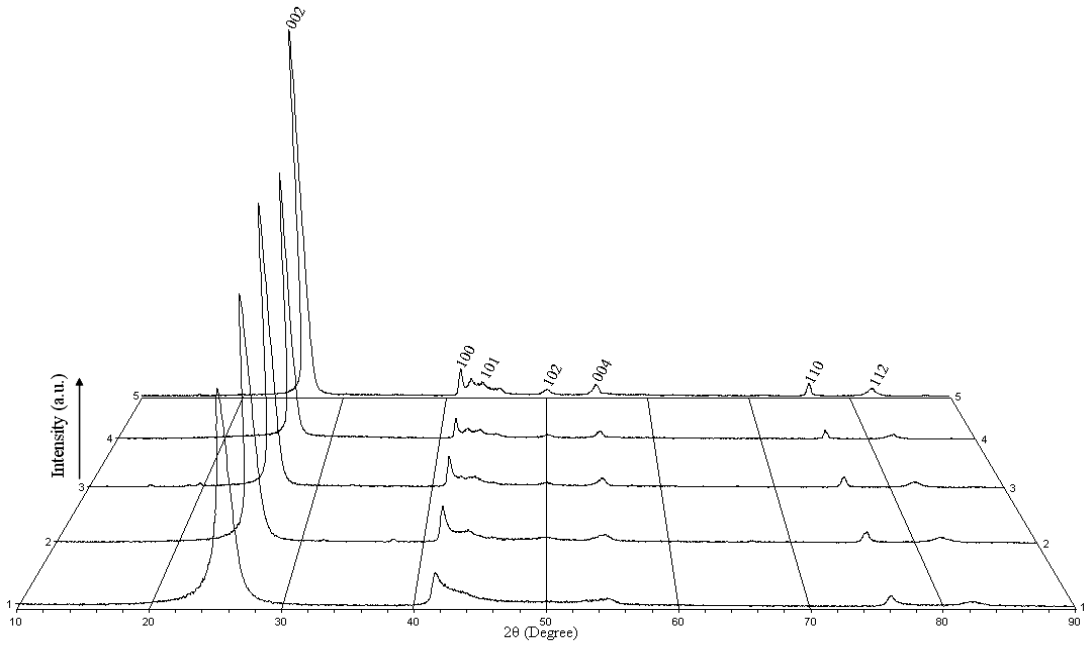

Figure 4.45 XRD patterns of the hBN in the presence of NaOH where, 1) 1 %, 2) 10 %, 3) 20 %, 4) 30 %, and 5) 40 % NaOH.

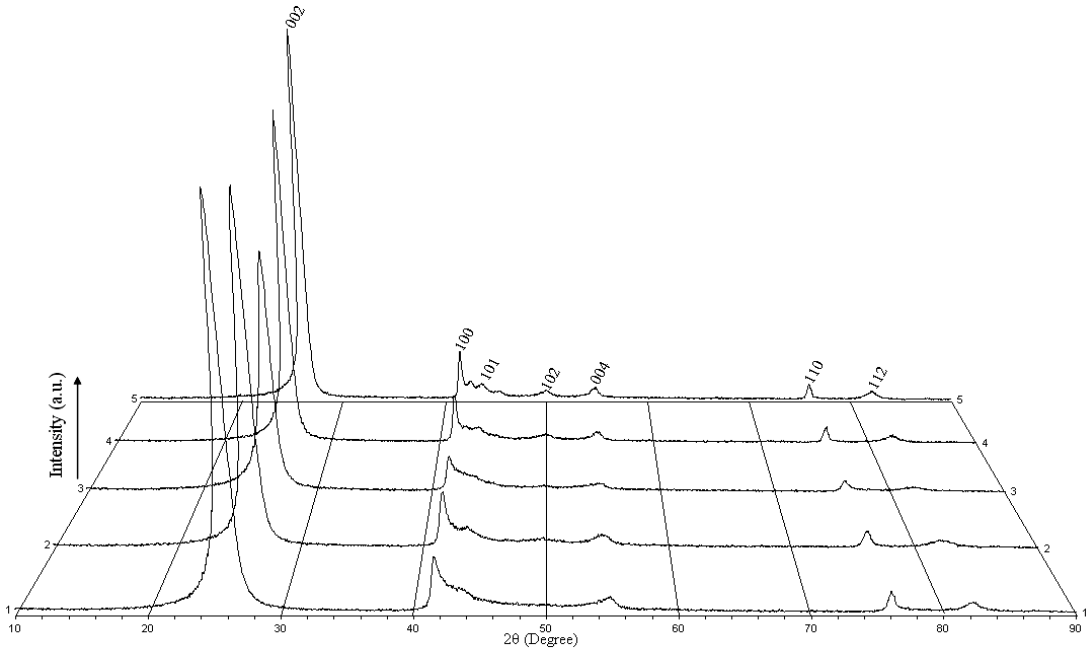

Figure 4.46 XRD patterns of the hBN in the presence of KOH where, 1) 1 %, 2) 10 %, 3) 20 %, 4) 30 %, and 5) 40 % KOH.

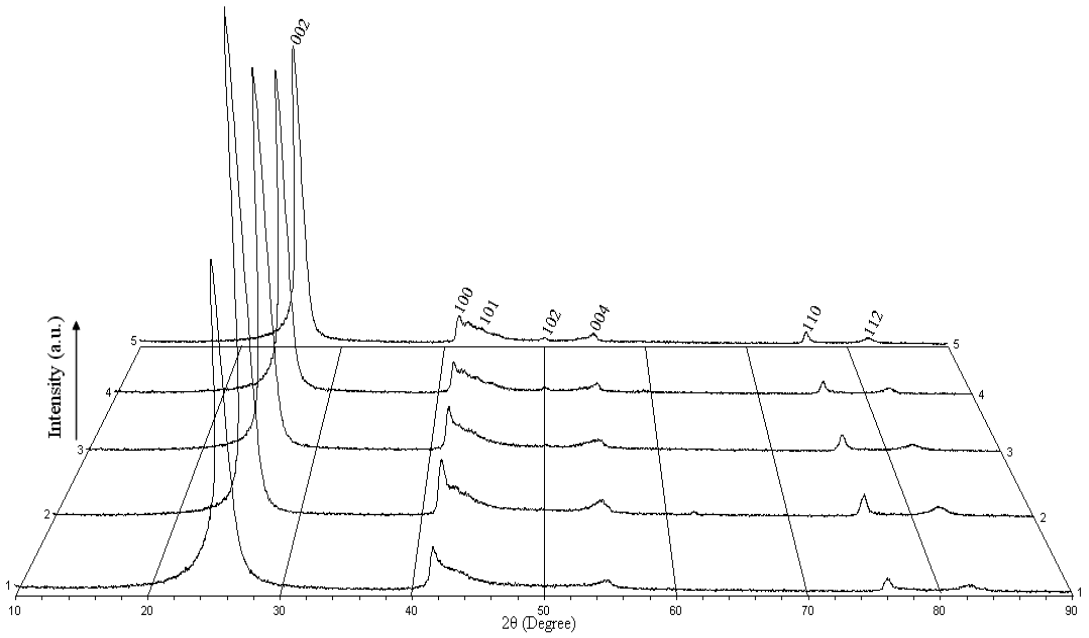

Figure 4.47 XRD patterns of the hBN in the presence of $Mg(OH)_2$ where, 1) 1 %, 2) 10 %, 3) 20 %, 4) 30 %, and 5) 40 % $Mg(OH)_2$.

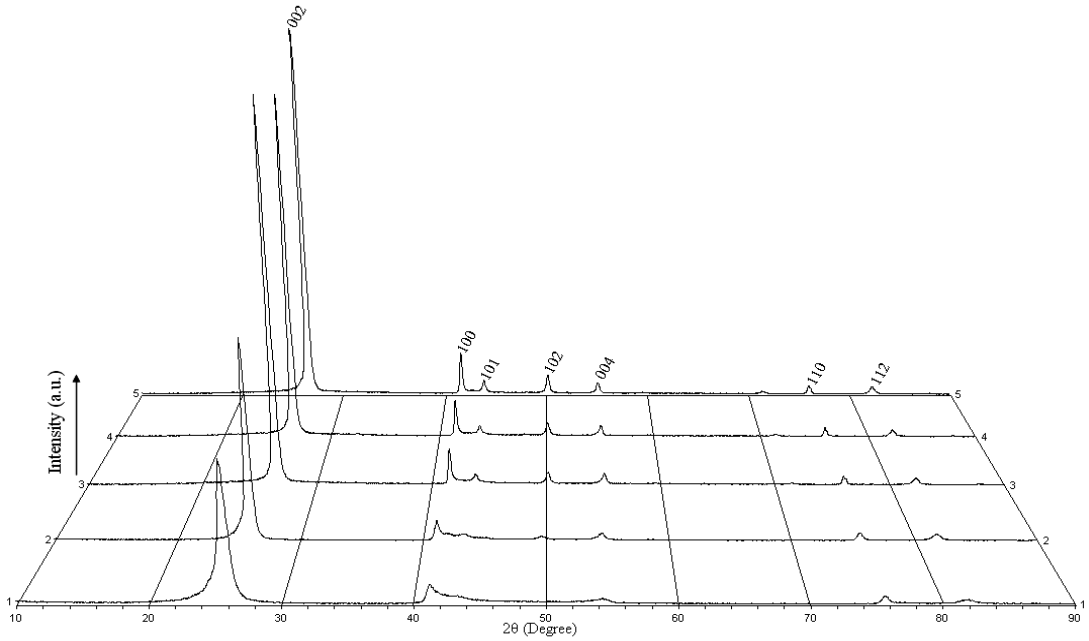

Figure 4.48 XRD patterns of the hBN in the presence of $Ca(OH)_2$ where, 1) 1 %, 2) 10 %, 3) 20 %, 4) 30 %, and 5) 40 % $Ca(OH)_2$.

The Debye-Scherrer and Williamson-Hall average grain size of the hBN samples (Table 4.3) were calculated from XRD diffractograms (Figure 4.49 and 4.50). $Ca(OH)_2$ additions into boron oxide and urea mixture had significant contribution to the grain size as a result of promoted better hydroxyl and hydride loss at the end of macromolecules due to the basic reduction of side groups of intermediate products of mixture. However, KOH, NaOH, and $Mg(OH)_2$ had the lowest effect with less hydroxyl and hydride loss. It was not possible to calculate the Williamson-Hall average grain size when the $Mg(OH)_2$ was used as additives due to unoccupied 102 and inseparable 100 and 101 peaks and less grain spread at those directions indicating turbostratic nature of the sample. But its Debye-Scherrer average grain size was similar to the calculated grain sizes with KOH and NaOH additions.

Table 4.3. Lattice Parameters, Average Grain Size, Microstrain and Graphitization Index of Metal Hydroxides

	Lattice Parameters (Å)			**Average Grain Size (nm)**			
Flux Agents	**a**	**c**	**d**	**Debye-Scherer Method**	**Williamson-Hall Method**	**M* (%)**	**G****
1 % LiOH	2.504	6.730	3.365	10.564	N.A.	N.A.	N.D.
10 % LiOH	2.506	6.702	3.351	24.360	12.36	0.005	2.48
20 % LiOH	2.506	6.702	3.351	33.086	25.31	0.057	2.28
30 % LiOH	2.506	6.688	3.344	35.337	38.06	0.043	1.86
40 % LiOH	2.504	6.682	3.341	38.964	44.46	0.086	2.24
1 % NaOH	2.502	6.736	3.368	7.651	N.A.	N.A.	N.D.
10 % NaOH	2.502	6.722	3.361	11.037	N.A.	N.A.	N.D.
20 % NaOH	2.504	6.708	3.354	16.427	N.A.	N.A.	N.D.
30 % NaOH	2.504	6.680	3.340	24.556	8.94	-0.082	3.47
40 % NaOH	2.504	6.690	3.345	20.459	7.64	-0.248	2.91
1 % KOH	2.504	6.726	3.363	10.344	N.A.	N.A.	N.D.
10 % KOH	2.502	6.748	3.374	8.780	N.A.	N.A.	N.D.
20 % KOH	2.504	6.754	3.377	7.517	N.A.	N.A.	N.D.
30 % KOH	2.504	6.726	3.363	12.191	4.39	-0.107	2.50
40 % KOH	2.504	6.720	3.360	15.649	7.55	0.012	3.04
1 % $Mg(OH)_2$	2.504	6.736	3.368	10.081	N.A.	N.A.	N.D.
10 % $Mg(OH)_2$	2.502	6.732	3.366	11.161	N.A.	N.A.	N.D.
20 % $Mg(OH)_2$	2.502	6.742	3.371	9.138	N.A.	N.A.	N.D.
30 % $Mg(OH)_2$	2.504	6.716	3.358	10.679	N.A.	N.A.	N.D.
40 % $Mg(OH)_2$	2.506	6.720	3.360	10.840	N.A.	N.A.	N.D.
1 % $Ca(OH)_2$	2.514	6.840	3.420	10.741	N.A.	N.A.	N.D.
10 % $Ca(OH)_2$	2.516	6.810	3.405	23.435	7.36	-0.414	3.26
20 % $Ca(OH)_2$	2.516	6.824	3.412	21.921	87.90	0.168	2.92
30 % $Ca(OH)_2$	2.504	6.674	3.337	82.330	176.87	0.183	2.86
40 % $Ca(OH)_2$	2.504	6.666	3.333	119.179	297.08	0.148	2.15

N.A.; Not Applicable, N.D.; Not detected, M*; Microstrain, G**; Graphitization Index.

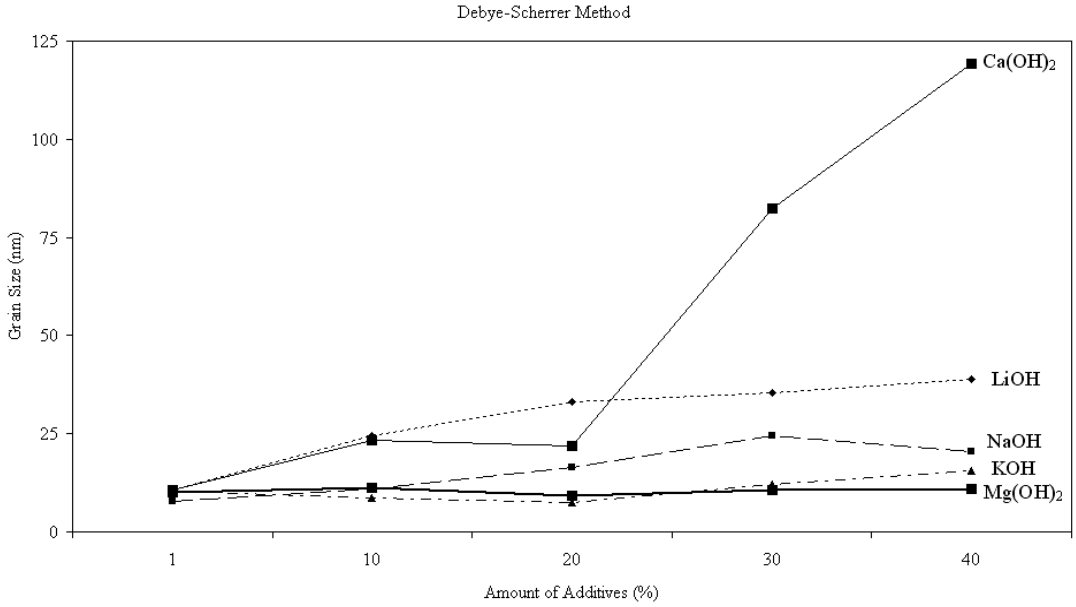

Figure 4.49 Average grain size (Debye-Scherrer Method) of hBN versus amount with the use of metal hydroxides.

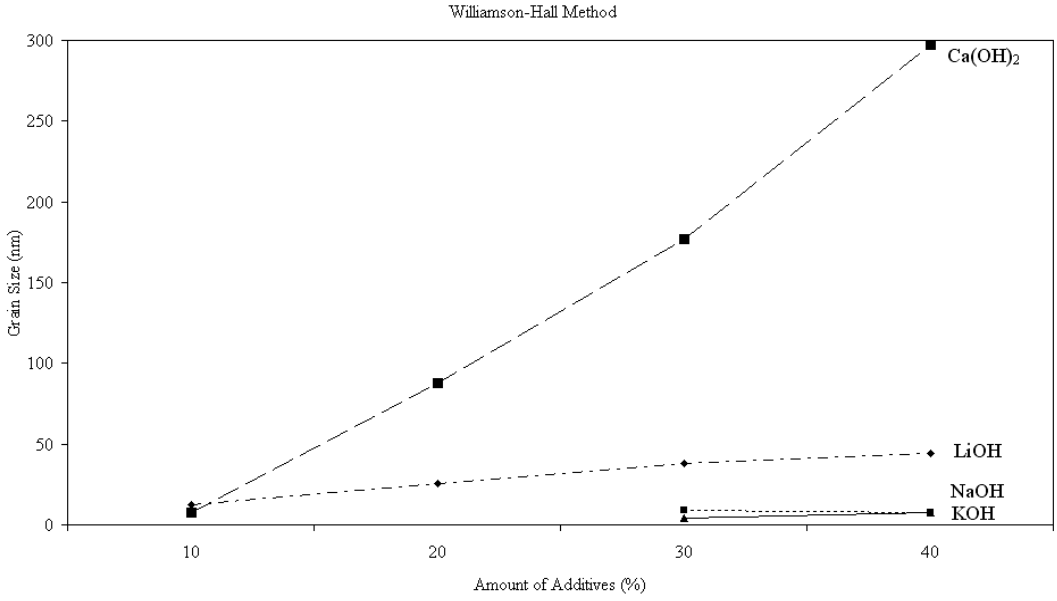

Figure 4.50 Average grain size (Williamson-Hall Method) of hBN versus amount with the use of metal hydroxides.

Graphitization index existed in low values indicating high graphitic order of the hBN at high amounts of metal hydroxides use (Figure 4.51). The LiOH and $Ca(OH)_2$ additions contributed better results to graphitization index even the lower amounts. However, the best graphitization index of hBN was obtained at 30 % addition of LiOH as well as lithium carbonate and acetate. It was not able to calculate the graphitization index of hBN if $Mg(OH)_2$ and low amounts of NaOH and KOH. Because low grain spread on the directions of 100, 101, and 102 or disordered structure of BN might be resulted addition of these salts.

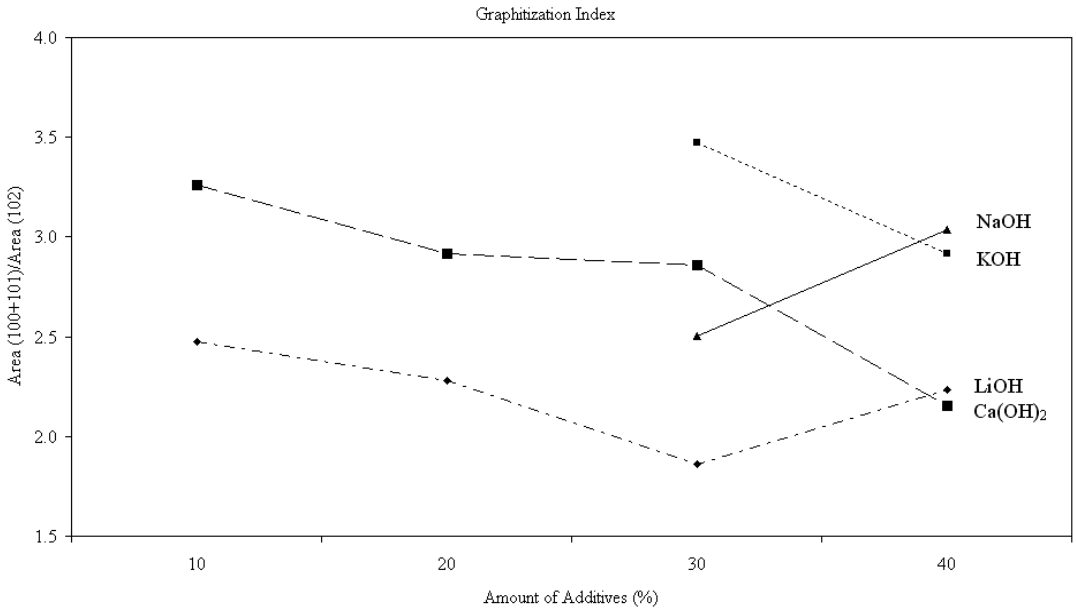

Figure 4.51 Graphitization index of hBN synthesized with different metal hydroxides.

4.3.3. Scanning Electron Microscopy Observations of hBN Samples in the Presence of Metal Hydroxides

The SEM images given in figures 4.52, 4.53, 4.54, 4.55, and 4.56 exhibit that synthesized hBN samples had homogeneous plates ($Ca(OH)_2$, LiOH, and KOH), rod-like, tubular form (LiOH and NaOH), and helix ($Mg(OH)_2$). The SEM images included the an irregularly dispersed ($Ca(OH)_2$, $Mg(OH)_2$, NaOH, and KOH) powder whereas some of SEM images of hBN particles appeared plate-like (LiOH) when metal hydroxides were used as fluxing agents. Also some SEM images stated that mixed grain formation pronounced in the addition of NaOH while some had homogenous expanded flaky shapes (KOH and LiOH).

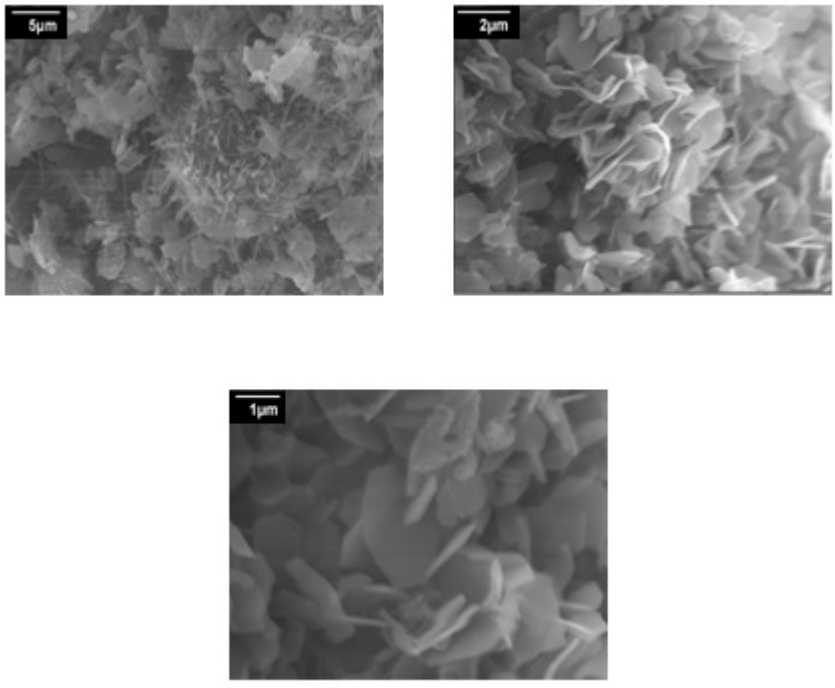

Figure 4.52 Selected SEM images of hBNs synthesized in the presence of LiOH.

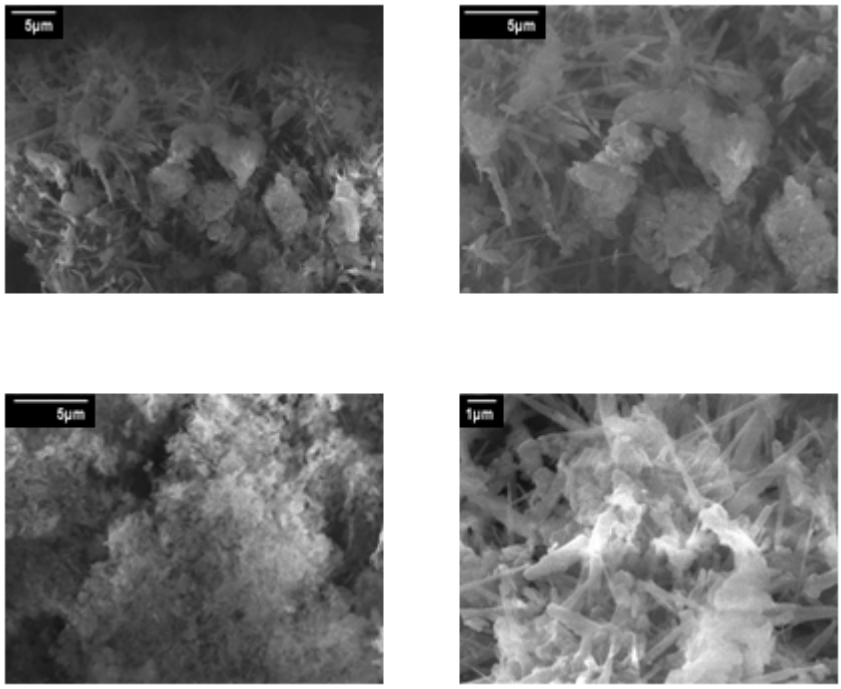

Figure 4.53 Selected SEM images of hBNs synthesized in the presence of NaOH.

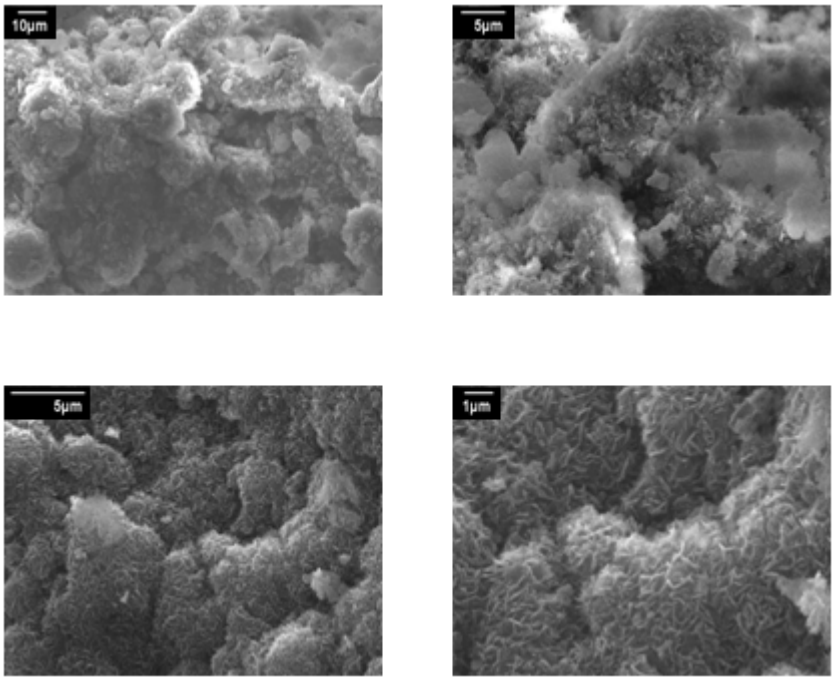

Figure 4.54 Selected SEM images of hBNs synthesized in the presence of KOH.

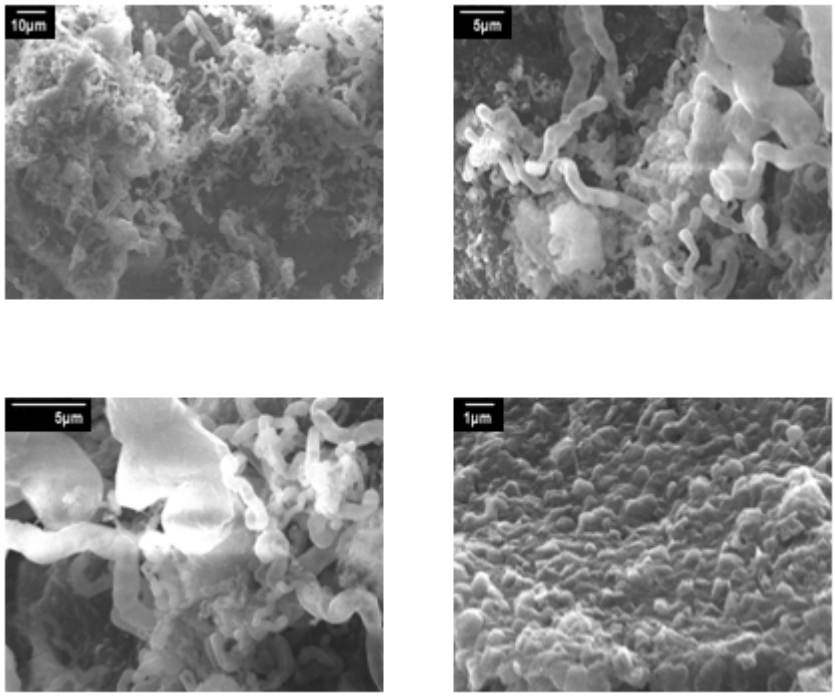

Figure 4.55 Selected SEM images of hBNs synthesized in the presence of $Mg(OH)_2$.

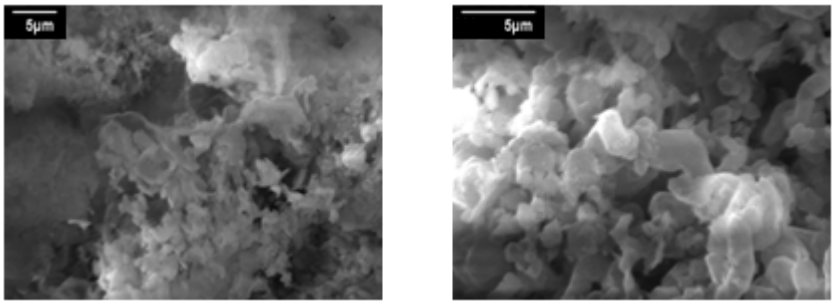

Figure 4.56 Selected SEM images of hBNs synthesized in the presence of $Ca(OH)_2$.

4.4. Low Temperature Trials of Representative Metals Salts Additions on hBN Synthesis

The temperature at which the boron oxide and urea systems are carried out in presence of fluxing agents had possibly influence on formation of hBN. Due to the hardness and expensiveness of high temperature synthesis of solid state reactions, BN synthesis performed at low temperatures such as 1300 and 1150 °C (and 1000 °C for Li_2CO_3).

4.4.1. FT-IR Spectroscopy of hBN Samples Synthesized at Low Temperatures

FT-IR spectra of hBN samples prepared at 1000, 1150, 1300 and 1450 °C are presented in figure 4.57 for Li_2CO_3. Low temperature hBN synthesis with $Li(CH_3CO_2)$ and LiOH were carried out at 1150, 1300 and 1450 °C (Figure 4.58 and 4.59). FT-IR spectra of low concentration additions of fluxes (10 % $CaCO_3$), which were performed at 1150, 1300 and 1450 °C, is given figure 4.60. Two strong peaks located at ~1400 cm^{-1} and ~800 cm^{-1} were identified as in-plane and out-of- plane vibrations of hBN , respectively. The broad bands near 3400 cm^{-1} ascribed to –BO–H and N–H bonds from terminal group of BN.

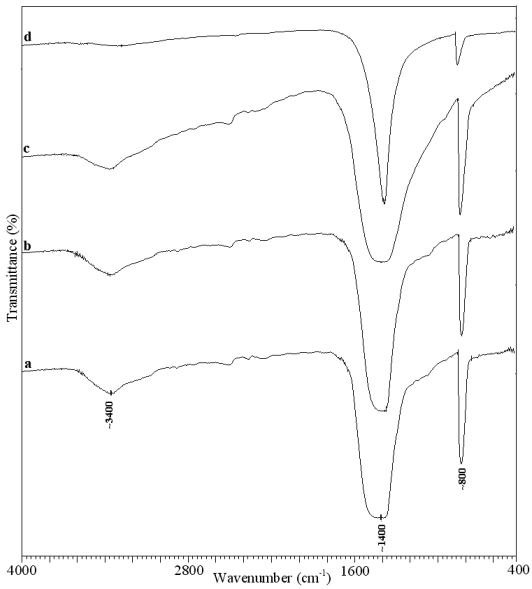

Figure 4.57 FT-IR spectra of the hBN samples synthesized with 40 % Li_2CO_3 at different temperatures a) 1000 °C, b) 1150 °C, c) 1300 °C, and d) 1450 °C.

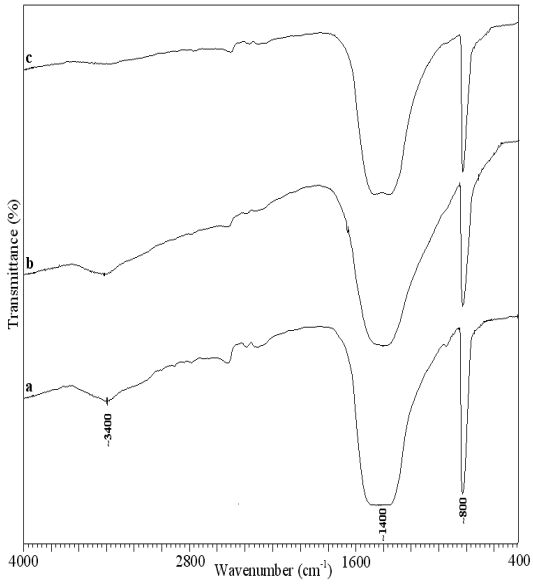

Figure 4.58 FT-IR spectra of the hBN samples synthesized with 40 % $Li(CH_3CO_2)$ at different temperatures a) 1150 °C, b) 1300 °C, and c) 1450 °C.

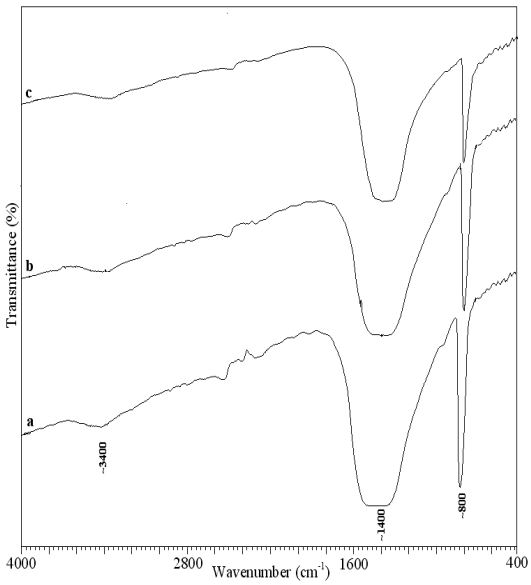

Figure 4.59 FT-IR spectra of the hBN samples synthesized with 40 % LiOH at different temperatures a) 1150 °C, b) 1300 °C, and c) 1450 °C.

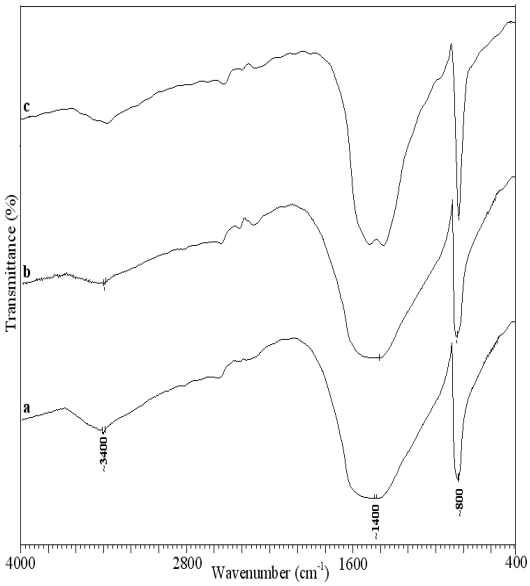

Figure 4.60 FT-IR spectra of the hBN samples synthesized with 10 % $CaCO_3$ at different temperatures a) 1150 °C, b) 1300 °C, and c) 1450 °C.

4.4.2. XRD Analysis of hBN Samples Synthesized at Low Temperatures

XRD analysis was performed in order to determine composition and crystallinity of hBN in the presence of the fluxing agents at lower temperatures and results were compared to original XRD pattern of standard hBN. The main peaks, 002, 10X, 004, 110, and 112 were observed in all diffractograms even low temperatures (Figures 4.50, 4.51, 4.52, and 4.53). The lattice parameters of hBN samples were calculated from the XRD patterns and were compared with literature values.

All diffractograms indicated the formation of BN however hexagonal form of BN persisted when the amount of additives and temperature increased (Figures 4.61, 4.62, 4.63, and 4.64). The XRD diffractograms of hBN synthesized with calcium carbonate included the 100 and 101 peaks together as a result of decreasing temperature. Moreover, the 102 peak was detected and other main peaks sharpened at high temperatures in the synthesis with lithium carbonates, acetates, and hydroxides.

Highly crystalline hBN was formed at a lower temperature such as 1150 ºC with Li_2CO_3 additions to boron oxide and urea mixture. That had the best contribution to the hBN formation among metal carbonates at 1450 ºC. The formation of the high crystalline hBN decomposed and small grain size hBNs were derived from the lower temperature than 1150 ºC as a result of disappearance of 102 peak. Thus the stacking regularity of the B–N layers along (002) direction was destroyed, and hBN gradually transformed into tBN and aBN or nanoscale BN [1, 56].

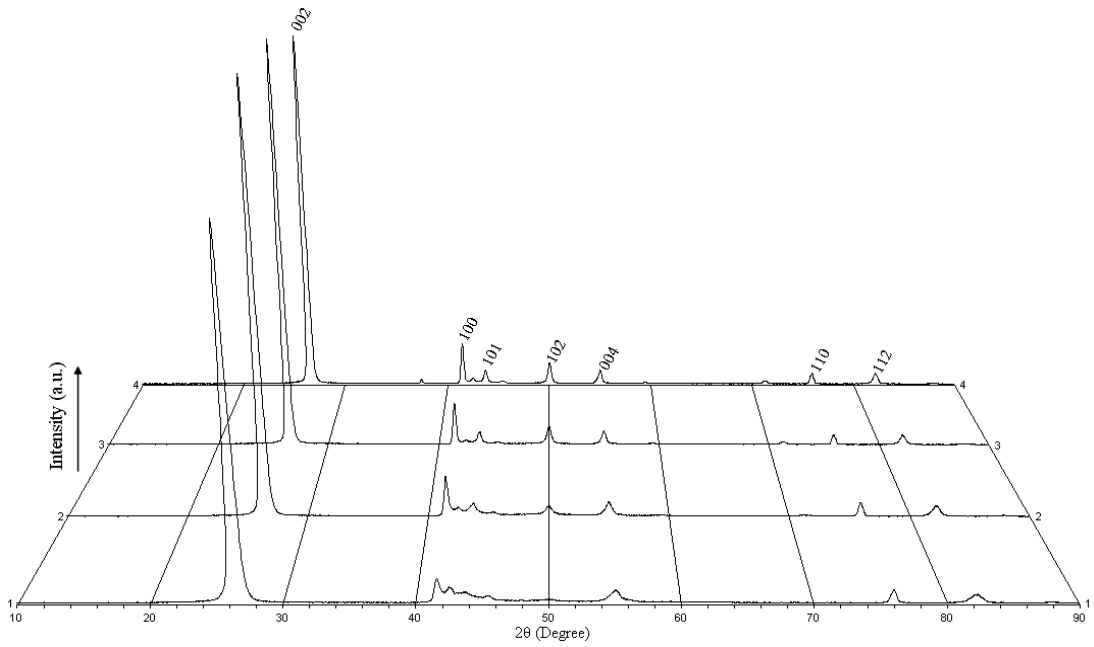

Figure 4.61 Synthesis of hBN with the addition of 40 % Li_2CO_3 at different temperatures, where, 1) 1000 °C, 2) 1150 °C, 3) 1300 °C, and 4) 1450 °C.

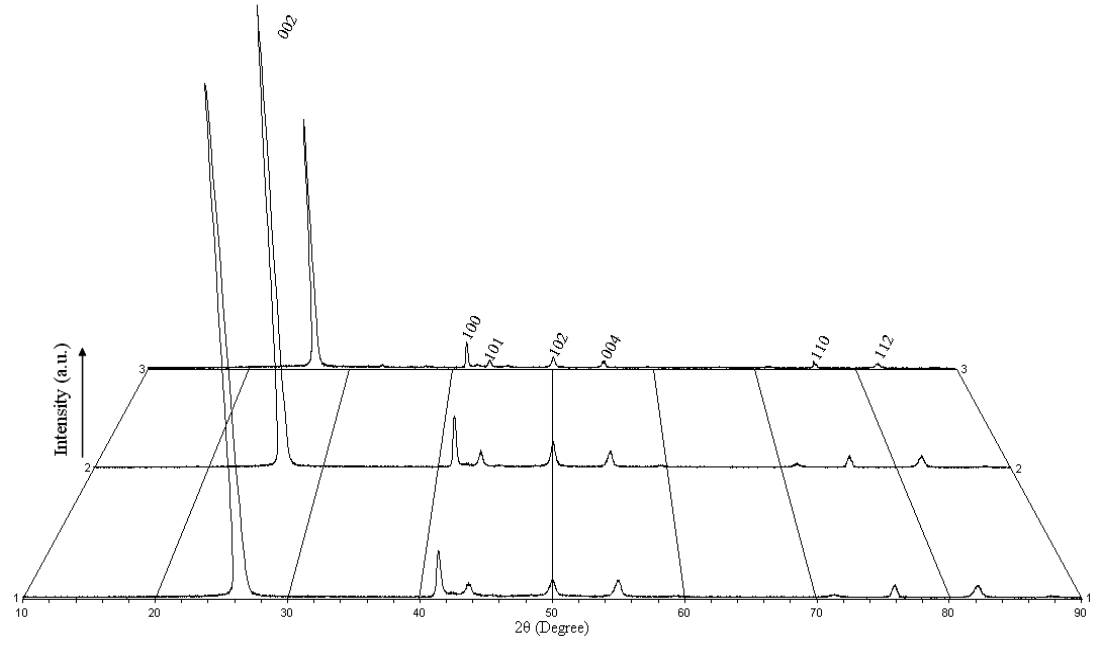

Figure 4.62 Synthesis of hBN with the addition of 40 % $Li(CH_3CO_2)$ at different temperatures, where, 1) 1150 °C, 2) 1300 °C, and 3) 1450 °C.

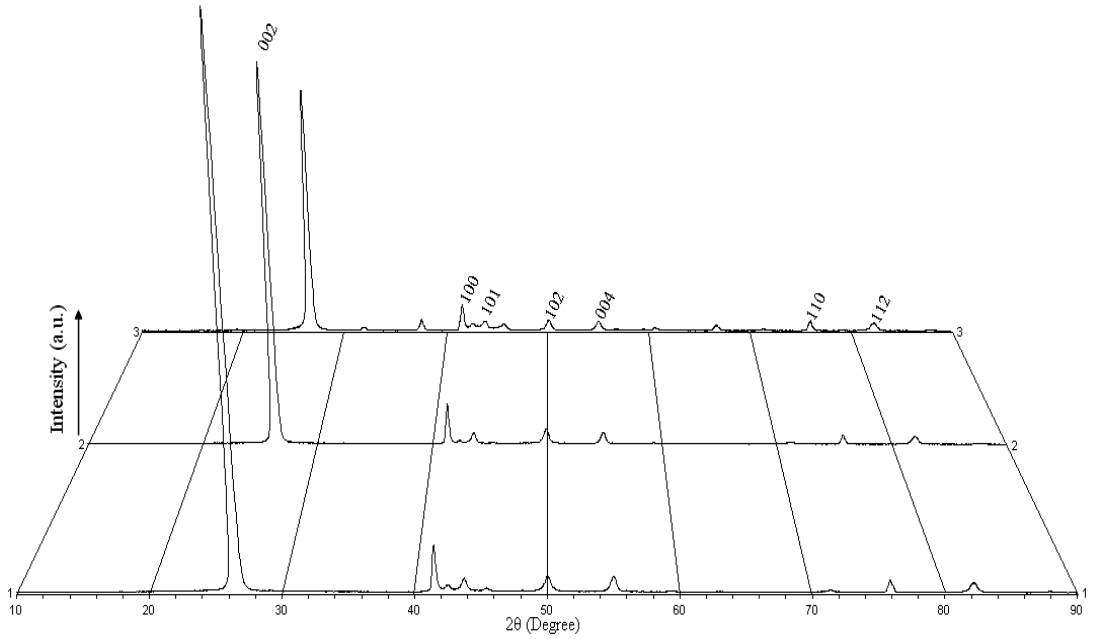

Figure 4.63 Synthesis of hBN with the addition of 40 % LiOH at different temperatures, where, 1) 1150 °C, 2) 1300 °C, and 3) 1450 °C.

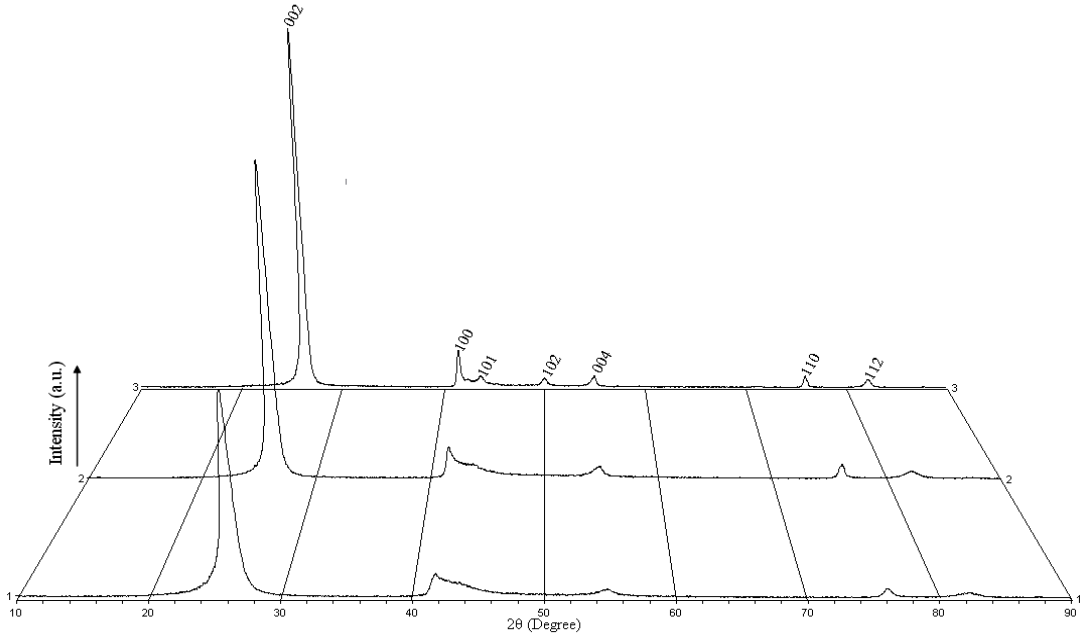

Figure 4.64 Synthesis of hBN with the addition of 10 % $CaCO_3$ at different temperatures, where, 1) 1150 °C, 2) 1300 °C, and 3) 1450 °C.

The temperature had significant importance to the crystallite and average grain size determined according to Debye-Scherrer and Williamson-Hall method (Table 4.4). The Debye-Scherrer average grain size of hBN decreased with temperature is given in figure 4.65. However they still had higher grain sizes than the some of high temperature synthesis of hBN with additives. The Williamson-Hall average grain sizes also went down with the decreasing temperature and it was only detectable at 1450 ºC for $CaCO_3$ (Figure 4.66). Williamson-Hall method was not applicable to the lower temperatures such as 1150 ºC for whole synthesis because of the incomplete transformations of intermediate ions, radicals or molecules to hBN lattices.

Table 4.4. Lattice Parameters, Average Grain Size, Microstrain and Graphitization Index of Low Temperature Trials

		Lattice Parameters (Å)			**Average Grain Size (nm)**			
Flux Agent	**T[1]**	**a**	**c**	**d**	**Debye-Scherer Method**	**William son-Hall Method**	**M* (%)**	**G****
40 % Li_2CO_3	1450 ºC	2.504	6.674	3.337	42.953	44.41	0.014	1.91
	1300 ºC	2.506	6.688	3.344	46.654	46.65	0.061	1.95
	1150 ºC	2.506	6.690	3.345	27.436	15.85	-0.064	2.86
	1000 ºC	2.504	6.680	3.340	17.514	N.A.	N.A.	N.D.
40 % Li(Ac***)	1450 ºC	2.506	6.672	3.336	54.049	89.43	0.110	1.97
	1300 ºC	2.506	6.676	3.338	40.296	38.45	0.014	1.88
	1150 ºC	2.506	6.696	3.348	31.004	29.58	-0.004	2.55
40 % LiOH	1450 ºC	2.504	6.682	3.341	38.964	44.46	0.086	2.24
	1300 ºC	2.510	6.726	3.363	40.279	93.72	0.130	1.99
	1150 ºC	2.506	6.688	3.344	41.752	N.A.	N.A.	N.D.
10 % $CaCO_3$	1450 ºC	2.506	6.704	3.352	27.181	12.12	-0.142	3.64
	1300 ºC	2.502	6.712	3.356	13.622	N.A.	N.A.	N.D.
	1150 ºC	2.500	6.714	3.357	8.938	N.A.	N.A.	N.D.

N.A.; Not Applicable, N.D.; Not detected, M*; Microstrain, G**; Graphitization Index, T[1]; Temperature, Ac***; $CH_3CO_2^-$.

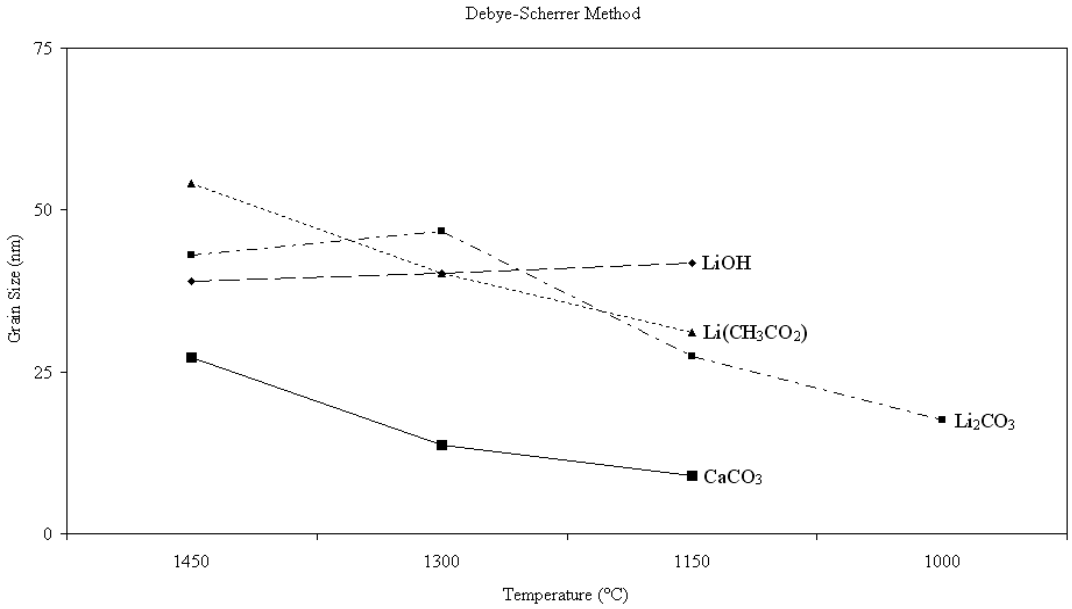

Figure 4.65 Average grain size (Debye-Scherrer Method) of hBN at increasing temperatures with the use of representative metals.

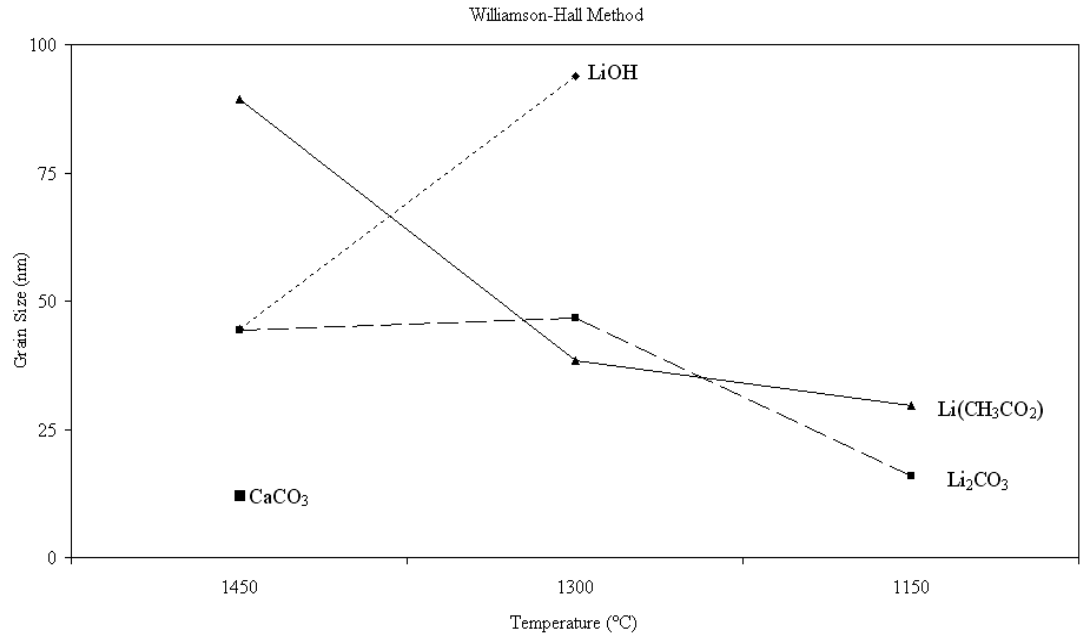

Figure 4.66 Average grain size (Williamson-Hall Method) of hBN at increasing temperatures with the use of representative metals.

The graphitization index of hBN was calculated for low temperature synthesis (Figure 4.67). It was clear from the graphitization index calculations that the lowest ones were obtained at 1300 ºC for lithium salts and there was no significant difference between the samples carried out at 1450 ºC and 1300 ºC. However the graphitization index reasonably increased at 1150 ºC.

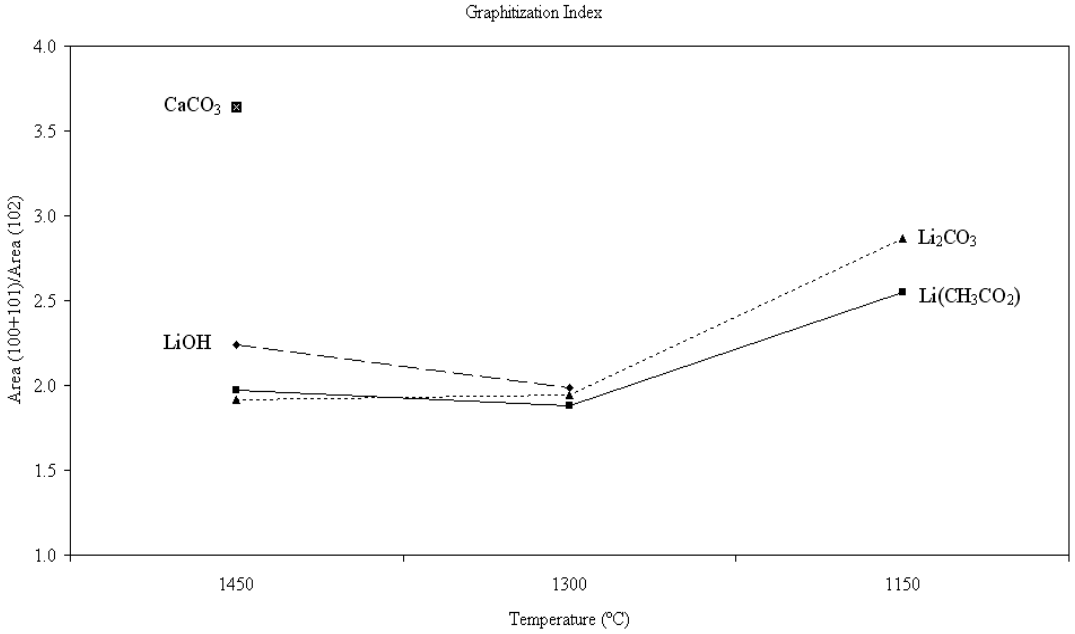

Figure 4.67 Graphitization index of hBN synthesized at low temperatures with different additives.

4.4.3. Scanning Electron Microscopy Analysis of hBN Samples Synthesized at Low Temperatures

SEM images of BN samples show a tubular mixed shape (Figure 4.68) and some of them appear irregularly grained powder (Figure 4.69). However, in some SEM images indicate that the surfaces of hBN were coated by amorphous materials

(Figure 4.70 and 4.71). It was obvious that the temperature decrease caused the deformation of regularity and flaky hexagonal form of BN.

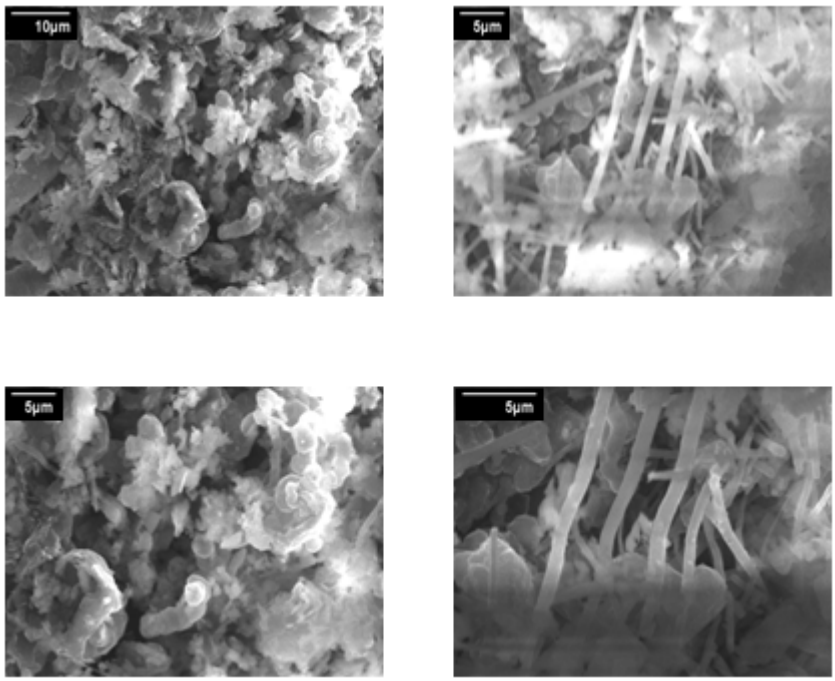

Figure 4.68 Selected SEM images of hBNs synthesized in presence of Li_2CO_3 at 1300 °C.

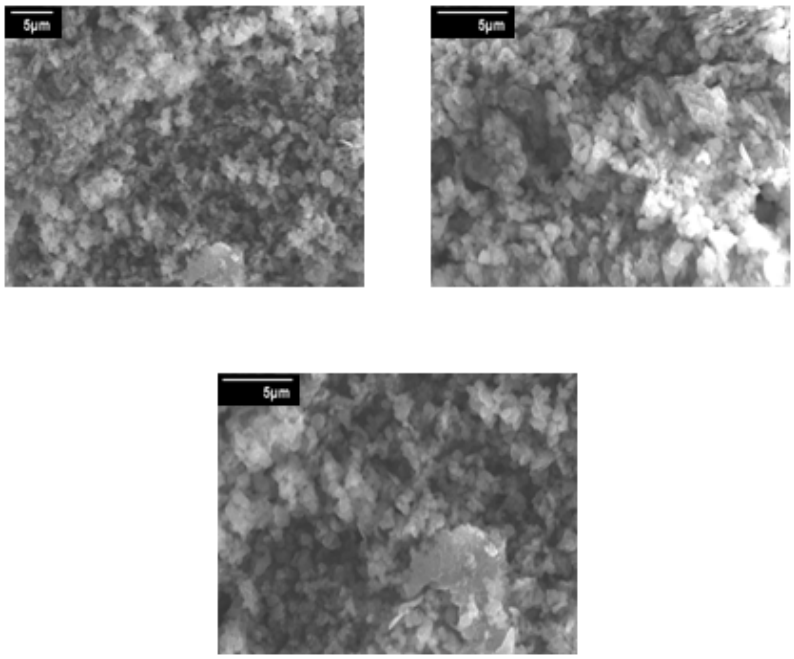

Figure 4.69 Selected SEM images of hBNs synthesized in presence of Li_2CO_3 at 1150 °C.

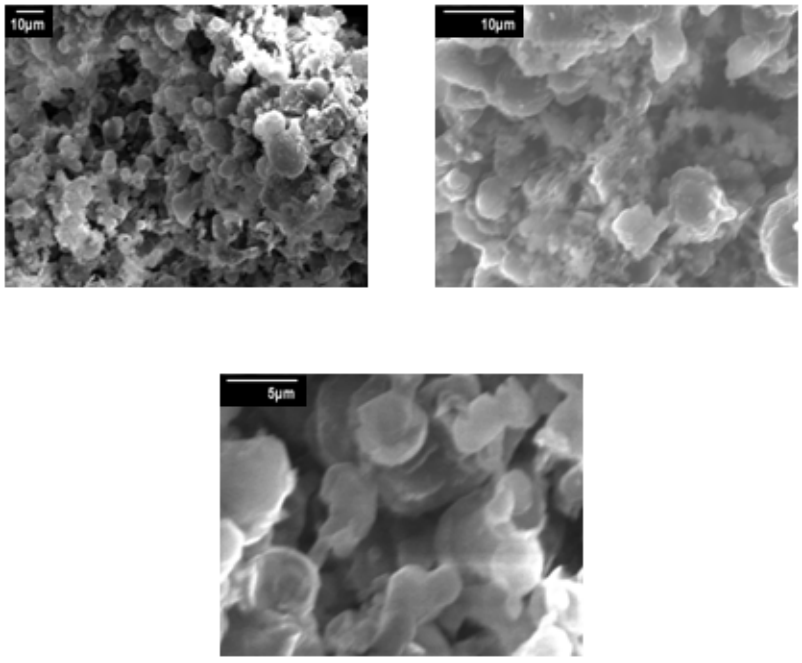

Figure 4.70 Selected SEM images of hBNs synthesized in presence of $Li(CH_3CO_2)$ at 1300 °C.

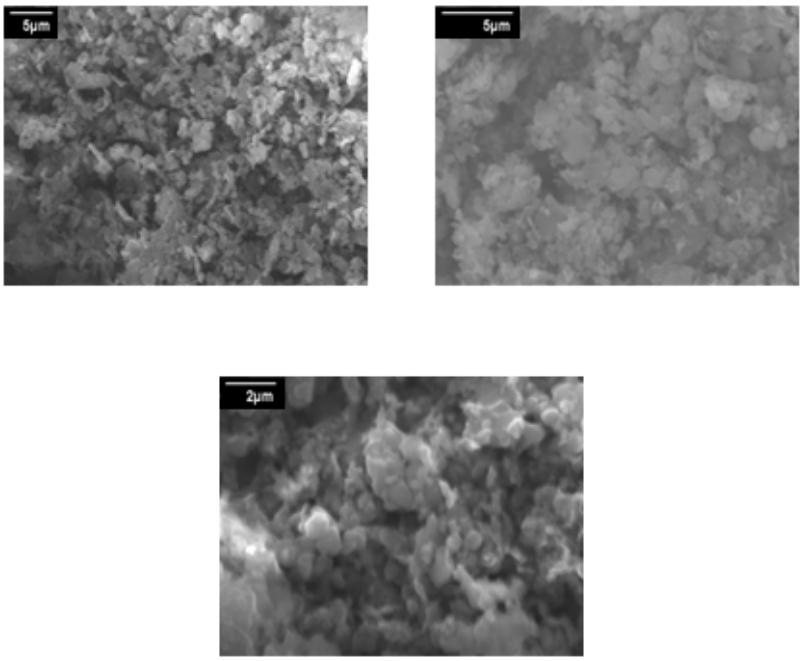

Figure 4.71 Selected SEM images of hBNs synthesized in presence of $Li(CH_3CO_2)$ at 1150 °C.

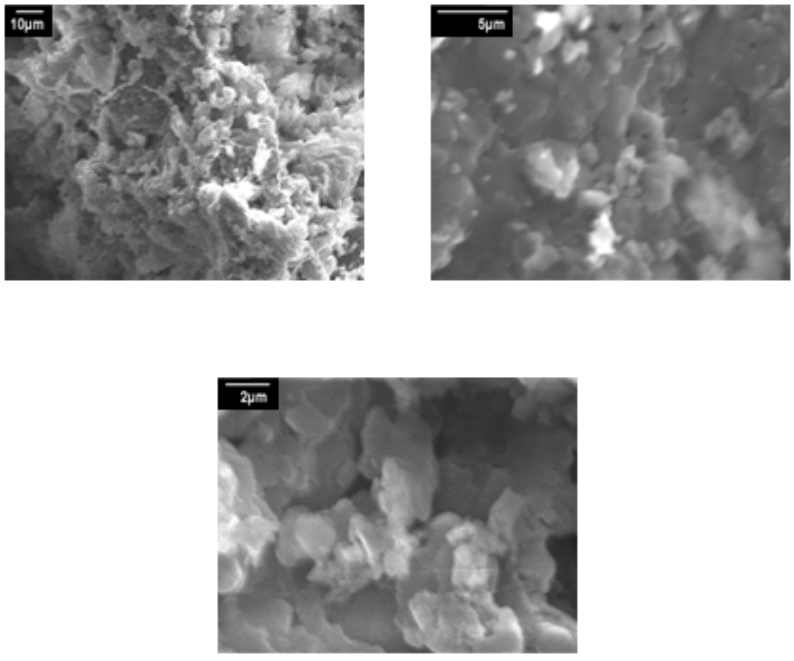

Figure 4.72 Selected SEM images of hBNs synthesized in presence of LiOH at 1300 °C.

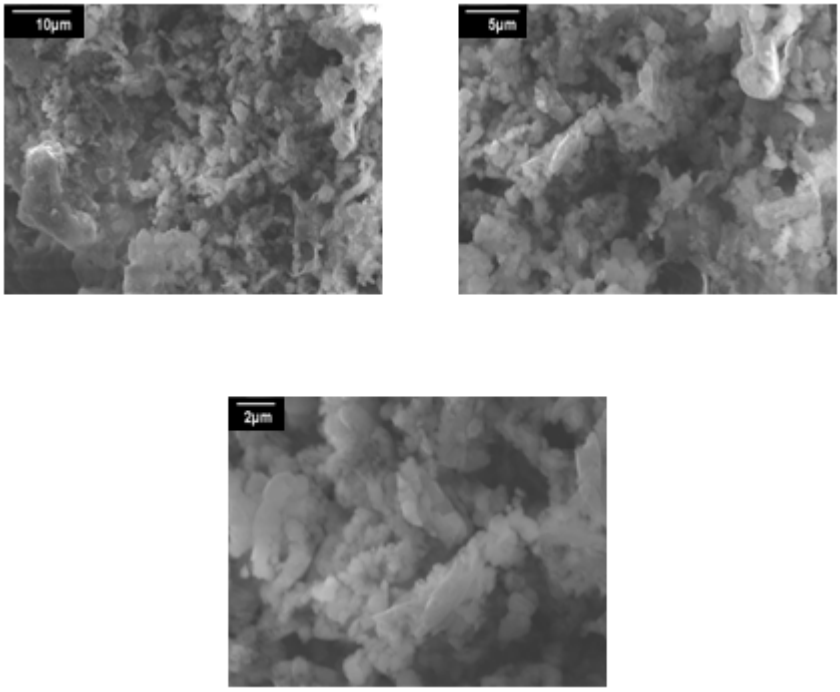

Figure 4.73 Selected SEM images of hBNs synthesized in presence of LiOH at 1150 °C.

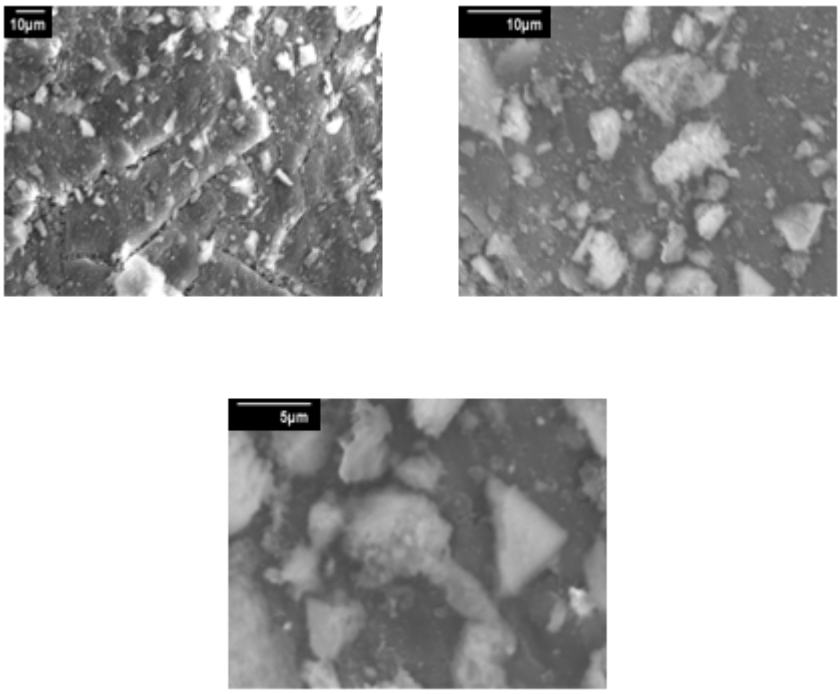

Figure 4.74 Selected SEM images of hBNs synthesized in presence of $CaCO_3$ at 1300 °C.

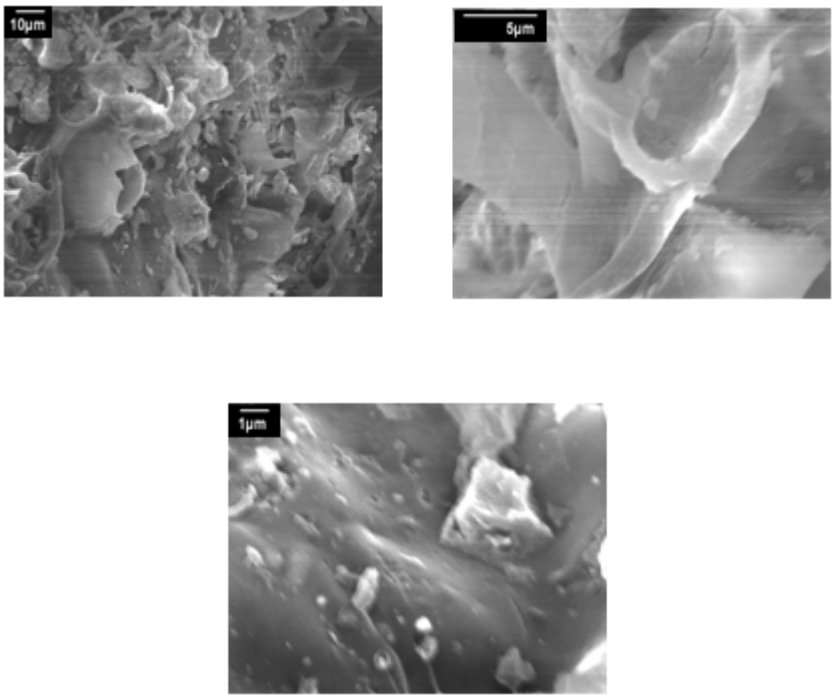

Figure 4.75 Selected SEM images of hBNs synthesized in presence of $CaCO_3$ at 1150 °C.

4.5. Effect of Metals of the Metal Salts on the Formation of hBN

In FT-IR, the main vibration bands of hBN were determined such as 810, 1370, 2520, and 3424 cm^{-1} denoting the out of plane B–N, in plane B–N, vibrations of B–H, and end group vibrations of O–H and N–H, respectively. Also, there was no evidence for the other polymorphs of BN such as cBN which would be assigned with the peak at around 1050 cm^{-1} [54].

The characteristic peaks of hBN (002, 10X (X:0 and 1), 102 004, 110, 112) were observed in XRD diffractograms. The plane mixture of the boric oxide and urea had the turbostratic polymorph or amorphous phases, in contrast to the original hBN. Some of the XRD diffractograms of hBN included the 100 and 101 peaks together

indicating the small crystallite size and turbostratic or nanocrystalline form of BN when magnesium, potassium, and sodium acetates and hydroxides were added in boric oxide and urea mixture. But they were completely separated in carbonates, acetates and hydroxides of lithium and calcium additions and they were nearly same peaks as in original hBN. Moreover appearance of the 102 peak indicated the high crystalline hBN with the additions of lithium and calcium carbonate into the boron oxide and urea mixture (Figure 4.76).

Addition of calcium and lithium acetates into boron oxide and urea mixture had the best contribution among the other acetates deriving from the formation of separated peaks at 100 and 101 and existence of 102 peak (Figure 4.77). In addition, the sharp 002 peaks of patterns were attributed to addition of calcium and lithium acetates, while sodium, potassium, and magnesium acetates had broad indicating the turbostratic nature of BN. Also appearance of the 102 peak with high intensity indicated the formation of highly crystalline hBN (as in $Li(CH_3CO_2)$, $K(CH_3CO_2)$, $Mg(CH_3CO_2)_2$, $Ca(CH_3CO_2)_2$ diffractograms).

LiOH and $Ca(OH)_2$ had significant effect on the formation of hBN among the metal hydroxide additions as in figure 4.78. In some of hBN samples synthesized in presence of NaOH, KOH, and $Mg(OH)_2$ had low grain size and less three dimensional ordered sturucture. The effectiveness of hydroxides decreased with the increasing atomic mass however $Ca(OH)_2$ usage increased independent from its atomic mass of metal ion.

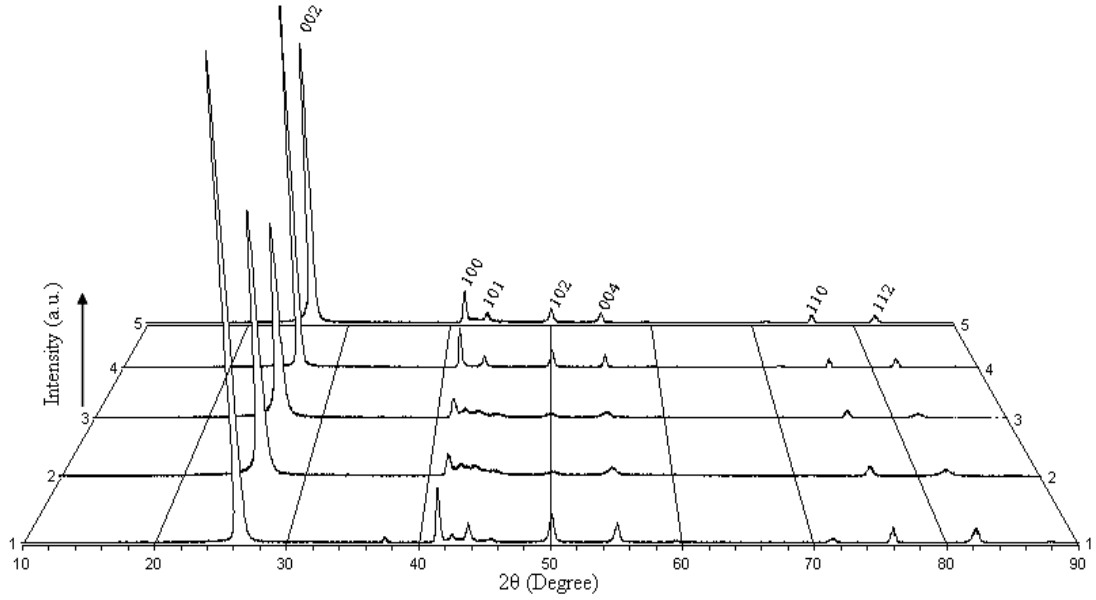

Figure 4.76 Comparison of XRD patterns of hBNs prepared with different additives, where 1) 40 % Li_2CO_3, 2) 40 % Na_2CO_3, 3) 40 % K_2CO_3, 4) 40 % $MgOHCO_3$, and 5) 40 % $CaCO_3$.

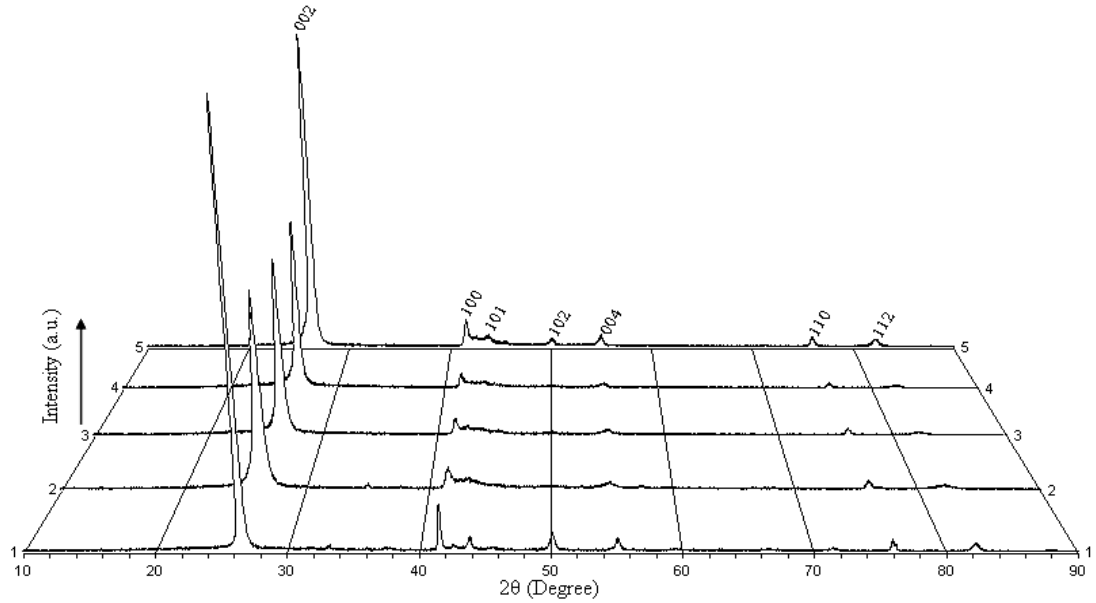

Figure 4.77 Comparison of XRD patterns of hBNs prepared with different additives, where 1) 40 % $Li(CH_3CO_2)$, 2) 40 % $Na(CH_3CO_2)$, 3) 40 % $K(CH_3CO_2)$, 4) 40 % $Mg(CH_3CO_2)_2$, and 5) 40 % $Ca(CH_3CO_2)_2$.

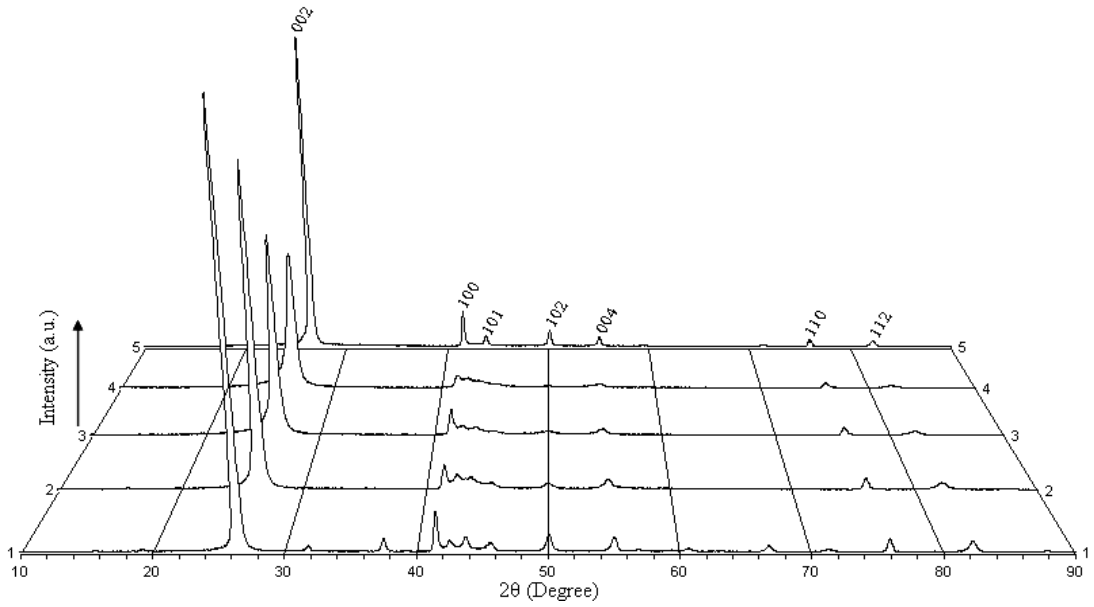

Figure 4.78 Comparison of XRD patterns of hBNs prepared with different additives, where 1) 40 % LiOH, 2) 40 % NaOH, 3) 40 % KOH, 4) 40 % $Mg(OH)_2$, and 5) 40 % $Ca(OH)_2$.

4.6. The Effect of Anions in the Metal Salts on the hBN Synthesis

The anion effects of representative metal compounds were discussed according to the XRD patterns of the hBN samples. Type of the side groups present with metal ions slightly influence the formation of hBN. When the calculated grain sizes of hBN (Table 4.5 and Figure 4.79, 4.80, 4.81, 4.82, and 4.83) samples considered, carbonates had considerable effect due to the intermediate product in heating at high temperatures.

Table 4.5. Comparison of effect of the anions of salts

	Carbonate			Hydroxide			Acetate		
	G.S.[a]	G.S.[b]	G.I.*	G.S.[a]	G.S.[b]	G.I.*	G.S.[a]	G.S.[b]	G.I.*
Lithium	43.0	44.4	1.91	39.0	44.5	2.24	54.1	89.4	1.97
Sodium	20.1	10.8	3.06	20.5	7.64	2.91	13.1	N.A.	N.A.
Potassium	23.9	10.9	3.18	15.6	7.55	3.04	16.6	11.8	3.31
Magnesium	52.9	46.4	2.30	10.8	N.A.	N.A.	22.8	16.8	4.09
Calcium	34.4	31.5	2.27	119.2	297.1	2.15	26.2	15.5	3.99

G.S.[a]: Avarege grain size calculated according to Debye-Scherrer
G.S.[b]: Avarege grain size calculated according to Williamson-Hall
G.I.*: Graphitization index.
N.A.: Not applicable

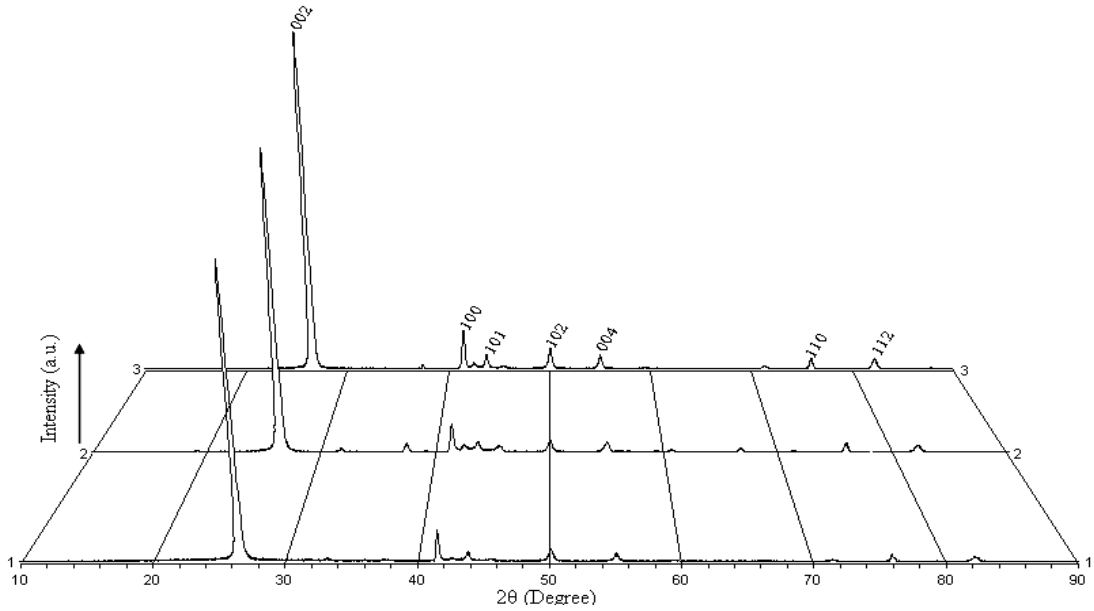

Figure 4.79 Comparison of XRD patterns of hBNs prepared with lithium in different anions, where 1) 40 % $Li(CH_3CO_2)$, 2) 40 % LiOH, and 3) 40 % Li_2CO_3.

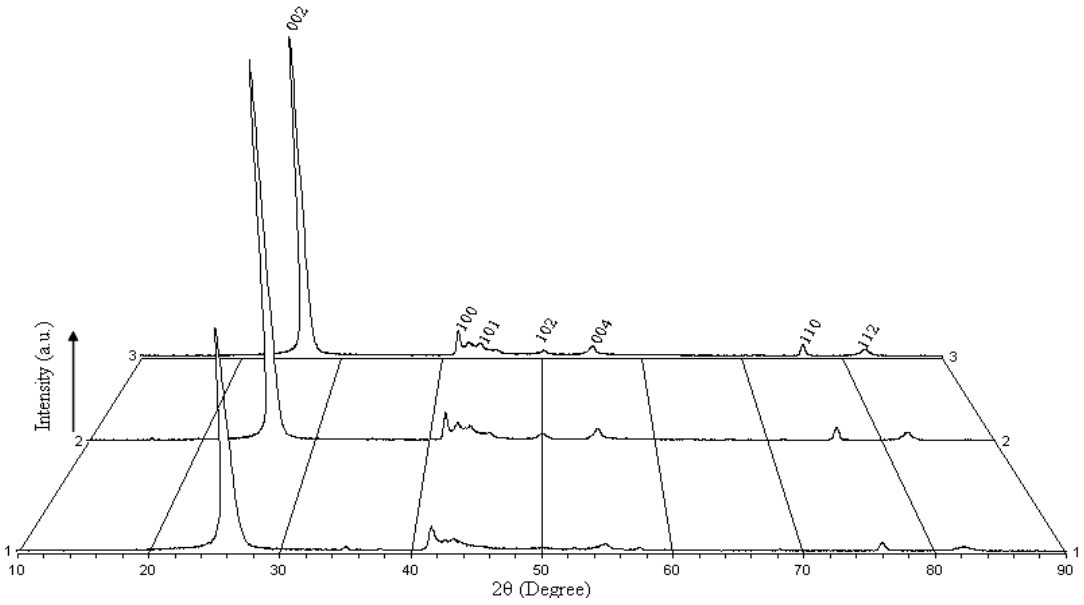

Figure 4.80 Comparison of XRD patterns of hBNs prepared with sodium in different anions, where 1) 40 % $Na(CH_3CO_2)$, 2) 40 % NaOH, and 3) 40 % Na_2CO_3.

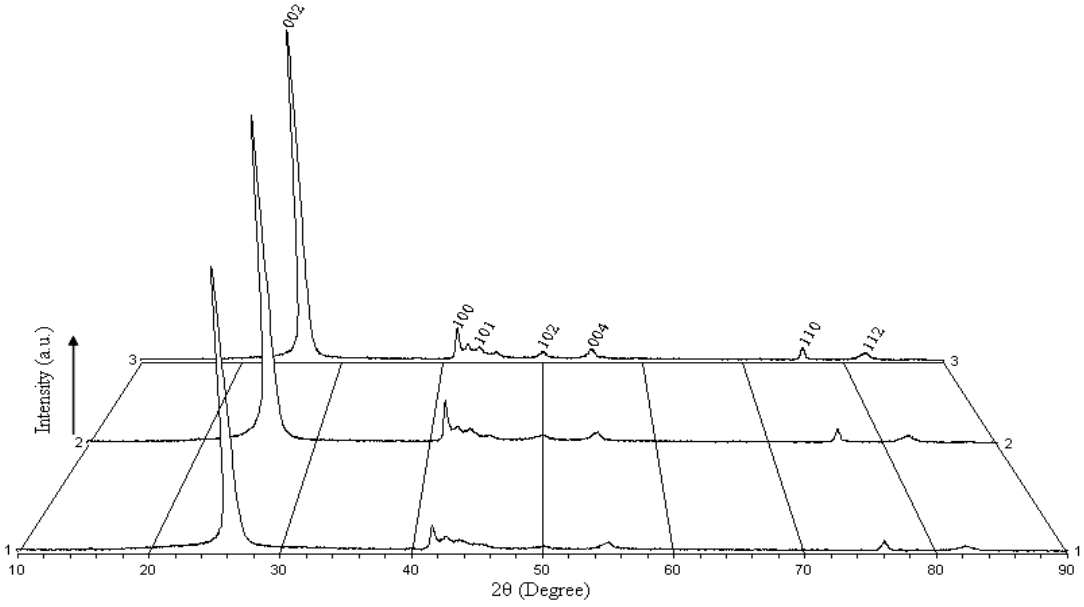

Figure 4.81 Comparison of XRD patterns of hBNs prepared with potassium in different anions, where 1) 40 % $K(CH_3CO_2)$, 2) 40 % KOH, and 3) 40 % K_2CO_3.

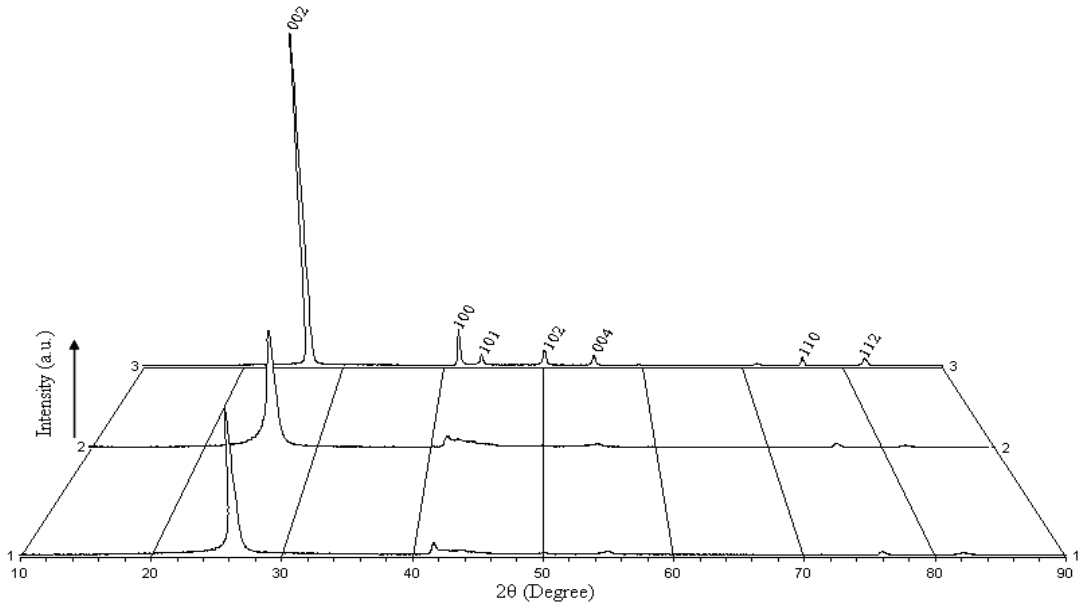

Figure 4.82 Comparison of XRD patterns of hBNs prepared with magnesium in different anions, where 1) 40 % $Mg(CH_3CO_2)_2$, 2) 40 % $Mg(OH)_2$, and 3) 40 % $MgOHCO_3$.

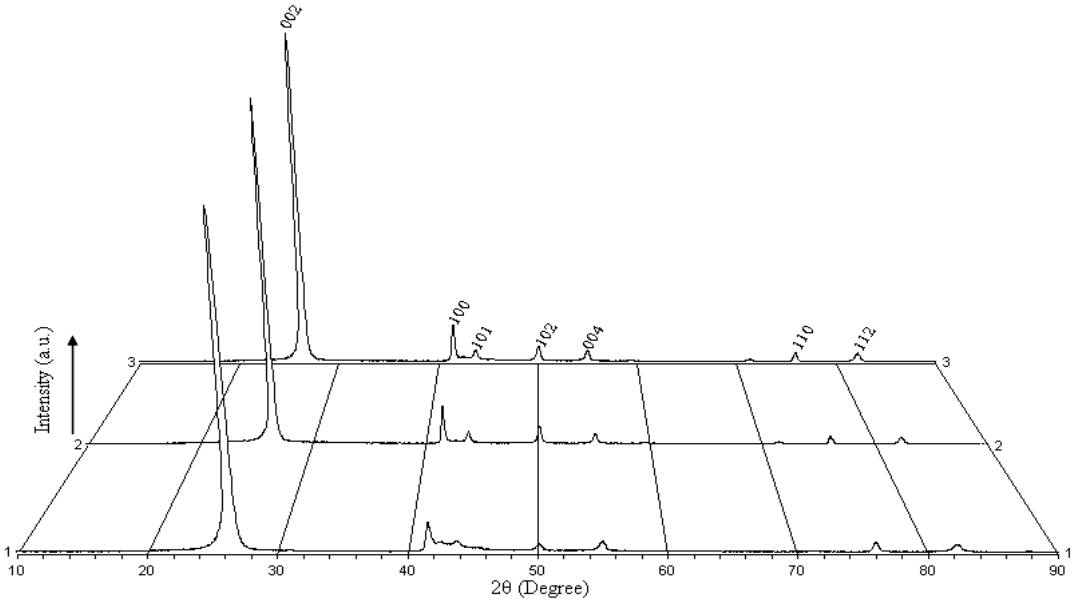

Figure 4.83 Comparison of XRD patterns of hBNs prepared with magnesium in different anions, where 1) 40 % $Ca(CH_3CO_2)_2$, 2) 40 % $Ca(OH)_2$, and 3) 40 % $CaCO_3$.

4.7. Transmission Electron Microscopy Observations for hBN Samples

In this study, the nano forms of hBN were observed in the samples with other crystalline forms. Therefore, further particle size images were obtained using transmission electron microscopy (TEM) as well as in SEM. hBN formed in presence of flux agents were in the irregularly nanotubes a kind of the multi-walled cylindrical and bamboo nanotubes as well as nanowires (Figure 4.84, 4.85, 4.87, and 4.89). Moreover, flaky nature of hBN form was also appeared in TEM images and some of them were covered with amorphous material (Figure 4.86 and 4.87). Furthermore nanocrystalline hBN with needle-like was seen in the samples prepared with presence of LiOH (Figure 4.87). TEM images indicated that the multi-walled hBN was composed of sheets, nanorods and they were parallel to each other. The distance between the two parallel layers was calculated as 0.337 nm from TEM images that was in accordance with the calculated lattice parameters from XRD.

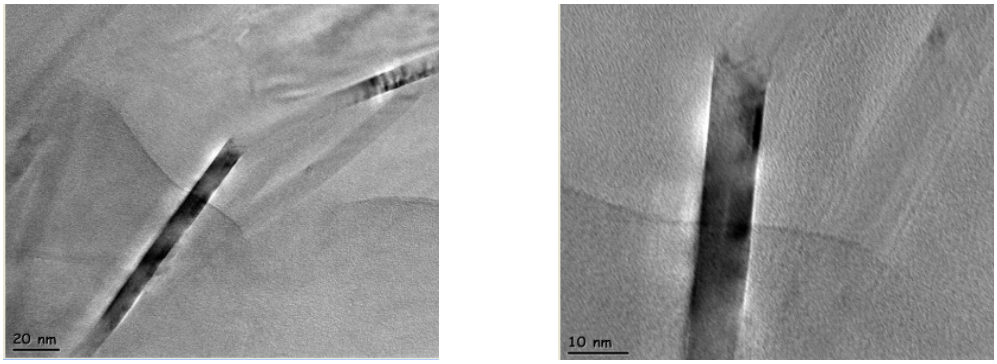

Figure 4.84 Selected TEM images of hBN synthesized in the presence of Li_2CO_3 at 1450 °C.

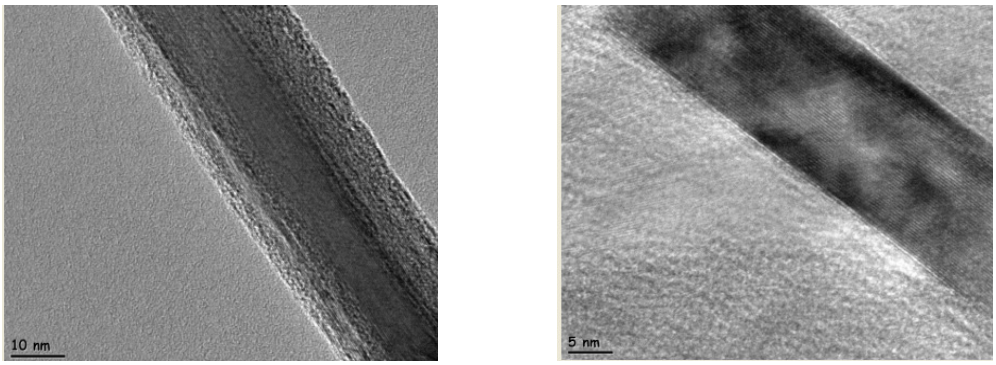

Figure 4.85 Selected TEM images of hBN synthesized in the presence of Li_2CO_3 at 1300 °C.

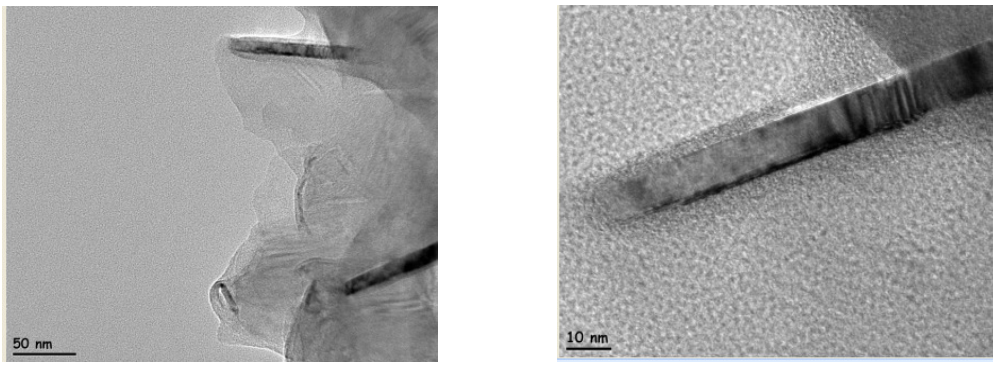

Figure 4.86 Selected TEM images of hBN synthesized in the presence of Li_2CO_3 at 1150 °C.

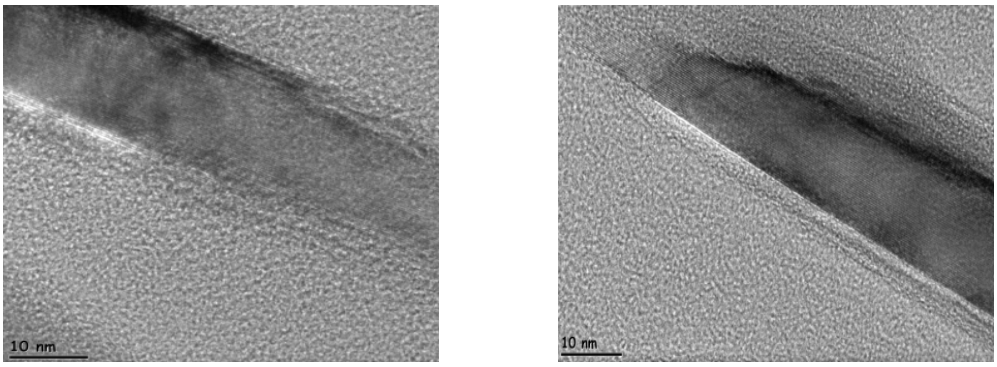

Figure 4.87 Selected TEM images of hBN synthesized in the presence of $Li(CH_3CO_2)$ at 1150 °C.

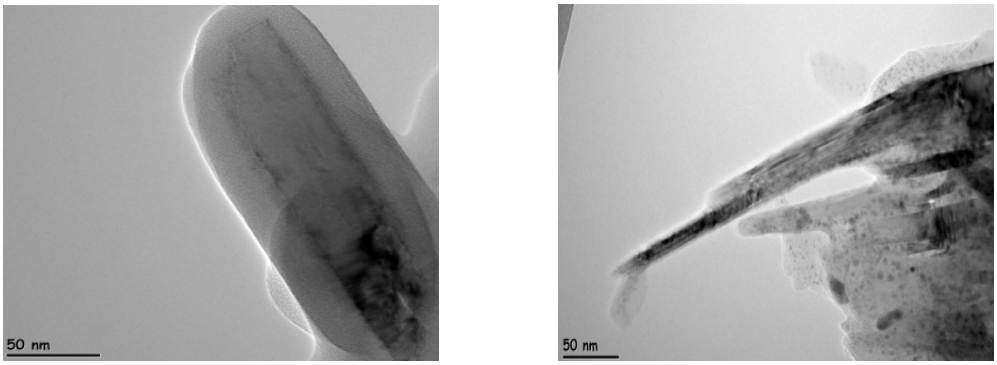

Figure 4.88 Selected TEM images of hBN synthesized in the presence of LiOH at 1450 °C.

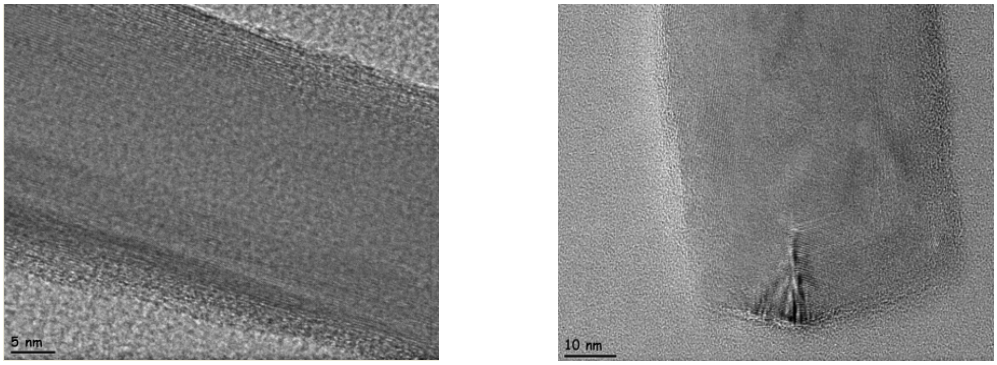

Figure 4.89 Selected TEM images of hBN synthesized in the presence of $CaCO_3$ at 1450 °C.

CHAPTER 5

5. DISCUSSION

Boron nitride samples were synthesized by using modified O'Connor method with the presence of representative metal carbonates, acetates, and hydroxides of lithium, sodium, potassium, magnesium, and calcium. That method was preferred to synthesize of hBN because of easiness. The characterization was performed with FT-IR, XRD, SEM, and TEM [1, 8, 38, 40, 63] to clarify the structure.

Initially, hBN formation was determined by FT-IR measurements which explained the structure by vibrational modes in hBN. The synthesized samples in the presence of fluxing agents indicated hBN formation and also, there was no evidence for cBN [54]. The XRD measurements supported that the cBN phase could not occur at this reaction conditions. Another phase of rBN was determined from XRD patterns with a peak at 003 direction and presence a peak between the 100 and 101. The main peak of rBN at 003 coincides with the peak of hBN at 002 [64], therefore, it was confusable.

The average grain size, crystallinity, lattice parameters, and graphitization index of hBN samples were calculated from XRD patterns when the fluxing agents were added into the boron oxide and urea mixture. Addition of more than 20 % of metal carbonates, hydroxides, and acetates enhanced the hBN formation because the reaction surface area and reduction in molten phase for a long time or reductive

properties of fluxes [19, 20, 21]. However, there was no significant change in the use of 30 % and 40 % of additives. Because high amount of additives might decrease the interaction between nitrogen and boron containing compounds.

In addition, the intermediates such as HCN, HNCO, NO, N_2O, CO, and CO_2, the products of thermal decomposition of fluxes at high temperatures, might increase the formation of hBN [65, 66] in the ammonia atmosphere. The accompanying anions had no significant effect on formation of hBN, however, the addition of carbonates had comparatively improved results than the hydroxides and acetates because of thermally stable intermediate products at high temperatures and high melting point [65, 66].

The hBN formations were also determined at high temperatures such as 1450 ºC. The addition of sodium and potassium salts into reaction medium was also indicated to turbostratic or nanocrystalline BN with small crystallite size while lithium, magnesium, and calcium salts promoted highly crystalline hBN formation. This might be due to the melting temperatures of species in the mixture that would be effective on formation of hBN. However, the significant contribution of lithium, magnesium, and calcium salts might be explained retention of the melt for a long time and increase in surface area. However, calcium salts caused turbostratic or nanocrystalline form of BN at the temperatures lower than 1450 ºC although addition of lithium salts into the reaction mixture increased the crystallinity of hBN even low temperatures such as 1300 ºC and 1150 ºC.

Electronic interactions such as d-π interaction enhanced hBN formation by addition of transition metal salts [1, 38, 67] in other studies. However, atomic size and coordination numbers of metal atoms possibly have not significant effect on the

formation of hBN although the metals used in the study have relatively high coordination number [68].

The importance of the usage of metal salts could be seen clearly from electron microscopy images. The disc-shape homogeneous plates of hBN were first reported by Shimomura [60] in literature. In this study, lithium and calcium salts provided the best contribution to layered structure and disc-shape homogeneous plate formation of hBN. Further information could be obtained from TEM images in which BN samples consisted of uniform needle-like and multi-walled nano particles. The grains of BN synthesized in the presence of potassium salts were coagulated in SEM images.

The effect of various fluxing agents in different concentrations was investigated by the FT-IR, XRD, SEM, and TEM. The use of metal salts decreased the synthesis temperature of highly crystalline hBN and increased the amount of nano-scale hBN, which were clarified with XRD. The crystallinity, grain size, and lattice parameters were found to be very close to the literature values. The SEM and TEM images were also supported the calculation of specified parameters from XRD pattern for hBN. The structural and compositional effects of additives must be apparently determined with other instrumental methods.

CHAPTER 6

6. CONCLUSION

In this study, the hexagonal boron nitride (hBN) formations were confirmed in the presence of the representative metal carbonates, acetates, and hydroxides by using FT-IR, XRD, SEM, and TEM analysis.

1. The formation of hBN was found to be dependent on the amount of additives.
2. Higher than 20 % of additives had positive contribution to hBN formation.
3. The grain size of the synthesized hBN increased due to the concentration and type of the fluxing agent.
4. The improved crystallinity was obtained at high temperatures such as at 1450 ºC comparatively lower temperature than O'Connor method.
5. Anions of the used metal salts had no significant effects on formation of hBN.
6. The nanoscale hBN samples were synthesized at high temperatures that nano rod and tubular structures were observed in hBN samples.
7. The intermediate products at the synthesis had possibly important role in the synthesis of hBN. Therefore they are questionable.
8. Further studies are necessary to determine the actual effect of additives.

9. Nanocrystalline, nanorod, and nanowire structures obtained in the synthesis of hBN must be investigated for the different applications of nano-scale particles.
10. The rBN formation was observed in this study is a suitable phase to convert the other phases especially cubic BN.
11. It was possible to obtain high crystalline hBN powder at lower temperature such as 1150 ℃, which would be convenient temperature for commercial applications.

REFERENCES

[1] Budak, E. and Bozkurt, Ç. 2010. Synthesis of hexagonal boron nitride with the presence of representative metals. *Journal of Physics: Condensed Matter* 405: 4702–4705.

[2] Özkol, E. 2008. Production of Boron Nitride. M.Sc. Thesis. Department of Chemical Engineering, Middle East Technical University, Ankara. p. 5.

[3] Ruprecht, P., Konkol, W., Cornils, B., Langhoff, J., Brunke W. and Schäfer, W. 1985. Slagging gasification of coal under addition of flux agents. *Fuel Processing Technology* 11 (1): 1–12.

[4] Wang, D.Y., Liu, C.J., Shi, P.Y., Jiang, M.F. 2004. Effect of Rare Earth Oxide on Crystallization Temperature of Mold Flux for Continuous Casting. *Journal of Iron and Steel Research* 16 (5): 28–32.

[5] Vaynman S. and Fine, M.E., 1999. Development of Fluxes for Lead-Free Solders Containing Zinc. *Scripta Materialia* 41 (12): 1269–1271.

[6] Miclea, C., Tanasoiu, C., Spanulescu, I., Miclea, C. F., Gheorghiu, A., Amarande, L., Cioangher, M., Miclea, C. T. 2007. Microstructure and Properties of Barium Titanate Ceramics Prepared by Mechanochemical Synthesis, *Romanian Journal of Information Science and Technology*, 10 (4): 335–345.

[7] Anonymous- 1. Chamber of Mining Engineers of Turkey Web Site. http://www.maden.org.tr/resimler/ekler/6358599b7afb250_ek.pdf?tipi=5&turu=R&sube=0.

[8] Budak, E. 2009. Comparison of the Effect of Representative Metal and Transition Metal Salts on the Formation of Hexagonal Boron Nitride. Ph.D. Thesis, Department of Chemistry, Abant Izzet Baysal University, Bolu. p. 5.

[9] Haubner R., Wilhelm M., Weissenbacher R. and Lux B. 2002. Boron Nitrides - Properties, Synthesis and Applications. *High Performance Non-Oxide Ceramics II Structure and Bonding*, 102: 1–45

[10] Mishima, O. and Era, K. 2000. Science and Technology of Boron Nitride. *In:* Kumashiro, Y. (ed.): *Electric Refractory Materials*. 498. Mercel Dekker, Inc. New York.

[11] Hubacek, M., and Ueki, M., 1996. Chemical Reactions in Hexagonal Boron Nitride System. *Journal of Solid State Chemistry* 123: 215–222.

[12] Paine, R. T. and Narula, C. K. 1990. Synthetic Routes to Boron Nitride, *Chemistry Review*, 90: 73–91.

[13] O'Connor, T. E. 1962. Synthesis of Boron Nitride. *Journal of American Chemical Society* 84: 1753–1754.

[14] Hubacek, M. and Brozek, V. 1991. Kinetics of Deoxidizing of Hexagonal Boron Nitride Preparations. *Journal of Solid State Chemistry* 95: 253–259.

[15] Hubacek, M. and, Sato, T. 1995. Preparation and Properties of a Compound in the B-C-N System. *Journal of Solid State Chemistry* 114: 258–264.

[16] Rijnders, M. R., 1996. Periodic Layer Formation During Solid State Reactions. Ph.D. Thesis, Faculty of Chemical Engineering and Chemistry, Eindhoven University of Thecnology, Nedherlands.

[17] Ropp, R.C., Solid State Chemistry. 2003. Mechanisms and Reactions in the Solid State. 129–150 Elsevier Science B.V. First Edition New Jersey, USA.

[18] West, A.R., 2003, Solid state chemistry and its applications. John Wiley and Sons, U.S.A.

[19] Çamurlu, H. E. 2011. Effect of Na_2CO_3 on Hexagonal Boron Nitride Prepared from Urea and Boric Acid. *Ceramics International* 37 (6): 1993-1999.

[20] Çamurlu, H. E., Sevinç, N., and Topkaya, Y., 2008. Effect of Calcium Carbonate Addition on Carbothermic Formation of Hexagonal Boron Nitride. *Journal of European Ceramic Society* 28: 679–689.

[21] Çamurlu, H. E., Sevinç, N., and Topkaya, Y., 2009. Catalytic effect of alkaline earth oxides on carbothermic formation of hexagonal boron nitride. *Ceramics International* 35: 2271–2275.

[22] West, A. R., 2001, Basic Solid State Chemistry, Second Edition, John Wiley and Sons, U.S.A.

[23] Smart, L. E. and Moore E. A. 2005, Solid State Chemistry: An Introduction, Third Edition, Taylor and Francis, U.S.A.

[24] Gillan E. G. and Kaner R. B. 1996. Synthesis of Refractory Ceramics via Rapid Metathesis Reactions between Solid-State Precursors, *Chemistry of Materials,* 8, 333–343.

[25] Haber, J., 1984. The Role of Surfaces in the Reactivity of Solids, *Pure and Applied Chem*istry, 56 (12): 1663–1676.

[26] Alkoy, S., Toy, Ç., Gönül, T., and Tekin, A. 1997. Crystallization Behavior and Characterization of Turbostratic Boron Nitride, *Journal of the European Ceramic Society* 17: 1415–1422.

[27] Bello, I., Chan, C.Y., Zhang, W.J., Chong, Y.M., Leung, K.M., Lee, S.T. and Lifshitz, Y. 2005. Deposition of thick cubic boron nitride films: The route to practical applications, *Diamond and Related Materials* 14: 1154–1162.

[28] Balint M. G. and Petrescu M. I. 2009. An attempt to identify the presence of polytype stacking faults in hBN powders by means of X-ray diffraction. *Diamond and Related Materials* 18: 1157–1162.

[29] Thomas, J., Weston N. E. and O'Connor T. E. 1962. Turbostratic Boron Nitride, Thermal Transformation to Ordered-layer-lattice Boron Nitride. *Journal of American Chemistry Society* 84: 4619–4622.

[30] Egerton, R.F. 2005. Physical Principles of Electron Microscopy: An Introduction to TEM, SEM, and AEM, Springer, U.S.A.

[31] Zeng, H., Kan, Y. M. and Zhang, G.J. 2010. Synthesis of boron carbide powder from hexagonal boron nitride. *Materials Letters*, 64 (18): 2000–2002.

[32] Reddy, A. L. M., Tanur, A. E. and Walker, G. C. 2010. Synthesis and hydrogen storage properties of different types of boron nitride nanostructures. *International Journal of Hydrogen Energy*, 35, 4138–4143

[33] Balmain, W. H. 1842. Bemerkungen über die Bildung von Verbindungen des Bors und Siliciums mit Stickstoff und gewissen Metallen. *Journal für Praktische Chemie* 27: 422–430.

[34] Leitner, J., Voňka, P., Brožek, V. and Hubáček M. 1988. Thermodynamic analysis of the refining of technical boron nitride. *Journal of Materials Science*, 23 (10): 3594–3599.

[35] Brožek, V. and Hubáček M. 1992. A contribution to the crystallochemistry of boron nitride. *Journal of Solid State Chemistry*, 100 (1): 120–129.

[36] Choi, J. Y., Kang, S. J. L., Fukunaga, O., Park, J. K. and Eun, K. Y. 1993. Effect of B_2O_3 and hBN Crystallinity on cBN Synthesis. *Journal of American Ceramic Society,* 76 (10): 2525–2528.

[37] Kubota, Y., Watanabe, K., Tsuda O. and Taniguchi, T. 2007. Deep Ultraviolet Light-Emitting Hexagonal BN Synthesized at Atmospheric Pressure. *Science*, 317: 932–934.

[38] Budak, E. and Bozkurt, Ç. 2004. The effect of transition metals on the structure of h-BN intercalation compounds, *Journal of Solid State Chemistry*, 177 (4-5): 1768–1770.

[39] Bartnitskaya, T. S., Kurdyumov, A. V., Lyashenko, V. I., Ostrovskaya, N. F. and Rogovaya, I. G. 1996. Catalytic Synthesis of Graphite-Like Boron Nitride. *Powder Metallurgy and Metal Ceramics,* 35 (5-6): 296–300.

[40] Bartnitskaya, T. S., Lyashenko, V. I., Kurdyumov, A. V., Ostrovskaya, N. F. and Rogovaya, I. G. 1994. Effect of Lithium on Structure of Graphite-Like Boron Nitride with Carbothermal synthesis. *Powder Metallurgy and Metal Ceramics,* 33 (7-8): 335–340.

[41] Nihal Yücel, "Effect of Metal Carbonyls on the formation of Hexagonal Boron Nitride", Master Thesis, Department of Chemistry, Abant Izzet Baysal University, 2005, Bolu.

[42] Chopra, N. G., Luyken, R. J., Cherrey, K., Crespi, V. H., Cohen, M. L., Louie S. G. and Zettl, A. 1995. Boron Nitride Nanotubes, *Science*, 269: 966–967.

[43] Solin, S. A. 1982. The nature and structural properties of graphite intercalation compounds. *Advances in Chemical Physics*, 49: 455–532.

[44] Loiseau, A., Willaime, F., Demoncya, N., Schramchenko, N., Hug, G., Colliexe, C. and Pascard, H. 1998. Boron nitride nanotubes. *Carbon*, 36 (5-6): 743–752.

[45] Cumings, J. and Zettl, A. 2000. Mass-production of BN double-wall nanotubes and nanococoons. *Chemical Physics Letters,* 316: 211–216.

[46] Chen, Y., Gerald, J. F., Williams, J.S. and Bulcock, S. 1999. Synthesis of boron nitride nanotubes at low temperatures using reactive ball milling. *Chemical Physics Letters*, 299 (3-4): 260–264.

[47] Li, L., Li, C. P. and Chen, Y. 2008. Synthesis of boron nitride nanotubes, bamboos and nanowires. *Physica E: Low-dimensional Systems and Nanostructures*, 40 (7): 2513–2516.

[48] Chen, H., Chen, Y., Yu, J. and Williams, J. S. 2006. Purification of boron nitride nanotubes. *Chemical Physics Letters*, 425 (4-6): 315–319.

[49] Hirano, T., Oku, T. and Suganuma, K. 2000. Atomic structure and electronic state of boron nitride fullerenes and nanotubes. *Diamond and Related Materials*, 9 (3-6): 625–628.

[50] Deepak, F.L., Vinod, C.P., Mukhopadhyay, K., Govindaraj, A. and Rao, C. N. R. 2002. Boron nitride nanotubes and nanowires. *Chemical Physics Letters*, 353 (5-6): 345–352.

[51] Shi, L., Gu, Y., Chen, L., Qian, Y., Yang, Z., and Ma, J. 2004. Synthesis and Morphology Control of Nanocrystalline Boron Nitride. *Journal of Solid State Chemistry* 177 (3): 721–724.

[52] Kılıç, A., Olutaş, M., Kılıç, K. and Altınkök, A. 2011. Organization of flux line system and voltage oscillations in superconducting MgB_2. *Journal of Applied Physics* 110: 113917.

[53] Hubacek, M., Sato, T., and Ishii, T. 1994. A Coexistence of Boron Nitride and Boric Oxide. *Journal of Solid State Chemistry,* 109: 384–390.

[54] Hu, J. Q., Lu, Q. Y., Tang, K. B., Yu, S. H., Qian, Y. T., Zhou, G. E., Liu, X. M. and Wu, J. X. 1999. Synthesis and Characterization of Nanocrystalline Boron Nitride. *Journal of Solid State Chemistry*, 148: 325–328.

[55] Chen, L., Gu, Y., Li, Z., Qian, Y., Yang, Z. and Ma, J. 2005. Low-Temperature Synthesis and Benzene-Thermal Growth of Nanocrystalline Boron Nitride. *Journal of Crystal Growth*, 273: 646–650.

[56] Zhu, L., Tan, M., Lian, G., Zhang, X., Cui, D. and Wang, O. 2009. Hydrothermal hot-pressing induced phase transition in hexagonal boron nitride. *Solid State Sciences*, 11: 1283–1287.

[57] Bartnitskaya, T. S., Vlasova, M. V., Lyashenko, V. I., Serebryakova, T. I., Timofeeva, I. I. and Tomila, T. V. 1993. Formation of Highly Disperse Boron Nitride in Carbothermal Reduction in The Presence of Lithium Compounds. *Translated from Poroshkovaya Metallurgiya*, 361: 64–73.

[58] Hubacek, M. and, Sato, T. 1995. Preparation and Properties of a Compound in the B-C-N System. *Journal of Solid State Chemistry*, 114: 258–264.

[59] Al-Jawhari H. A., Baeraky T. A. and Afandi Y. H. 2011. The influence of microwave frequencies at high temperatures on structural properties of h-BN. *International Journal of Engineering and Technology* 11: 87–90.

[60] Shimomura, J., Funahashi, T. and Koitabashi, T. 1995. Electron Microscopy of Hexagonal Boron Nitride Powder. *Journal of Material Science,* 30: 3193–3199.

[61] Perdigon-Melon J. A., Auroux, A., Cornu, D., Miele, P., Toury, B. and Bonnetot, B. 2002. Porous Boron Nitride Supports Obtained From Molecular Precursors: Influence of the Precursor Formulation and of the Thermal Treatment on the Properties of BN Ceramic. *Journal of Organometallic Chemistry*, 657: 98– 106.

[62] Yoo, C. S., Akella, J. and Cynn, H. 1997. Direct Elementary Reactions of Boron and Nitrogen at High Pressures and Temperatures. *Physical Review B*, 56: 140–146.

[63] Koç, G. 2004. Synthesis of Cadmium Intercalated Hexagonal Boron Nitride. MSc Thesis. Department of Chemistry, Abant Izzet Baysal University, Bolu. p. 35.

[64] Taniguchi, T., Sato, T., Utsumi, W., Kikegawa, T. and Shimomura, O. 1997. In-situ X-ray observation of phase transformation of rhombohedral boron nitride under static high pressure and high temperature. *Diamond and Related Materials*, 6(12): 1806–1815.

[65] Mu, J. and Perlmutter, D. D. 1981. Thermal decomposition of carbonates, carboxylates, oxalates, acetates, formates, and hydroxides, *Thermochimica Acta*, 49 (2-3): 207–218.

[66] Abul-Milh, M. and Steenari, B. M. 2001. Effect of calcination on the reaction of ammonia over different carbonates and limestone s in fluidized bed combustion conditions. *Enery and fuel,* 15: 874–880.

[67] Hubacek, M., Sato T. and Ueki M. 1997. Copper - Boron Nitride Interaction in Hot-Pressed Ceramics. *Journal of Materials Research*, 12 (1): 113–118.

[68] Hause J. E., 2008, Inorganic Chemistry. 237-244, Academic Press, Elsevier, Canada.

CIRRICULUM VITAE

Name	**:**	Muhammed ÖZ
Permanent Address	**:**	Abant Izzet Baysal University Faculty of Art & Science of Chemistry 14280,Bolu
Degree and date to be conferred	**:**	M.S., 2009
Place/Date of Birth	**:**	İslahiye 22.08.1982
Secondary education	**:**	Opet Anatolian High School, Gaziantep, 2000.

Collegiate institutions attended	**Dates**	**Degree**	**Date of degree**
Abant Izzet Baysal University	2001-2005	B.S.	2005
Abant Izzet Baysal University	2006-2009	M.S.	2009

Publications:

1-Yenisoy-Karakas, S., Oz, M., Gaga, E. O., 2012. Seasonal variation, sources, and gas/particle concentrations of PCBs and OCPs at high altitude suburban site in Western Black Sea Region of Turkey, Journal of Environmental Monitoring, Volume: 14, Issue: 5 pp 1365-1374.

2- M. Gulen, G. Yildirim, S. Bal, A. Varilci, I. Belenli and M. Oz., 2013. Role of annealing temperature on microstructural and electro-optical properties of ITO films produced by sputtering, Journal of Materials Science: Materials in Electronics, Volume 24, Issue 2, pp 467-474.

Positions Held: Research Assistant at Department of Chemistry, Faculty of Arts & Science, Abant Izzet Baysal University since 2005.